ELFORSK

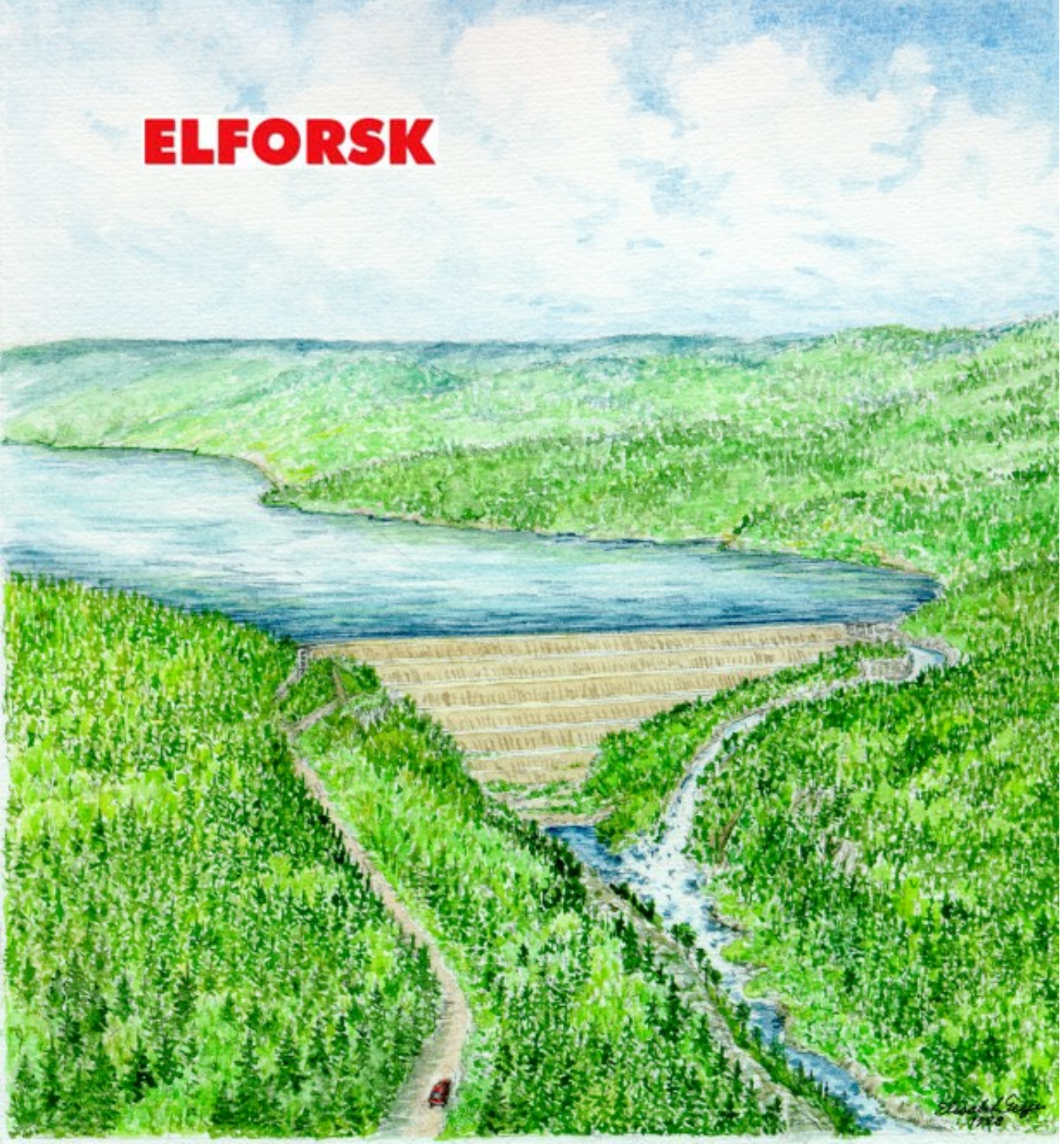

DAMMSÄKERHET

LONG TERM RESISTIVITY AND SELF POTENTIAL MONITORING OF EMBANKMENT DAMS – Experiences from Hällby and Sädva Dams, Sweden

Rapport 05:15

CEATI Project No. T992700-0205
Investigation of Geophysical Methods for Assessing Seepage and Internal Erosion in Embankment Dams

LONG TERM RESISTIVITY AND SELF POTENTIAL MONITORING OF EMBANKMENT DAMS –

Experiences from Hällby and Sädva Dams, Sweden

October 2003

Sam Johansson and Johan Friborg
HydroResearch Sam Johansson AB

Torleif Dahlin and Pontus Sjödahl
Lund University

Förord

Stockholm maj 2005

Denna rapport är ett delresultat inom Elforsk ramprogram Dammsäkerhet.

Kraftindustrin har traditionellt satsat avsevärda resurser på forsknings och utvecklingsfrågor inom dammsäkerhetsområdet, vilket har varit en förutsättning för den framgångsrika utvecklingen av vattenkraften som energikälla i Sverige.

Målen för programmet är att långsiktigt stödja branschens policy, dvs att:

- Sannolikheten för dammbrott där människoliv kan vara hotade skall hållas på en så låg nivå att detta hot såvitt möjligt elimineras.
- Konsekvenserna i händelse av dammbrott skall genom god planering såvitt möjligt reduceras.
- Dammsäkerheten skall hållas på en god internationell nivå.

Prioriterade områden är Teknisk säkerhet, Operativ säkerhet och beredskap samt Riskanalys.

Ramprogrammet har en styrgrupp bestående av: Jonas Birkedahl – FORTUM, Malte Cederström - Vattenfall Vattenkraft, Anders Isander – Sydkraft Vattenkraft, Lennart Markland – Vattenregleringsföretagen, Urban Norstedt - Vattenfall Vattenkraft, Gunnar Sjödin – Vattenregleringsföretagen samt Lars Hammar - Elforsk

Lars Hammar
Elforsk AB

Disclaimer

This report was prepared by the authors via HydroResearch and Lund University and administered and funded by:

- Elforsk AB,
- Svenska Kraftnät, and
- the CANADIAN ELECTRICITY ASSOCIATION on behalf of CONSORTIUM MEMBERS (hereinafter called "SPONSORS"), who do not necessarily agree with the opinions expressed herein.

Neither the SPONSORS, nor CEA, nor the authors, nor HydroResearch/Lund University, nor any other person acting on their behalf makes any warranty, expressed or implied, or assumes any legal responsibility for the accuracy of any information or for the completeness or usefulness of any apparatus, product or process disclosed, or accept liability for the use, or damages resulting from the use, thereof. Neither do they represent that their use would not infringe upon privately owned rights.

Furthermore, the SPONSORS, CEA and authors and HydroResearch/Lund University HEREBY DISCLAIM ANY AND ALL WARRANTIES, EXPRESSED OR IMPLIED, INCLUDING THE WARRANTIES OF MERCHANTABILITY AND FITNESS FOR A PARTICULAR PURPOSE, WHETHER ARISING BY LAW, CUSTOM, OR CONDUCT, WITH RESPECT TO ANY OF THE INFORMATION CONTAINED IN THIS REPORT. In no event shall the SPONSORS, CEA or HydroResearch/Lund University be liable for incidental or consequential damages because of use or any information contained in this report.

Any reference in this report to any specific commercial product, process or service by tradename, trademark, manufacturer or otherwise does not necessarily constitute or imply its endorsement or recommendation by HydroResearch/Lund University, CEA or the SPONSORS.

Acknowledgements

This study was funded by Elforsk AB, Svenska Kraftnät, and Dam Safety Interest Group, within the CEA DSIG Geophysics Research Project (T992700-0205).

It has been a pleasure to work with our North American colleagues in the DSIG project. Their experience, advice and comments have inspired us in this project. Especially, we would like to express our gratitude to DSIG project leader P.Eng. Ken Lum, Dr. Bob Corwin and Prof. F.D.Morgan.

Furthermore we are grateful to the staff at Hällby and Sädva for invaluable assistance during installations and maintenance of the data acquisition systems.

Moreover, the electrode positioning and offshore SP surveys could not have been realised without the skills of Kjell Andersson and Peter Jonsson (Dept. of Engineering Geology, Lund University).

SUMMARY

Methods for seepage monitoring and internal erosion detection are essential for the safety of earth embankment dams. This work aims at developing improved methodology to indirectly monitor seepage flow changes using resistivity and self-potential (SP), and is a continuation and expansion of previous research (funded by Elforsk AB). The project is built around an automatic monitoring system operating at Hällby since 1996, and a similar installation at Sädva in operation since May 2001. The project is funded by Elforsk AB, Svenska Kraftnät, and Dam Safety Interest Group. In parallel Elforsk and Svenska Kraftnät are also funding a Ph.D.-project that will continue until 2005.

The seasonal temperature variation in the dam is an indicator of seepage anomalies. Resistivity is also temperature dependent, and previous research projects have shown that the seepage induced temperature variation can be detected by repeated resistivity measurements. The rationale for the first installation at Hällby was to allow long term monitoring in order to improve the accuracy and temporal resolution. Since SP is influenced by resistivity there was also an interest to see if any seasonal SP variation could be detected.

Long term monitoring requires a stable monitoring system providing reliable data. Important steps to achieve this are: proper installations, appropriate monitoring equipment, optimised monitoring strategy, efficient data handling, optimal inversion parameters, data evaluation and presentation, and finally, a relevant evaluation of the dam status. All these steps have been studied to varying degrees in this project.

Electrodes should be installed where the soil temperature and humidity vary as little as possible, preferably below the freezing depth. Stainless steel electrodes are recommended for resistivity measurements only. Non-polarisable electrodes should be used for SP measurements. To maximize the signal-to-noise ratio in the SP observations it is important to locate the electrodes where there is maximum variation in SP. This location may often not coincide with ideal locations for resistivity monitoring electrodes. The optimum location should ideally be found through modelling of the SP response for the geometry of the dam. A second important electrode placement consideration is the location of the reference electrode. It is advisable to use reference electrodes placed at such a distance from the dam that changes in SP sources in the dam has little influence on the reference.

The monitoring equipment has been further developed and improved within the project. The operational reliability has been high at the Hällby dam. At Sädva reliability has been lower, due to stability problems with the monitoring equipment. These problems have now been reduced. The monitoring accuracy, however, is excellent at Sädva, with measurement errors typically less than 1%. At Hällby, monitoring accuracy is lower with particularly poor data quality on the right dam crest.

Several electrode configurations have been tested both theoretically and in practise at the dams. Arrays used include Wenner-Schlumberger, dipole-dipole, gradient and pole-

dipole. These sets of electrode configurations assume two-dimensional conditions, i.e. no variation perpendicular to the layout direction. This is obviously not the case when measuring along an embankment dam and the simplification of the dam geometry may lead to distorted results regarding depth estimation and absolute values. Repeated three-dimensional measurements are probably not yet realistic for embankments dams due to data processing limitations. Instead two-dimensional measurement must be accepted and modelling tools have been developed to estimate the size of these effects.

Data handling must be automated so that quality checks can be done before evaluation starts. Different filtering routines have been developed. An infinite impulse response low pass filter with spike removal has been applied to the monitoring data. This routine gives higher quality of the input data for the inverse numerical modelling (inversion) than the previously used approach, which was based on median filtering. Some initial examinations can be made from raw-data or filtered data, but inverted data is essential for full interpretation. Inversion has been carried out on filtered data using a variety of inversion parameters. The L_1-norm optimisation method in combination with time lapse inversion using a stronger filtered sliding damped reference data set have been preferred in the presentations.

Examples of data evaluation and presentation of data are given in the report. Sections of mean resistivity and variation have been found useful to give an overall picture of the investigated embankment. Detailed information in time series diagrams of the variation in individual model cells is also useful in order to compare the seasonal variation in the embankment dam with the variation in the reservoir.

The long-term measurements show that seasonal variation of both resistivity and SP is significant both at the Hällby and Sädva dams. The seasonal resistivity variation in the dam can be explained by seasonal change of water temperature and conductivity that depend on the seepage flow rate.

The seasonal variation of SP at Hällby cannot be explained by reservoir water level variations since the water level variation is less than 0.8 m. The seasonal variation is larger than the spatial variation of SP. The seasonal SP variation is most probably caused by resistivity variations. This implies that:

- One-time resistivity and SP measurements may be affected by seasonal variation that is larger than the spatial variation, i.e. interpretation from one survey may be misleading, and;
- SP measurements should be performed in combination with resistivity unless it can be shown that the resistivity variation can be neglected.

An increase of resistivity has been found in a specific region at Hällby left dam. However, this change cannot yet be fully explained due to lack of knowledge about material properties and behaviour at internal erosion. Near future monitoring results from this region will be followed with high interest. Laboratory tests that are to be performed at University of British Columbia will hopefully lead to a better understanding of this situation.

TABLE OF CONTENTS

APPENDICES

1 INTRODUCTION

Methods for seepage monitoring and internal erosion detection are essential for the safety of earth embankment dams. Several methods have been developed within other areas that can be used also on dams. There is however a need to improve their performance, and to adopt them to the special conditions that exist at embankment dams.

The project aims at developing improved methodology for monitoring of earth embankment dams, with the aim to study seepage flow changes, i.e. internal erosion. The work will focus on developing automatic monitoring through resistivity and self-potential (SP) measurements. The project is built around an automatic monitoring system operating at Hällby since 1996, and a similar installation at Sädva in operation since May 2001. The project is funded by Elforsk AB, Svenska Kraftnät, and DSIG (Dam Safety Interest Group) within CEATI Project No. T992700-0205 "Investigation of Geophysical Methods for Assessing Seepage and Internal Erosion in Embankment Dams". The project is a continuation and expansion of the previous research (funded by Elforsk AB since 1993), in order to further develop the resistivity and SP methods to seepage monitoring and detection techniques.

In parallel Elforsk and Svenska Kraftnät, are also funding a Ph.D. project that will continue until 2005. The future work within the Ph.D.–project will have a more academic approach including further development of monitoring methods, and extended evaluation of the data. Result will be collected in Ph.D.-thesis based on several scientific journal papers.

The seasonal temperature variation in the dam is an indicator of seepage anomalies. Resistivity is also temperature dependent, and within the previous research projects it was showed that the seepage induced temperature variation could be detected by resistivity measurements. The basic motive for the first installation at Hällby was to allow long term monitoring in order to evaluate if those variations could be detected and used. Since SP is dependent of resistivity there was also an interest to see if any seasonal SP variation could be detected.

A main issue is development of measurement methodology, for the above-mentioned methods in order to improve the data quality and resolution, allowing more information to be extracted from the data. Furthermore, the methodology for analytical and statistical processing of data, as well as inverse modelling and evaluation, is being developed. The ultimate aim is fully automated inverse modelling and an automated evaluation of the results versus the "normal condition of the dam", so that the system should be able to give a warning if anomalous change is detected, as well as the position and size of the anomaly. The aim is also to increase the understanding of the basic physical principles that control the seasonal variation in resistivity and SP, since these variations form the base for evaluation of the seepage flow through the dam.

2 HÄLLBY EMBANKMENT DAM

2.1 Site Description

The embankment dam at Hällby power plant was taken into operation in 1970. It is located in the Ångermanälven River in the middle part of Sweden. The power plant and the spillway are located in the central part of the old river section. Two embankment dams (called the left dam and the right dam) connect the spillway and power house to the abutments. The dams, as well as the power plant and spillway, are founded on grouted rock. Left dam is about 28 m high and about 120 m long, while the right dam is 30 m high and about 200 m long (Figure 2-1). Water level variations are less than 0.8 m (the allowed variation is between +290.2 m and +291.0 m) that gives ideal conditions for the measurements

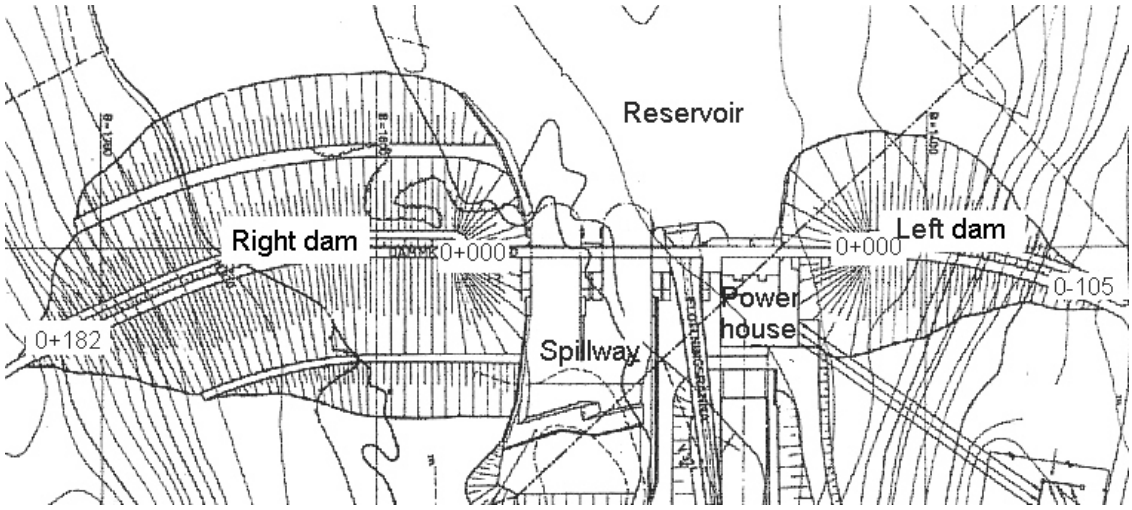

Figure 2-1: Plan over Hällby Power Plant.

Both dams have a vertical central core of moraine surrounded by filter and rockfill (Figure 2-2). There is a leakage monitoring system on the left dam. A new leakage monitoring system will be installed in 2003 also on the right dam.

There are also several piezometers installed where the dams connects to the spillway and water intake. Some are drilled from the crest, and some are drilled horizontally through the concrete walls into the dam core or into the bedrock below the dam (Figure 2-2).

A sinkhole was observed in 1986 at the connection between the left dam and the power plant. Repair was performed in 1987 by grouting about 250 m^3 of cement-bentonite and silicate. A significant volume (150 m^3) was also grouted at the connection between the right dam and the spillway. Additional grouting was also performed in the bedrock.

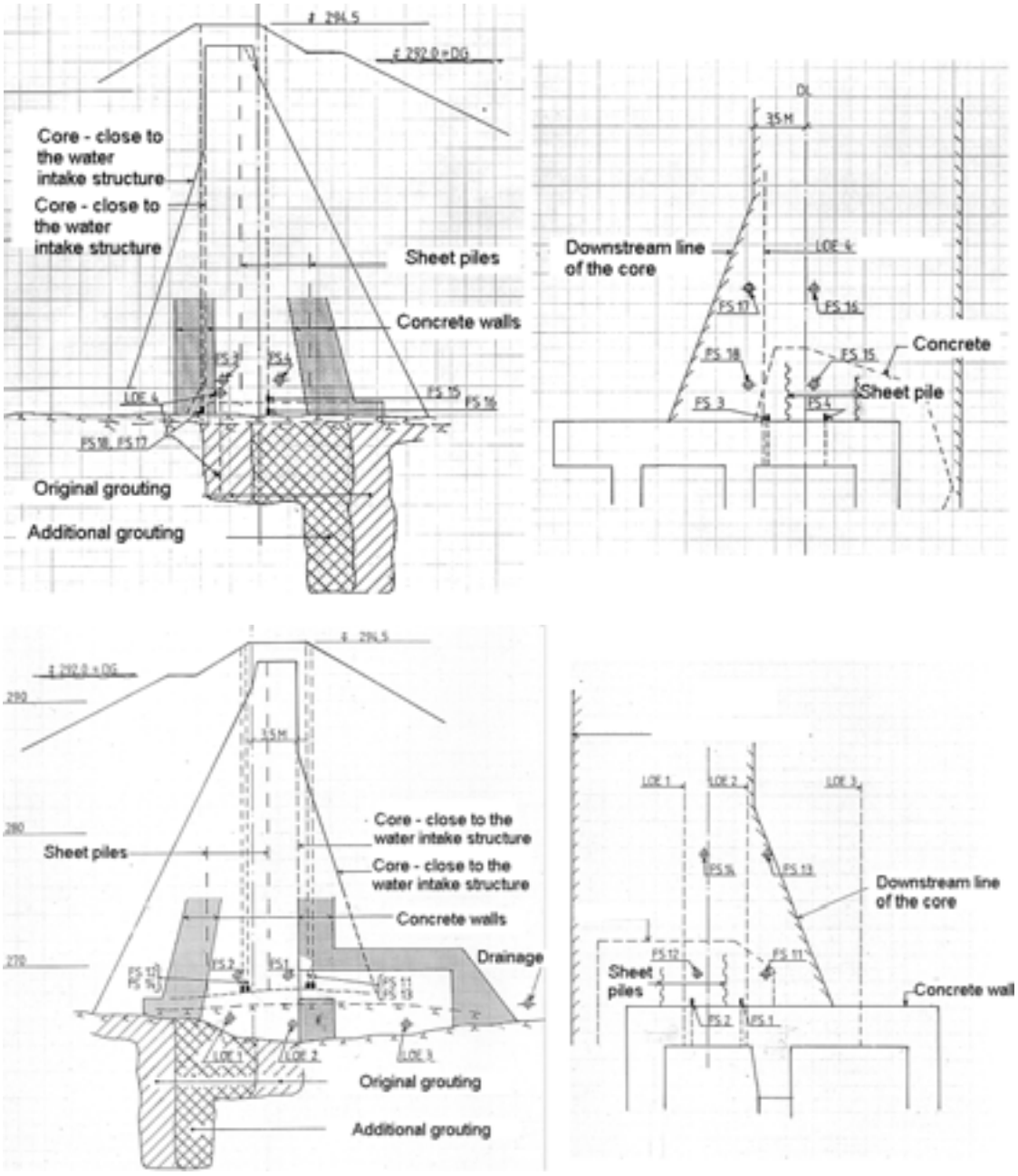

Figure 2-2: Principal cross sections at the connection to the power plant intake and the spillway showing the locations of the horizontal piezometers installed on the right dam (top) and the left dam (bottom).

2.2 Existing data acquisition system

A system for continuous resistivity monitoring was installed in the Hällby embankment dam in 1996. The installation comprises the following at the moment (Johansson et al. 2000):

- Full instrumentation for resistivity measurements. Self potential measurements can also be carried out, however with stainless steel electrodes
- Five cables with permanently installed electrodes:
  - on the reservoir bottom along the upstream side of the embankments,
  - buried along the dam crests, and
  - buried along the downstream toe (right dam only).
- Two remote electrodes (each placed around 1 kilometre from the dam but non-functional).
- Modem for remote control and data transfer.

There are in total 102 electrodes installed on the dam, of which 43 are installed on the crest and 21 on the downstream toe. Stainless steel plates were used as electrodes on land. The remaining 38 electrodes are installed in the reservoir on the dam upstream face, using underwater cables and ring electrodes in stainless steel (Table 2-1). The distance between each electrode is seven meters. This measuring layout gives a high flexibility and several types of resistivity measurements can be performed and the system is also used for monitoring of streaming potentials (SP).

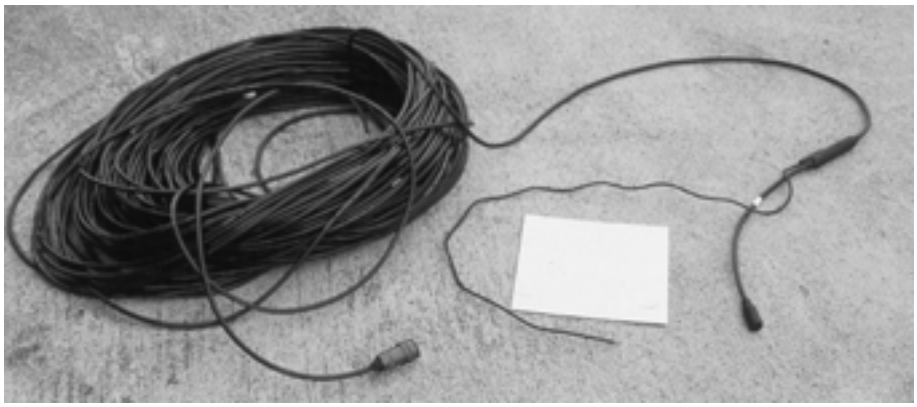

Figure 2-3: Electrode and multi-core cable used on the dam crest and the downstream toe.

Figure 2-4: Electrode mounted on multi-core cable used on the upstream side.

Some problems related to the data quality exist at Hällby due to high noise levels, especially on the right dam crest. These problems appear largely to be caused by high electrode contact resistance due to a thermal isolation layer at the dam crest. In order to improve the data quality to a level where it is meaningful to do a full evaluation of the data from the right dam crest it is necessary to re-install these electrodes.

Table 2-1: Summary of the design of the electrode cables and electrode type, where the electrode take-out separation is 7 metres along each cable throughout. The planned cable no 3 could not be utilised due to the rough terrain on the left downstream side.

No:	Location	Cable type	Electrode type	Take-outs	Active length/[m]	Blank cable/[m]	Total length/[m]
1	Left crest	Land	Steel plate	16	105	65	170
2	Right crest	Land	Steel plate	27	182	154	336
3	Left down-stream	-	-	(2)	-	-	-
4	Right down-stream	Land	Steel plate	19	126	190	316
5	Left upstream	Under water	Steel ring	14	91	115	206
6	Right upstream	Under water	Steel ring	24	161	195	356
Total				100(+2)	665	719	1384

2.3 Electrode positioning

During the installation of the upstream electrodes insufficient attention was paid to exact locations of the electrodes by the divers, and no documentation of the exact positions was made. The electrodes are placed along a cable with a seven-meter spacing, but when they were placed out there were no guarantees that the cable was fully stretched and the spacing was kept at seven meters. Also documentation of installation depth was missing. This means it has not been possible to carry out any meaningful inverse modelling of the offshore data in the past years, as it requires a good determination of the depth of water above the electrodes.

Because of these problems it was decided to perform a new positioning of the electrodes at a field campaign in September 2000. According to instructions the electrodes were to be installed in a line along the upstream toe of the dam. However, during the new positioning campaign it soon became clear that the electrodes in reality were placed not along the dam toe, but rather along a line just halfway down the upstream slope.

Raw data from the positioning were taken in WGS-84 longitude and latitude coordinates with an accuracy of +/- 1 meter under normal circumstances, and the depths were measured from the actual water table +291.60 meters above sea level (APPENDIX C, Figure 2-5, Figure 2-6).

The positioning was not carried out without complications. Windy conditions made the small boat that was available drift slightly back and forth. The visibility in the reservoir water was extremely low and obstacles such as trees, limbs and branches made conditions very unfavourable for the diver. When plotting the positions in the horizontal plane it was discovered that some electrode spacings exceeded the cable length 7 m. This could indicate that some electrodes were missed, but as the total length fits in well with the 7 m spacing it is probably explained by errors in positioning.

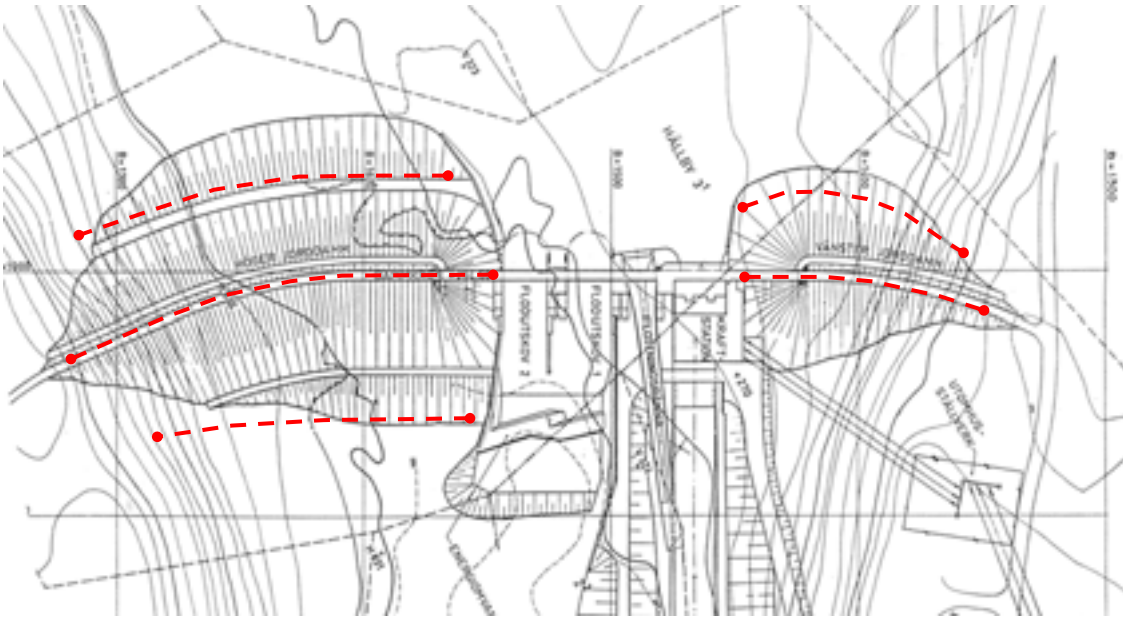

Figure 2-5: Principal location of electrode layouts at Hällby.

Moreover, at the right end of the right dam the electrode spacing was suspiciously low indicating that the same electrode had been positioned twice. According to the diver the last few electrodes at the right dam had not been correctly placed, but rather were put together in a mess. The particular uncertainties at the end of the right dam have caused some problems when it comes to processing and analysing the data. At this point, in the initial work of analysing the data from the downstream layouts, only 19 out of 24 electrodes at the right dam have been used.

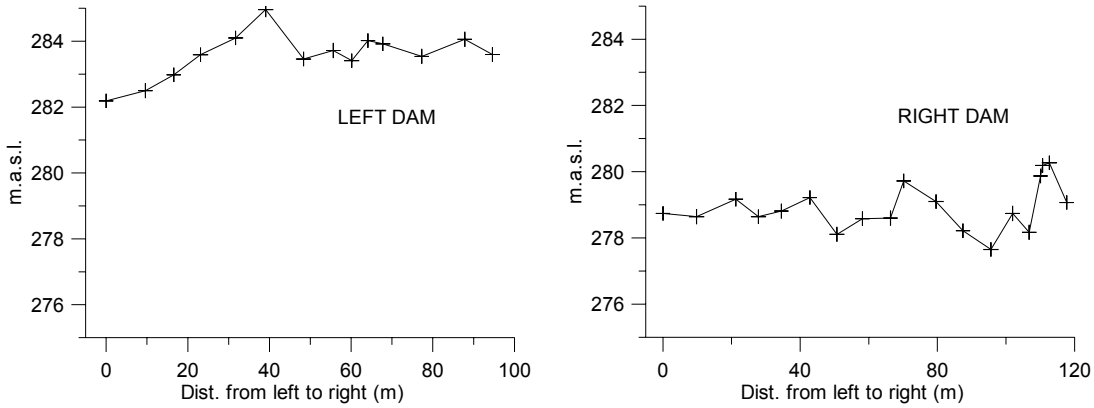

Figure 2-6: Altitude locations of the upstream electrodes at Hällby. Left dam and right dam. Distances are given from left to right seen from upstream, starting with zero for the first electrode.

2.4 Connection of LOE-pipes

In the project application it was planned to replace the faulty remote electrode cables at Hällby. However, it has been decided to reallocate the funds for this to connecting the so called LOE-pipes at Hällby, metal pipes installed in the connection with the concrete structure in the lower parts and below the core, to the data acquisition system.

The LOE-pipes were installed at the connection between the concrete structure of the dam and the embankments on both sides when the dam was built. They are used for manual measure of the piezometric head at various locations inside the embankment and a few of them are still in use. The locations of the LOE-pipes were shown above in Figure 2-2.

Electrodes placed at large depths are of great interest for the resistivity monitoring as it has the potential of significantly raising the resolution in the lower parts of the core. Some preparatory theoretical work will be needed to make full use of the pipes for monitoring, however, because of the complicated geometry of the measurement array with the LOE-pipes acting as line electrodes.

At Hällby electrode lines are placed on the upstream slope (originally a placement along the upstream toe were intended, but at the positioning of the electrodes it was discovered that they are placed closer to the midpoint of the upstream slope), buried on the dam crests and along the right downstream toe. So far these electrode layouts have been used for measurements along each layout with normal measurement arrays. It is also possible, however, to measure across the dam in different ways using electrodes from more than one of the layouts at the same time, but the resulting data from such an operation is more difficult to handle, as regards inversion and interpretation. As the main interest is to be able to find changes in the central part of the dam, i.e. the lower part of the core, the option of using the LOE pipes is highly interesting.

3 SÄDVA EMBANKMENT DAM

3.1 Site Description

The Sädva dam is located in the upper part of the Skellefteälven River just south of the Arctic Circle. The reservoir has a storage volume of 600 million m^3. The dam and power plant was put into operation in 1985.

The dam is a rock fill embankment dam with a total length of 620 m, divided in 210 m long main dam across the old river channel, and a 410 m long dyke, see Figure 3-1. This dam replaced an older dam, which can be seen at low water levels. The intake to the power station is on the right side of the dam about 50m from the right abutment. There is also an intake tower to the bottom outlet (sec 070) and a bottom intake to a mini hydro power plant (sec 140). The core is made of moraine and is slightly inclined as shown in Figure 3-2. The maximum height is 32 m. The main dam is entirely founded on grouted rock as is the dyke until sec 280. The remaining part of the dyke is founded on soil (moraine with clay).

The upper and lower retention levels are 477.00 m and 460.70 m respectively. The whole interval is fully made use of as can be seen in Figure 3-3 where the reservoir levels since 1999 is shown.

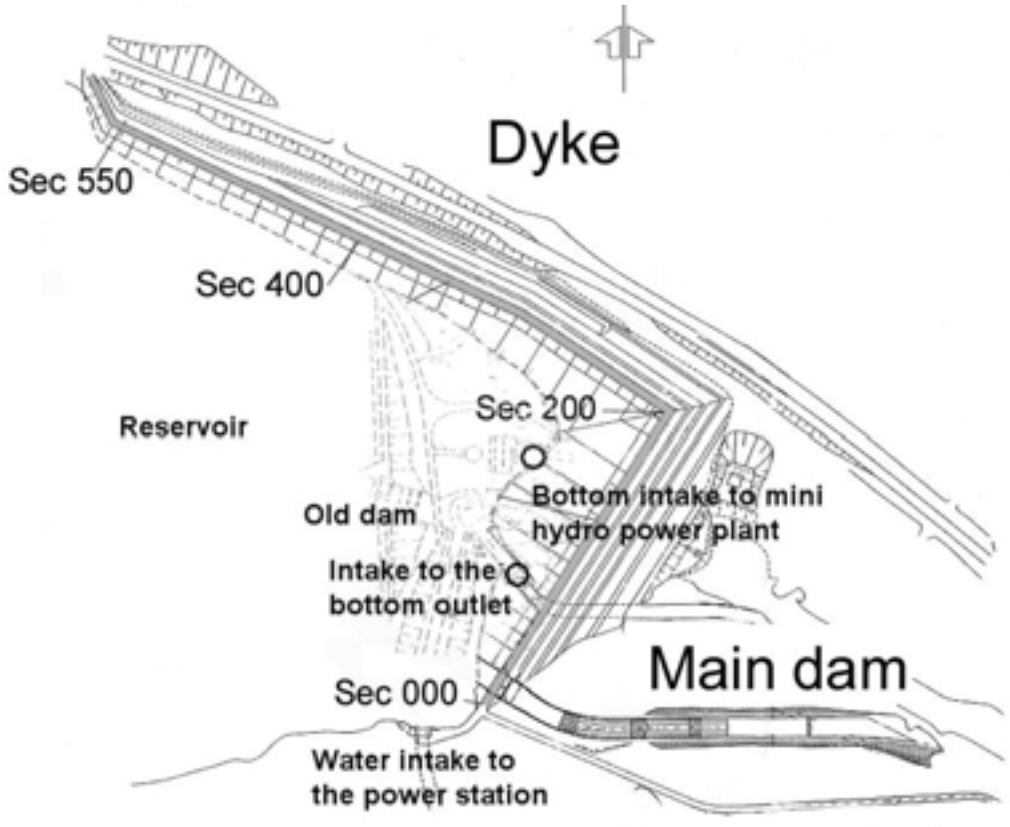

Figure 3-1: Plan over Sädva dam..

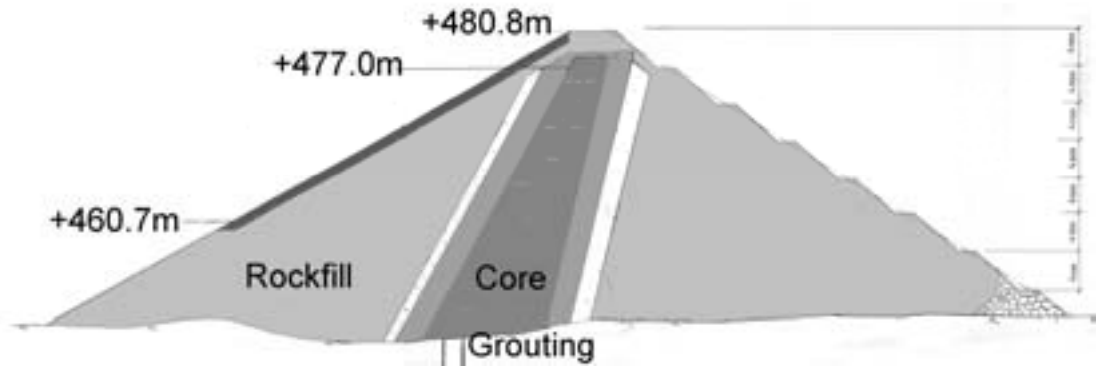

Figure 3-2: Cross-section of the Sädva embankment dam.

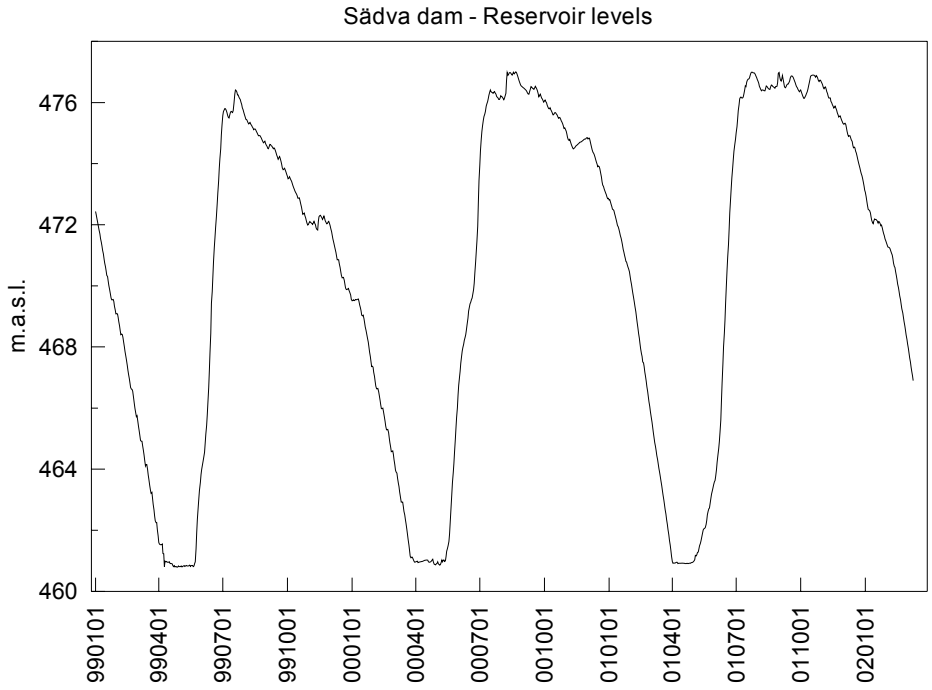

Figure 3-3: Reservoir levels at Sädva Dam.

3.2 Data acquisition system installation

A data acquisition system for automatic measurements of resistivity and SP data was installed at Sädva in May 2001. It was designed to make daily measurements on the electrodes installed in the upper part of the dam crest of the main dam and dyke, as well as measuring resistivity and temperature in the reservoir water via two probes.

The dam core electrodes were installed when the core crest was raised in the summer 1999. Similar construction work will be made in several Swedish dams as a consequence of the new Guidelines of Design floods. It is therefore of great value to

examine different ways of installation of new monitoring equipment, which easily can be made when the core is open. Experiences from this installation may therefore be valuable for future installations.

3.3 Electrodes

A correct electrode type and a proper installation are fundamental for all electric measurements. Based on the experience from Hällby dam it was decided to use the same type of electrodes for the resistivity measurements. However, it was decided also to install special electrodes for the SP-measurements on the main dam. This would allow comparisons between the different electrode types.

The resistivity electrodes consist of 0.25 m x 0.25 m stainless steel plates (Figure 3-4). The electrodes are connected to a polyurethane (PUR) covered stainless steel wire by bending and hammering one corner of the steel plate over the stripped wire end. These wires are joined to cables splits (pig-tail splits) on a PUR covered multi core cable. The multi core cables have 32 or 64 pig-tail splits each. The SP electrodes are so called non-polarisable copper-copper sulphate electrodes, Farwest Corrosion Control Company model SP-150 (Figure 3-5). These electrodes were delivered pre-packaged in a cloth bag filled with a bentonite mix designed to give a good coupling to the surrounding natural soil. The SP electrodes are joined to a multi core cable in the same way as the steel plate electrodes.

Figure 3-4: Installation of resistivity monitoring electrodes and cables.

A spacing of 6 m between the electrodes was chosen for the entire dam. The total number of electrodes is 128. Special SP-electrodes were also installed in the main dam, with a spacing of 6 m but shifted 3 m relative to the steel plate electrodes. Thus, there are electrodes at 3 m intervals on the main dam. The location of the electrodes is shown in Figure 3-6.

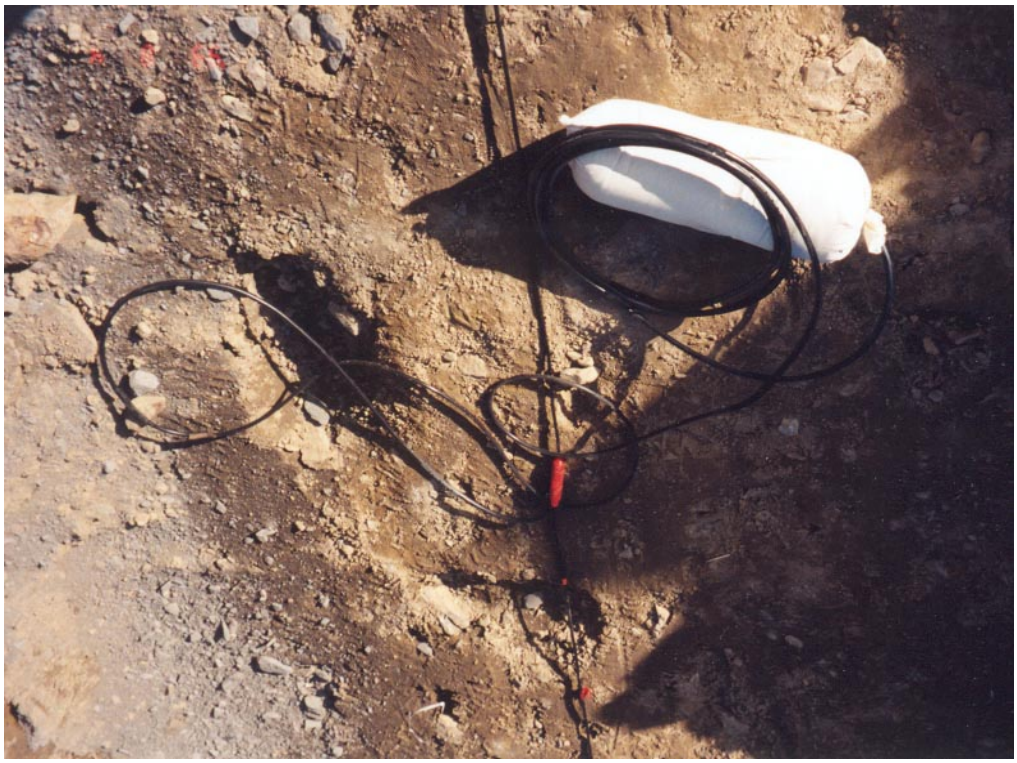

Figure 3-5: SP-electrode to be buried on the crest of the dam core.

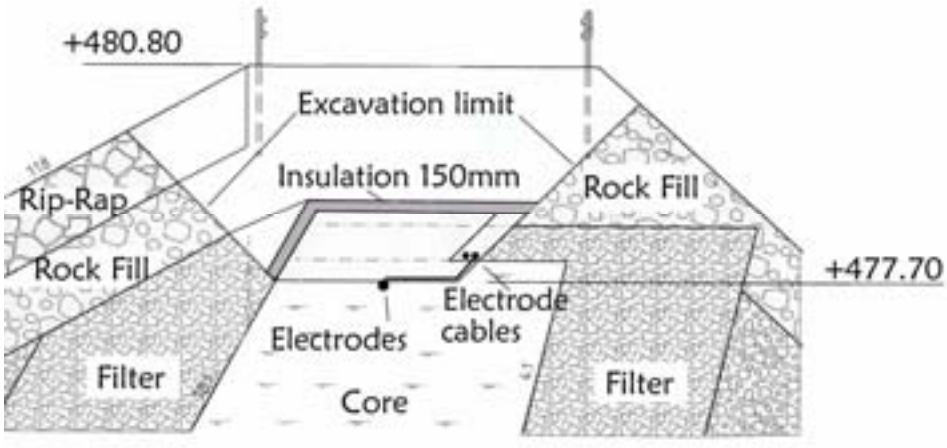

Figure 3-6: Cross-section of the dam crest showing the location of the installed electrodes.

3.4 Instrumentation

3.4.1 System Overview

The data acquisition system is a modified version of the ABEM Lund Imaging System. Figure 3-7 shows the system configuration in a schematic way.

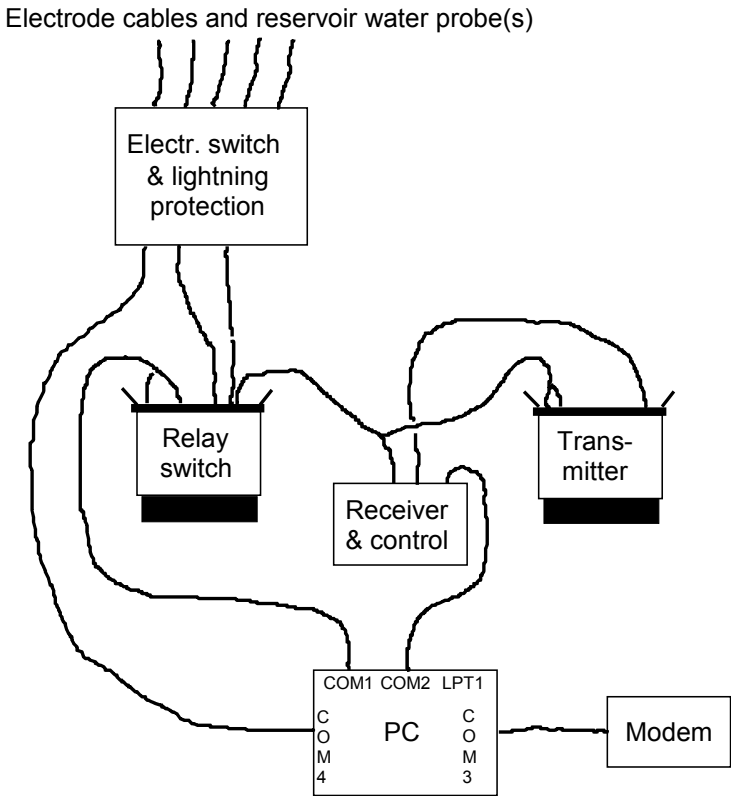

Figure 3-7: Sketch of system configuration.

The different components of the system can be seen in Figure 3-8, and are mounted in the following order from top to bottom:

- computer with modem,
- keyboard and mouse in drawer,
- receiver/control unit Terraohm RIP224,
- current transmitter ABEM Booster SAS2000,
- relay matrix switch Electrode Selector ES464,
- combined three-way relay switch and lightning protection,
- power supply adapters etc..

Figure 3-8: Photographs of data acquisition system mounted in 19" rack cabinet: Left: in operation with side panel removed, Right: rear view with electrode cables etc. connected.

3.4.2 Computer and software

The computer is a standard PC-type computer equipped with four serial ports configured as documented in APPENDIX A. The operating system is MS-DOS 6.22, and remote control is enabled via Symantec pcAnywhere 5.0 for DOS (initialised in AUTOEXEC.BAT by the line aw /o:h /m:a). The computer is re-booted every day, via a simple timer that switches off and on the power supply at midnight. The re-boot results in a call of Make_bat.exe that creates the batch file SAEDVA.BAT based on the script in SAEDVA.SCR. The filenames of the data files that are being created consists of a two-letter prefix for each protocol plus the date of the day. Rebooting every day and calling measurements from the computers start-up routine has the advantage of minimising the loss of data to one day if the system hangs.

3.4.3 Resistivity and SP measurement instrument

A data acquisition system for multi-electrode resistivity surveying developed at Lund University is used to acquire the resistivity and SP data (Dahlin 1993; Dahlin 1996). The data acquisition system is a modification of the ABEM Lund Imaging System.

The electrodes to be used in a specific measurement are connected via an ABEM Electrode Selector ES464 relay-switching unit. This relay matrix switch can multiplex 64 electrodes to four functions (C1, C2, P1, P2).

Current is transmitted by an ABEM Booster SAS2000 current transmitter, capable of transmitting a maximum of ±400 V (800 V peak-to-peak) or 500 mA with a power 40 W. The transmitter is controlled over the parallel port of the computer via an adapter.

A Lawson Labs AD201 controlled via a serial port was originally used to measure the voltages for resistivity as well as SP. It was in August 2002 replaced by a Terraohm RIP224 receiver/control unit that also took over the control of the current transmitter. The instrument is based on a 24-bit sigma-delta A/D-converter and has an input impedance of 10 GΩ.

The data acquisition process is completely controlled by the software ERIC, where the software scans through the measurement protocols selected by the user. The configurations so far have been Wenner, Schlumberger, dipole-dipole, pole-dipole and gradient array. Reciprocal measurements have been carried out in order to assess the measurement errors.

3.4.4 Combined relay switch and lightning protection

A combined relay switch and lightning protection has been tailor built for the installation at Sädva. The switching function is used to connect either the main dam electrodes, dyke electrodes or the two reservoir water probes to the ES464 relay matrix switch. It is also possible to select a combination of electrodes from the main dam and the dyke, e.g. to use all main dam electrodes except the last one and instead have access to the farthest dyke electrode as a "remote" electrode. The electrode cables and reservoir probes are physically and logically connected as listed in Table A-4.

Figure 3-9: Photograph of combined relay switch and lightning protection unit. A connector for the second reservoir water probe has been added after the photo was taken, as well as labels and caps for the open holes.

3.5 Probe for Measuring Resistivity and Temperature in the Reservoir Water

A submersible probe for monitoring the reservoir water resistivity and temperature was developed, and two units have been connected to the data acquisition system (Figure 3-10 and Figure 3-11). One probe is mounted immediately after the turbine in the mini power plant that is active 10 months a year, being closed during the spring flood in May-July. The other probe is mounted on the concrete structure at the old spillway, where water circulation is expected to be good during the period when the mini power plant is closed. In order to use the probes the relays of card number 5 the three way switch must be set, and the connection in relation to internal addresses in the relay switching unit ES464 will then be as documented in APPENDIX A.

Figure 3-10: Photograph of reservoir water resistivity and temperature probe. The electrodes are visible on the bottom of the probe, while a temperature sensor is placed inside the cylinder, which also houses a lead weight and is filled with polyurethane mould.

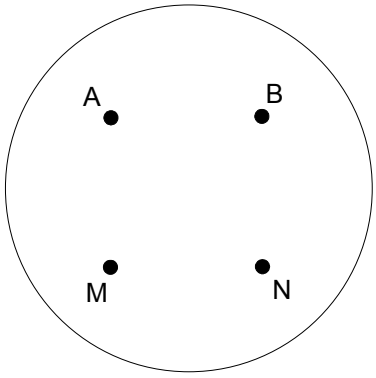

Figure 3-11: Sketch of electrode configuration on reservoir water resistivity probe viewed from below (diameter 50mm, electrode separation 20mm).

The geometrical factor for square array:

$$K = \frac{2\pi a}{2 - \sqrt{2}}$$

and an electrode separation of a = 20 mm gives the following formula for calculation of resistivity:

$$\rho_a = 0.2145 * \frac{U}{I}$$

However, this formula is valid if the probe is held at the water interface, and if submerged completely as it is at Sädva it modifies to approximately:

$$\rho_a = 0.236 * \frac{U}{I}$$

according to tank measurements in the laboratory.

Calibration in a controlled temperature fluid tank gave the following formulas for calculation of temperature for the two temperature sensors, see also APPENDIX B.

$T = 0.1004\,U - 275.65$ Probe 2 (in upstream reservoir)

$T = 0.0995\,U - 272.63$ Probe 1 (mounted in mini power plant)

where:

U = Voltage (mV)
T = Temperature (°C)

4 RESISTIVITY SURVEY AT SÄDVA

4.1 Survey description

A field campaign was conducted at Sädva in May/June 2001. The main objective was to measure SP in the surroundings of the dam site and thereby add further information on the geo-electrical context of the area to former measurements. SP measurements with a high reservoir level had already taken place in fall 2000 and at this time reservoir levels were low. The SP measurements are presented in another chapter in this report.

Low reservoir levels also made it possible to access some of the areas upstream the dam, which are normally below the water level. The opportunity was taken to perform some resistivity measurements as well. The ground conditions in the area lead to some problems with electrode contact and thus made it difficult to measure resistivity without a lot of preparing work. However, two profiles were possible to carry through, one on each side of the dyke (Figure 4-1). Wenner CVES measurements with five meters electrode spacing were carried out, using a mobile version of the data acquisition system installed at the site.

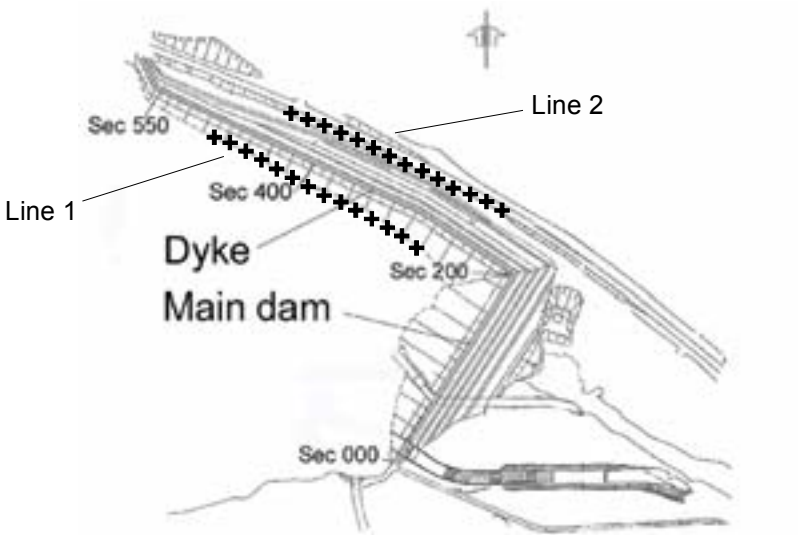

Figure 4-1: Location of the profiles marked with crosses on every third electrode location. Line 1 upstream the dyke and Line 2 downstream the dyke.

Figure 4-2 shows the downstream and upstream sides of the dyke, where the lines were located. The photos were taken in May 2001 with a reservoir at its lowest level. In the background the main dam can be seen and in front of that the old dam is indistinctly observable. The old dam, located 100-200 metres upstream the new location, is no longer in use and can only be seen when the reservoir level is low.

Figure 4-2: The downstream (left) and upstream (right) side of the dyke at low reservoir levels seen from the northwest end.

4.2 Data processing

The data sets were inverted using both the L_1-norm and the L_2-norm (see section 5.4 for description of these methods). Locations of the profiles were adjusted to the length coordinates used for the permanently installed electrodes on the main dam and the dyke. The resistivity ranges and the colour scale of the inverted models are chosen to be the same as for the inverted models from the permanently installed electrodes (section 7.4) to make comparisons easier.

4.3 Results and interpretation

The inverted sections are shown in Figure 4-3 and Figure 4-4. In the upstream profile the old dam is crossed at approximately section 360, which can be seen from the topography. The rock level at the location of the dyke, which is located within a few tenths of meters parallel to both profiles, varies around 463-467 meter above sea level. This indicates thin soil layers with approximately just a few metres depth along the lines. On the upstream profile there are shallow high resistivity regions on both sides of the old dam. Around section 420-440 metres there is a shallow low resistivity zone. The bedrock seems reasonably homogenous except for a quite extensive region beneath the old dam. It is hard to say whether this has something to do with possible actions taken when the old dam was constructed, such as grout curtains for instance which could influence bedrock resistivity. Before involving the old dam structure in any interpretation construction documents from when the old dam was built need to be checked.

The downstream profile has a large central zone of somewhat higher resistivity in the bedrock at depths around +465 metres and beneath. This zone is located with its centre at section 340 metres. Another zone with higher resistivity is found at the end of the profile around section 400. A quite large zone at medium and shallow depths extended from the leftmost part of the profile to the central high resistivity part exhibits remarkably low resistivity values. At shallow depths there is a distinct region with higher resistivity at section 350-390 metres.

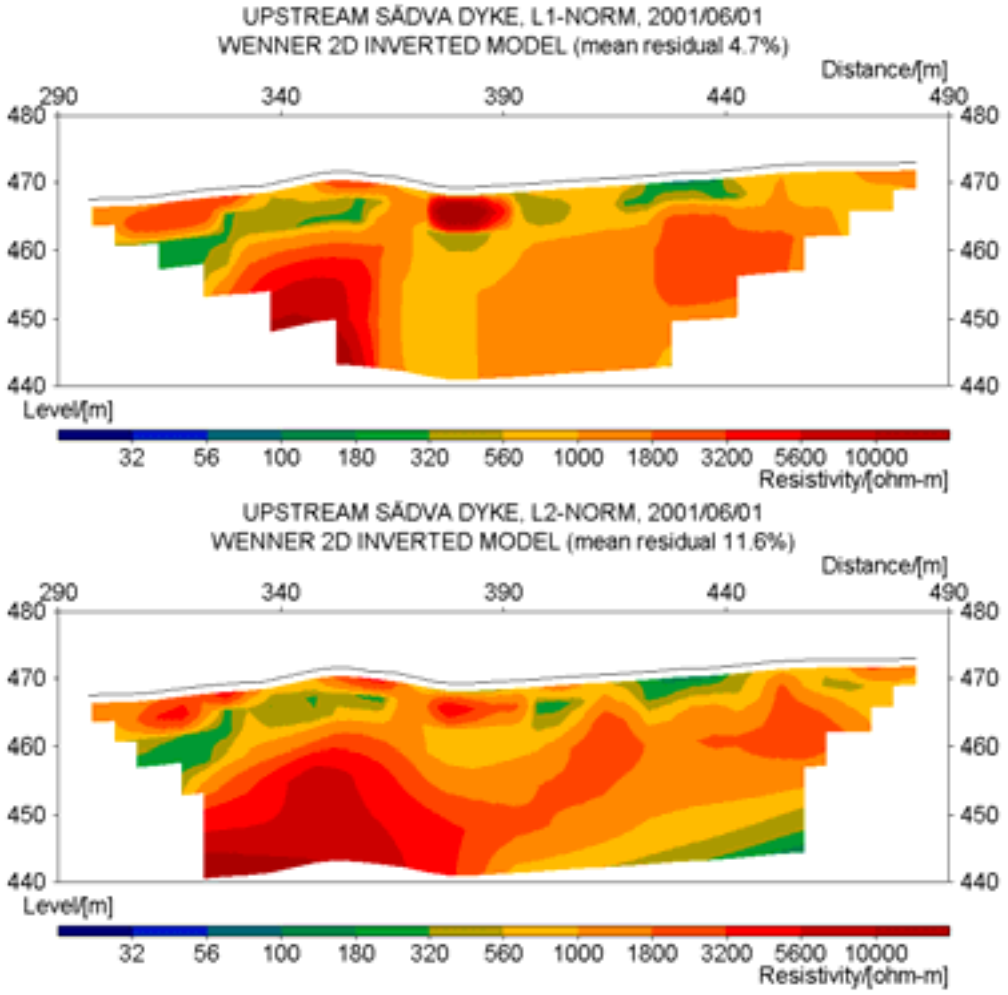

Figure 4-3: Line 1 upstream the dyke. L1 inversion (top) and L2 inversion (bottom). Seen from downstream. Distances indicate approximate position in relation to reference line along dam crest.

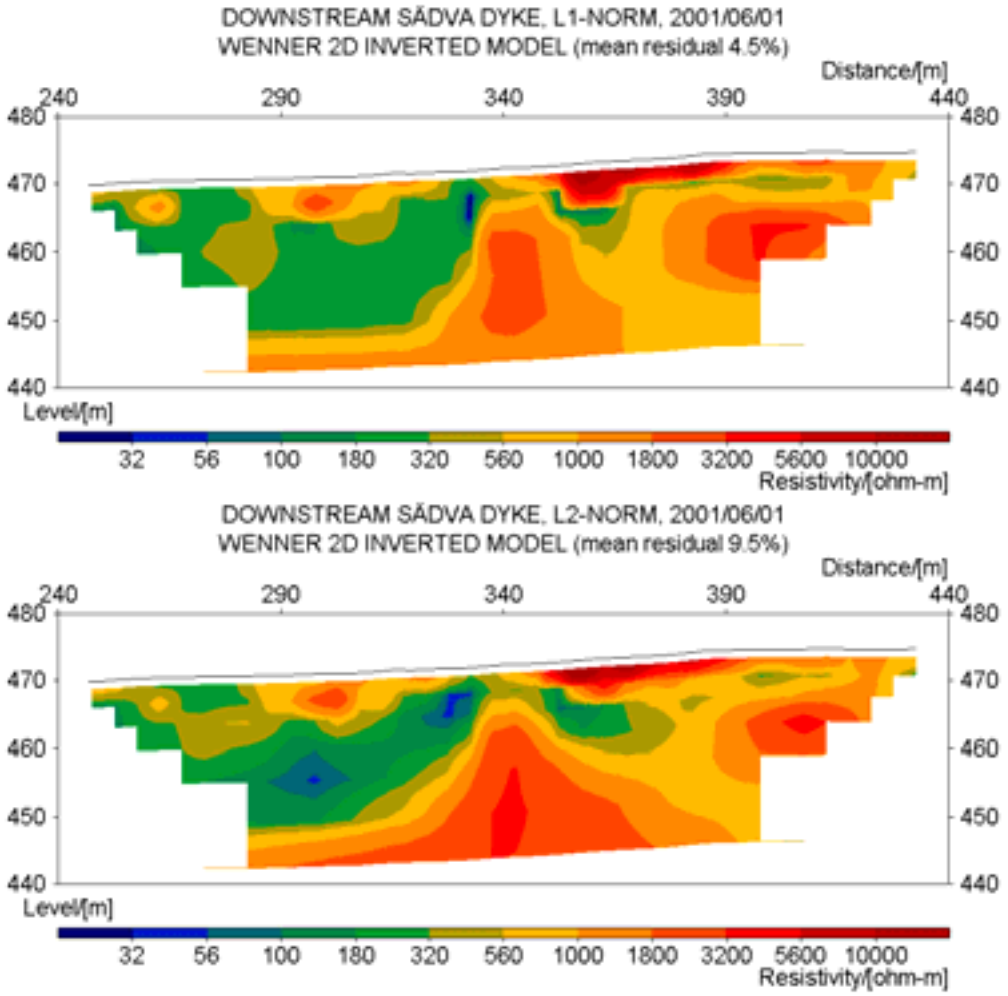

Figure 4-4: Line 2 downstream the dyke. L1 inversion (top) and L2 inversion (bottom). Seen from downstream. Distances indicate approximate position in relation to reference line along dam crest.

5 METHODOLOGY FOR TIME-LAPSE INVERSION AND ANALYSIS OF MONITORING DATA

5.1 Introduction

The inverted resistivities exhibit seasonal variation due to freezing of the ground, variation in water content and water level in the reservoir. However, a significant part of the variation is due to seepage of water with varying temperature and TDS.

The aim is to develop robust analytical and/or statistical methods for controlling and improving the data quality, and a methodology for automatic inverse modelling and evaluation of the resistivity data. The ultimate aim is fully automated inverse modelling and an automated evaluation of the results versus the "normal condition of the dam", so that the system should be able to give a warning if anomalous change is detected, as well as the position and size of the anomaly.

The methodology for the time-lapse inversion analysis of the monitoring data has been under revision. Significant work has been invested in conversion and upgrading of test software routines to pave the way for systematic tests and evaluation of different options for data processing and analysis.

There are, however, complications with the automation that have to be overcome. At Hällby the measurement errors are in some cases so large that it complicates the evaluation of seepage through the dam (especially for automatic evaluation). This applies in particular to the right dam crest. In the cases where data quality is satisfactory automatic evaluation has resulted in reasonable results. However, the data quality at Hällby is not in general of a quality that warrants reliable results from automatic evaluation. In order to achieve a fully automatic system de-spiking and low-pass filtering methods have been implemented in the data processing routines to filter the data before an inverse modelling is carried out. Since data is available from more than 6 years there is a good material to use as a base for the development of such methods.

5.2 Overview of data handling process

The measured data is processed by means of a time base filtering, where different approaches have been tested. Prototype software has been developed that automatically goes through the following procedure:

- Extract the desired data sets from the Zip-archives for a specified period (for example a year or the whole monitoring period).
- Carry out a time base median filtering over a specified number of days (e.g. 7), or apply combined predictive filtering and de-spiking technique.
- Calculate a data file consisting of the all time median as the time base median of the whole period (for example a year), or calculate sliding damped reference data sets.

- Convert all the time base filtered raw data files to the format used by the inversion software (see below). The all time median, or sliding damped, data sections can be incorporated into each of the data file to allow time-lapse inversion.
- Create a batch control file for the inversion software Res2dinv and run the inversion in batch mode.
- Extract the desired information from the inverted output files and save it in a format suitable for the continued processing and presentation.
- Scan through the inverted models and calculate statistical parameters for the whole period, such as annual median and mean resistivity sections, a section showing the variation coefficient, and sections showing the maximum and minimum interpreted resistivities of the period. A threshold for the mean model residual can be applied to filter away inverted model sections of too poor quality, which applies mainly to data recorded during the winter when the electrode contact resistances are highest and initially when the system was tuned in. The statistical evaluation can be repeated with different settings without necessarily re-doing the inversion

5.3 Raw data de-spiking and filtration

The measured data is processed by means of a time base filtering, where in particular median filtering (7-day or 15-day based) and an infinite impulse response (IIR) filtering (predictive filtering) has been tested. The median filtering simply means taking the median value of all daily measurements for a certain data point from e.g. a week. A low-pass filtering method using the IIR routine has been implemented as well, based on the following formula:

$$NewValue = \frac{(OldValue + factor \cdot NewData)}{(1 + factor)}$$

where *factor* may be for example 20%. In addition, a maximum threshold for the impact of a *NewData* (e.g. 40% of the present filtered value) acts as a de-spiking filter. In order not to shift the filtered data series towards higher dates the filter is run forwards and backwards, and the average taken as the filtered data.

The success of this approach is dependent on good start values at each end of the time series, if a heavily distorted start value is used it will shift a large portion of the filtered series. To avoid this, an approach that can be described as a median-mean is adopted to find suitable start values, in which the initial data points (from e.g. a couple of weeks) are sorted and a mean is taken after excluding a number of data points in each end of the sorted table. However, if a longer break in the data series should occur particular care needs to be taken to assure a good filter function.

5.4 Inversion methods

The true resistivity structure is interpreted using the commercially available software Res2dinv (Loke 2003), which does 2D smoothness constrained inverse modelling (inversion). In the inversion 2D structures are assumed, i.e. the ground properties are

assumed constant perpendicular to the line of the profile, while the current electrodes are modelled as 3D sources. A finite difference or finite element model of the resistivity distribution in the ground is generated, which is adjusted iteratively to fit the data so that the differences between the model response and the measured data (the model residuals) are minimised. This can be done either minimising the absolute values of the differences (inversion with L_1-norm or robust inversion), or minimising the squares of the differences (inversion with L_2-norm or smoothness-constrained least-squares inversion).

The smoothness-constrained (L_2-norm) method is one commonly used version of regularised least-squares optimisation. This method minimises the sum of squares of the spatial changes in the model resistivity and the data misfit. It gives good results where the subsurface geology exhibits a smooth variation, such as a gradual change in fine material content in a soil or a gradual change in chemical composition. However, in cases when a sharp transition in the subsurface resistivity is expected, e.g. the contact between a fine-grained dam core and fresh igneous rock of the foundation, this method tends to smear out the boundaries and create overshooting and undershooting on each side of the boundary. An alternative method is the L_1-norm optimisation method that tends to produce models with regions that are more blocky, i.e. piecewise constant and separated by sharp boundaries. This might be more consistent with the known geology in some situations (Loke et al. 2001). An outline of the mathematical formulations used by the L_2-norm and L_1-norm optimisation methods is given below.

The smoothness-constrained least-squares optimisation method is based on the following equation:

$$(\mathbf{J}_i^T\mathbf{J}_i+\lambda_i\mathbf{W}^T\mathbf{W})\boldsymbol{\delta}\mathbf{m}_i=\mathbf{J}_i^T\boldsymbol{\delta}\mathbf{d}_i-\lambda_i\mathbf{W}^T\mathbf{W}\mathbf{m}_{i-1}, \qquad (1)$$

where i is the iteration number, $\mathbf{J}_i$ is the Jacobian matrix of partial derivatives, $\boldsymbol{\delta}\mathbf{d}_i$ is the discrepancy vector which contains the differences between the logarithms of the measured and calculated apparent resistivity values, λ_i is the damping factor, $\boldsymbol{\delta}\mathbf{m}_i$ is the perturbation vector to the model parameters for the ith iteration, and $\mathbf{m}_{i-1}$ is the model parameters vector for the previous iteration. The model parameters are the logarithms of the resistivity value of the cells in the model. $\mathbf{W}$ is the roughness filter that constrains the roughness of the model parameters, and can be adjusted on basis of available information to emphasise the nature of the spatial changes in the model resistivity values.

Since the standard least-squares method uses the square of the data misfit, it tends to give greater importance to data points with larger misfits. This makes it particularly sensitive to bad data points. A more robust method is to minimise the sum of the absolute values of the data misfit, or an L_1-norm measure of the data misfit. One method to implement an L_1-norm based optimisation method using the standard least-squares formulation is the iteratively reweighted least-squares method. The optimisation equation in (1) is modified to

$$\left(\mathbf{J}_i^T\mathbf{R}_d\mathbf{J}_i + \lambda_i\mathbf{W}^T\mathbf{R}_m\mathbf{W}\right)\Delta\mathbf{r}_i = \mathbf{J}_i^T\mathbf{R}_d\mathbf{g}_i - \lambda_i\mathbf{W}^T\mathbf{R}_m\mathbf{W}\mathbf{r}_{i-1}, \quad (2)$$

where $\mathbf{R}_d$ and $\mathbf{R}_m$ are weighting matrices introduced so that different elements of the data misfit and model roughness vectors are given approximately equal weights in the inversion process. When the L_1-norm is applied to the model roughness filter, the inversion method tends to produce models consisting of areas with piecewise constant resistivity values (Loke et al. 2001).

For the monitoring data from Hällby and Sädva the inversion was carried out using the L_2 (smooth) inversion method as well as the L_1 (blocky) norm inversion method. Nevertheless, eventually a higher preference has been given to the L_1 norm due to its better robustness against noise (see chapter 8 and 9).

5.5 Time-lapse inversion

Time lapse inversion means that two data sets from different points of time are inverted together, where the first recorded data set would normally be regarded as a reference. In time-lapse inversion, a smoothness constrain is applied not only on the spatial variation but also on the temporal variation between the data sets. This approach has been shown to focus the difference between the data sets on the actual change in the model and suppress artefacts due to the resistivity structure (Loke 1999; Loke 2001).

The model obtained from the inversion of the initial data set is used as a reference model to constrain the inversion of the later time-lapse data sets. The smoothness-constrained inversion method in equation (1) is modified to:

$$(\mathbf{J}_i^T\mathbf{J}_i + \lambda_i\mathbf{W}^T\mathbf{W})\delta\mathbf{m}_i^k = \mathbf{J}_i^T\delta\mathbf{d}_i - \lambda_i\mathbf{W}^T\mathbf{W}\mathbf{m}_{i-1}^k - \beta_i\mathbf{V}^T\mathbf{V}\left(\mathbf{m}_{i-1}^k - \mathbf{m}_{i-1}^0\right), \quad (3)$$

where $\mathbf{m}_{i-1}^0$ and $\mathbf{m}_{i-1}^k$ are the model parameter vectors for the initial data set and the *k*th time data set. The additional term, $\beta_i\mathbf{V}^T\mathbf{V}\left(\mathbf{m}_{i-1}^k - \mathbf{m}_{i-1}^0\right)$, on the right-hand side of the above equation constrains the change in the model for the *k*th time data set such that the difference between the model resistivity values for this data set and the initial time data set model (which serves as a reference model) is also minimised. β is the weight given to this cross-model constrain and $\mathbf{V}$ is the cross-model weighting matrix that determines the characteristic that we wish to introduce in the differences in the model resistivity values.

In dams, the resistivity can be expected to vary in a cyclic manner over the year, and hence some average of the variation over the year might be used as a reference data set. In the initial work carried out on the data presented here, the median over the selected period (one or more years) was used as reference data set, against which all the 7-day or 15-day median data sets were constrained in the inversion. With the implementation of combined filtering and de-spiking an approach using a sliding damped reference data set has also been tested. Whenever used the sliding damped reference data set has been

filtered using the same filter but with parameters adjusted to make the filter function stronger.

5.6 Discussion

The approach of using a yearly mean as reference data set in the time-lapse inversion must be expected to give a rather large damping effect on the extreme situations, so it may be reasonable to use a small time damping factor. Inversion with the time based smoothness constrain linked to the preceding data can be expected to allow more subtle variations in the resistivity to come out.

The inversion routines employed do not account for the true three-dimensional (3D) structure of the modelled dams, but assume that the properties of the dam are constant in the direction perpendicular to the extension of the profile. This is a poor approximation of reality considering the cross section of the dams, and it is important to be aware that the 3D effects can be expected to distort the inverted sections. Still, it can be a useful approach since the higher conductivity of the dam core compared to the surrounding filters and fill is expected to create a focussing of the sensitivity of the measurements to the dam core, which is of primary interest, see Chapter 10 for modelling results on this issue.

6 RESISTIVITY MONITORING AT HÄLLBY

6.1 General

Monitoring at Hällby has been carried out on a daily basis throughout the reporting period, however during the winter 1999-2000 there was an extended period without resistivity data due to a failure of the polarity switching relay in the current transmitter. In addition, problems with the telephone line communication and troubles of identifying these problems led to a further loss of data for the main part of the winter 2002-2003. The monitoring includes SP-data, however only with steel electrodes. Evaluation of all results measured until late March 2003 has been carried out.

6.2 Reservoir water

Temperature and resistivity in the reservoir are measured automatically on a daily basis since February 1997. The typical appearance of the temperature variation over time resembles a sinusoidal variation with a one-year period but with the lower bend cut off (Figure 6-1).

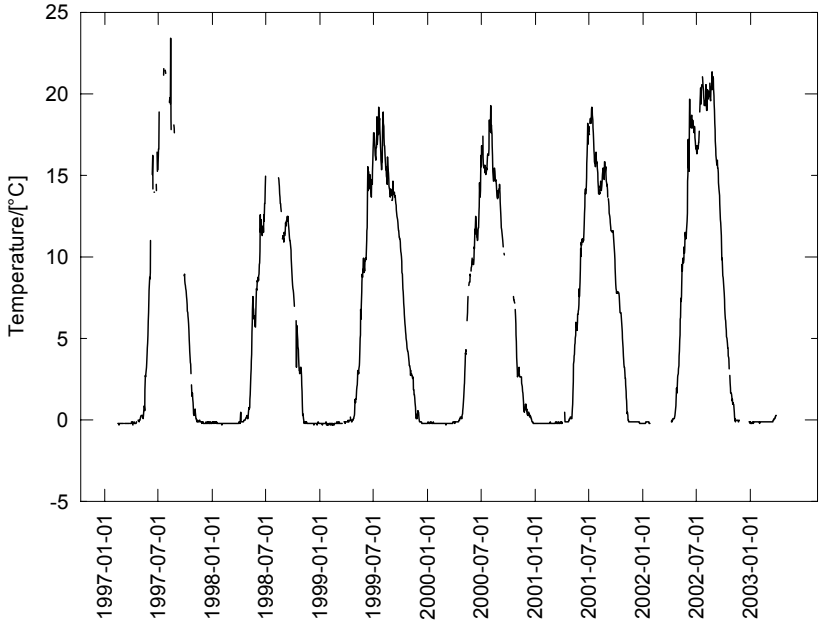

Figure 6-1: Temperature variation in the reservoir water at Hällby.

The results of the resistivity monitoring, seen in Figure 6-2, show a resistivity variation similar to prior measurements in reservoir water in the embankment dams at Lövön and Moforsen (Johansson and Dahlin 1996). Monthly measurements of water resistivity approximately 100 km downstream in Sollefteå performed by the Swedish University of Agricultural Sciences indicate less variation and slightly lower resistivities. This is expected as effects from mixing and dilution increase towards the mouth of the river and decreases the variations, and some peaks might be missed due to the fact that only one sample each month has been taken. Furthermore, lower absolute values are also

likely to be expected due to the normal occurrence of higher rates of TDS further downstream in a river system.

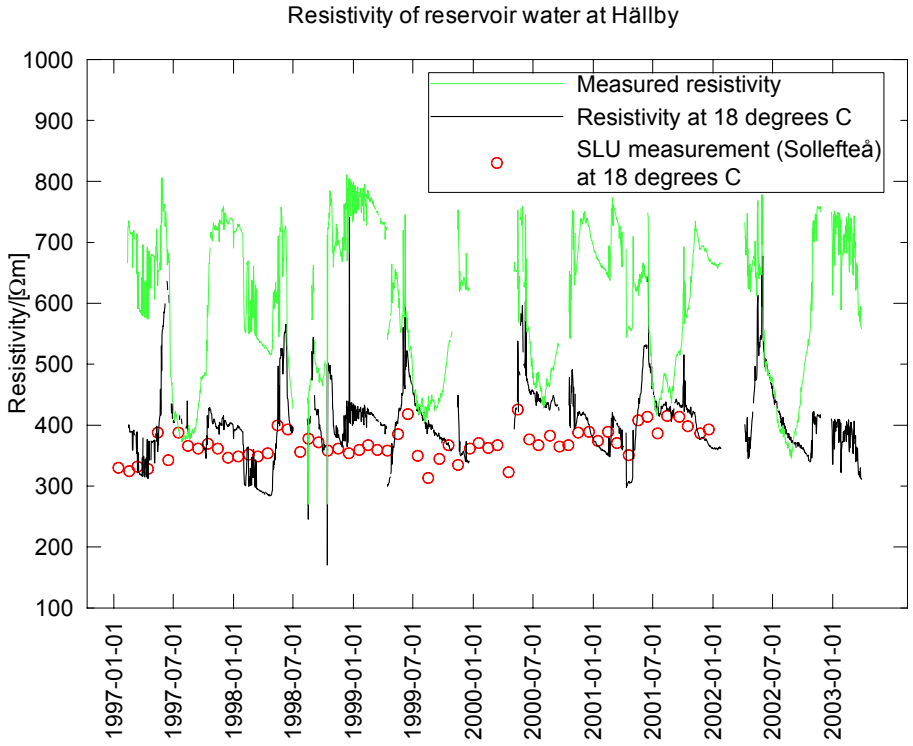

Figure 6-2: Resistivity variation in the reservoir water at Hällby, plotted as absolute resistivity and equivalent resistivity at 18°C. Rings mark measured values by Swedish university of Agricultural Sciences at Sollefteå approximately 100 km downstream.

The following formula has been used to transform measured resistivities to comparable values at 18 °C. T is the ambient temperature, ρ_t is the resistivity at the temperature T, ρ_t is the resistivity at 18 °C and α is the temperature coefficient of resistivity customarily chosen to about 0.025 $°C^{-1}$ (e. g. Ward 1990).

$$\rho_t = \frac{\rho_{18}}{(1 + \alpha(T - 18))}$$

6.3 Data quality

Previous analysis has shown that the data quality from the land based electrode layouts has been unsatisfactory and large scattering occur between daily measurements. In contrast, the underwater electrodes provide data with excellent quality (Johansson et al. 2000). Previous reports from the monitoring activities at Hällby included only data up till fall 1999, but no significant change in data quality has been observed during the following two years thereafter.

6.4 Raw data

Direct evaluation of raw data, i.e. apparent resistivities, is generally not performed in most applications because of the fact that different electrode arrays have a different sensitivity along the profile and with depth and therefore might give misleading resistivity values. However, in connection with monitoring over long time series and in situations where absolute values are less important it might be useful to also evaluate apparent resistivities, especially since it can be an important tool for data quality analysis.

Data from single measurement points, which represents single points in the pseudosections have been analysed over the full monitoring period. A few examples from the left dam crest (Figure 6-3, Figure 6-4, Figure 6-5), the right dam crest (Figure 6-6, Figure 6-7) and downstream the right dam (Figure 6-8, Figure 6-9) have been selected and are presented here.

All series include continuous daily data and extend over five years, fall 1996 to spring 2003, with three rather long interruptions during the winters of 2000, 2002 and 2003, and one shorter during summer 1998 due to technical problems. The sinusoidal pattern with a yearly period time, which was obvious for the measurements in the reservoir water, is also easily recognizable in this case. For the shallow measurement with short distances between the electrodes higher resistivity amplitudes appear whereas deep measurements give very low variations.

When evaluating the data, the attention has been directed towards finding changes from this typical pattern. Also trends with a general rise or lowering of the whole curve has been of particular interest. Another objective with the analysis of apparent resistivities has been to get a better understanding of the data quality. Previous analysis has shown that the data quality from the land based electrode layouts has been unsatisfactory. Particularly the right dam crest demonstrates poor data quality whereas on the left dam crest and downstream right dam conditions are reasonable (Johansson et al. 2000). Here it is seen that there are considerable variations in data quality between single measurements within the same layouts, see Figure 6-6 and Figure 6-7 as an example from the right dam crest. This suggests individual treatment of data points, rather than dealing with whole layouts, when it comes to evaluation and particularly so for layouts with poor data quality. Data quality typically deteriorates with increasing electrode distance, which could be expected as the signal levels decrease with increasing electrode distances.

The 7-day median filtering is a reasonable method to reduce noise from this kind of data. The method is working quite well in most cases but still needs some refining as can be seen in for instance Figure 6-3, where some outliers are still present in the median filtered data. As a further development of the filtering and de-spiking an IIR filter routine have been tried. This routine is described in chapter 5. Tuning of the filter parameters have been carried out for the raw data series by analysing the ability of the filtered curves to follow trends and remove obvious outliers without damping out the natural variations. Examples of filtered raw data time series with different filter parameters can be seen in the figures (Figure 6-3, Figure 6-4, Figure 6-5, Figure 6-6,

Figure 6-7, Figure 6-8, Figure 6-9), and from looking at the curves it appears obvious that the routine can be tuned to filter away much of the noise but maintain natural variation.

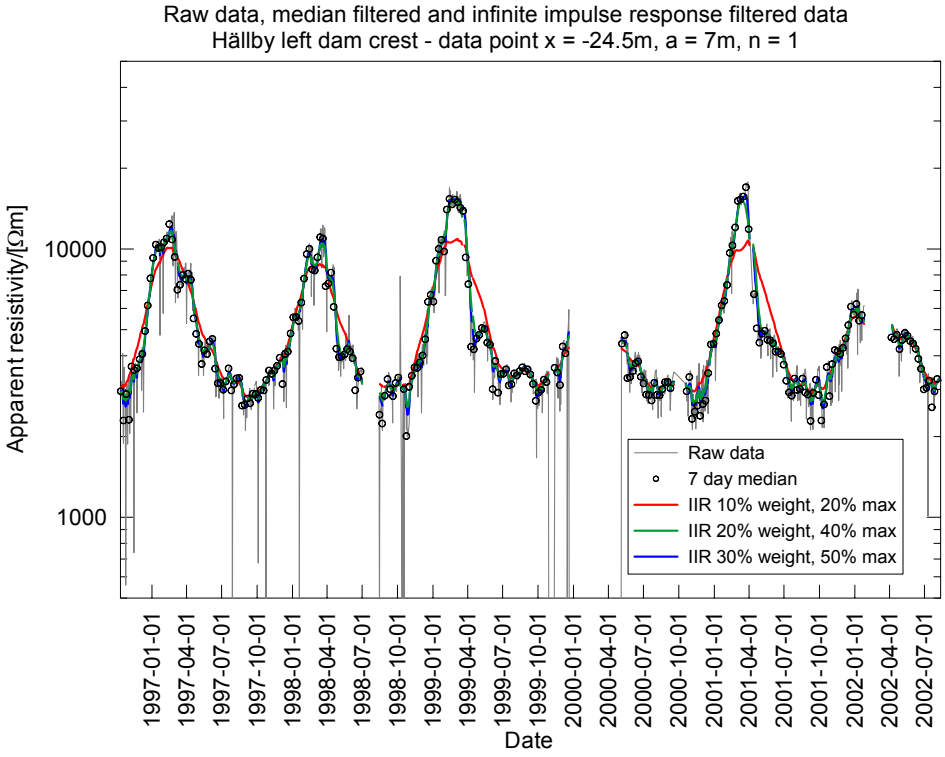

Figure 6-3: Apparent resistivity vs. time measured with 7 m a-spacing Wenner array with midpoint at section 10 m on Hällby left dam crest.

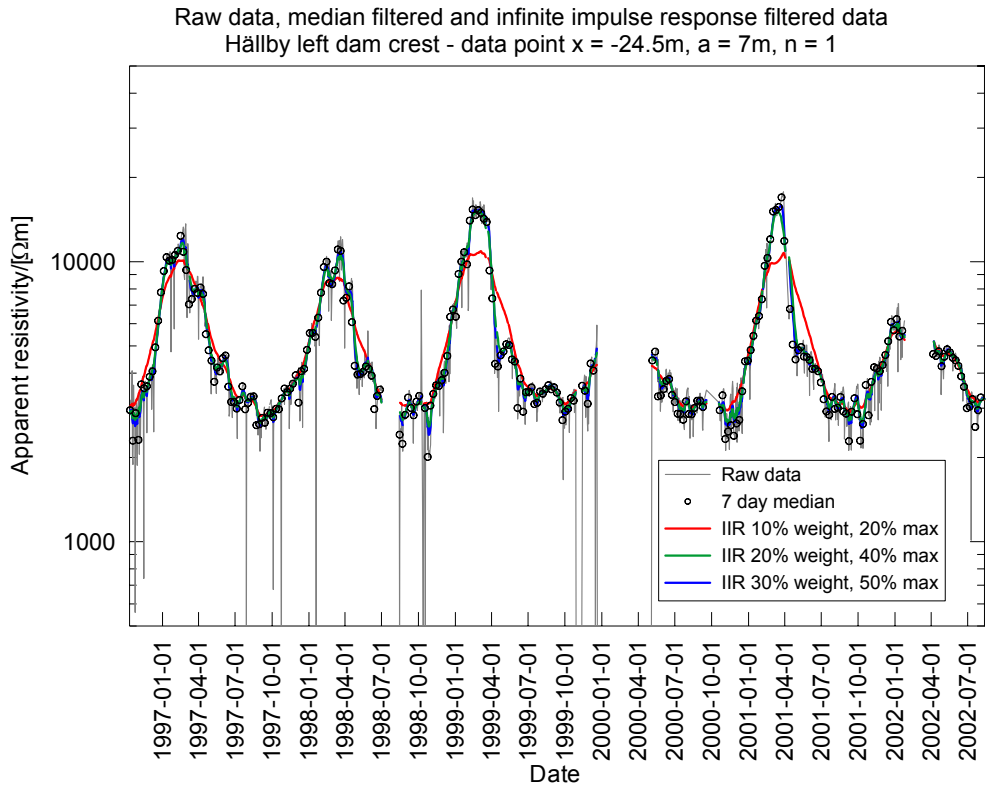

Figure 6-4: Apparent resistivity vs. time measured with 7 m a-spacing Wenner array with midpoint at section 24.5 m on Hällby left dam crest.

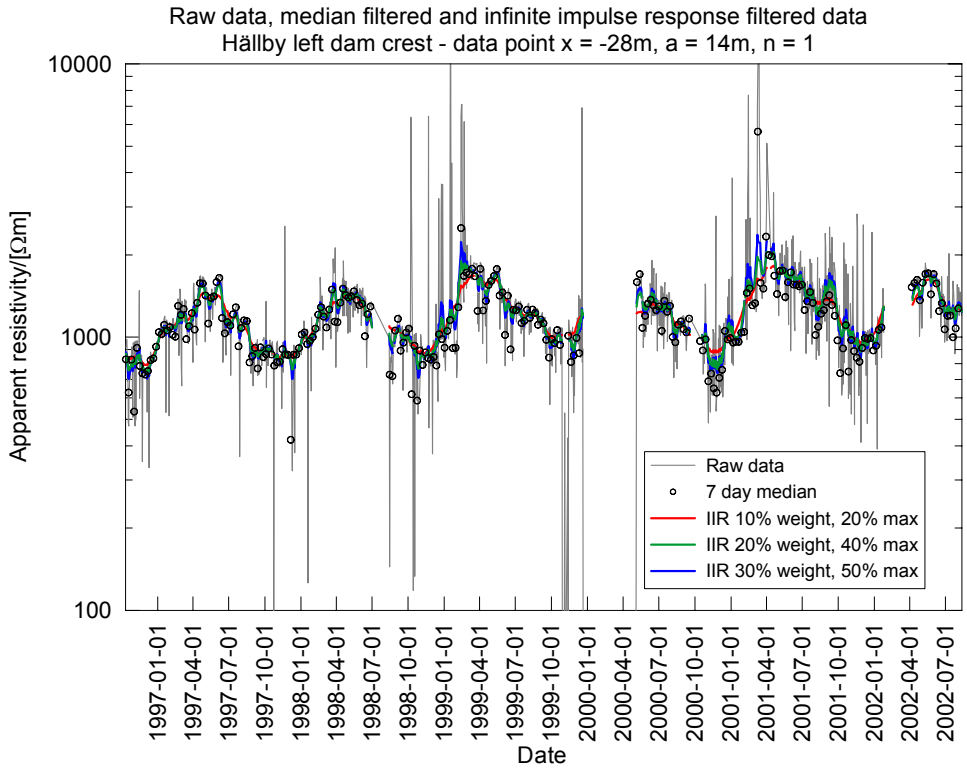

Figure 6-5: Apparent resistivity vs. time measured with 14 m a-spacing Wenner array with midpoint at section 28 m on Hällby left dam crest.

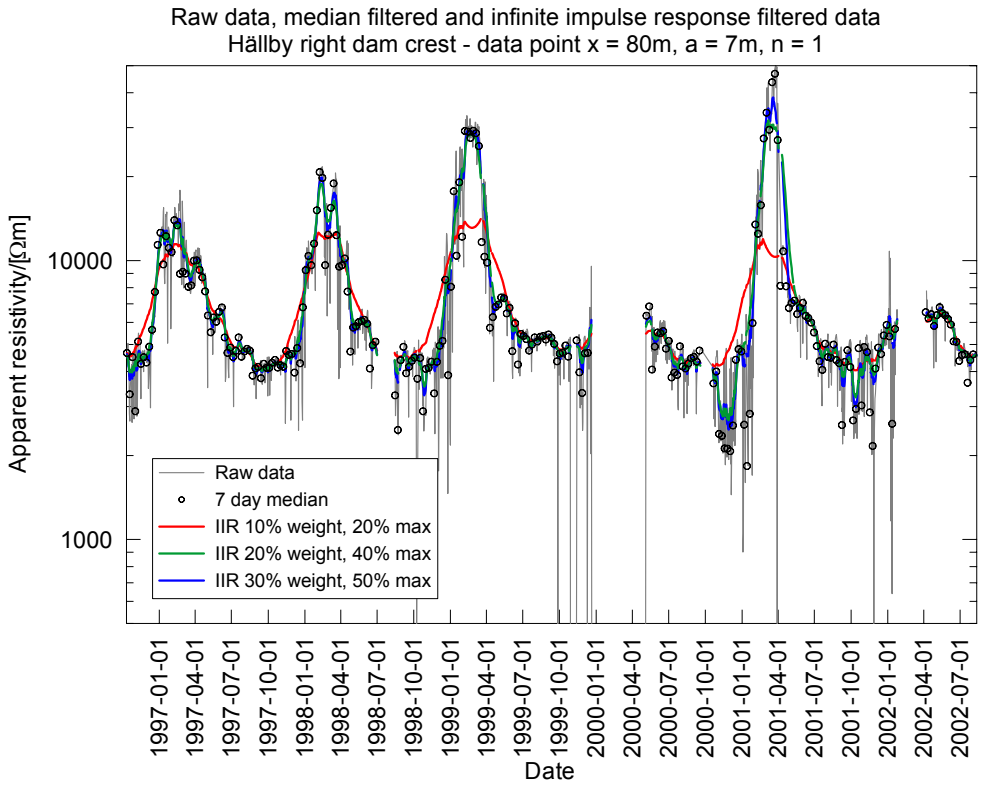

Figure 6-6: Apparent resistivity vs. time measured with 7 m a-spacing Wenner array with midpoint at section 80 m on Hällby right dam crest.

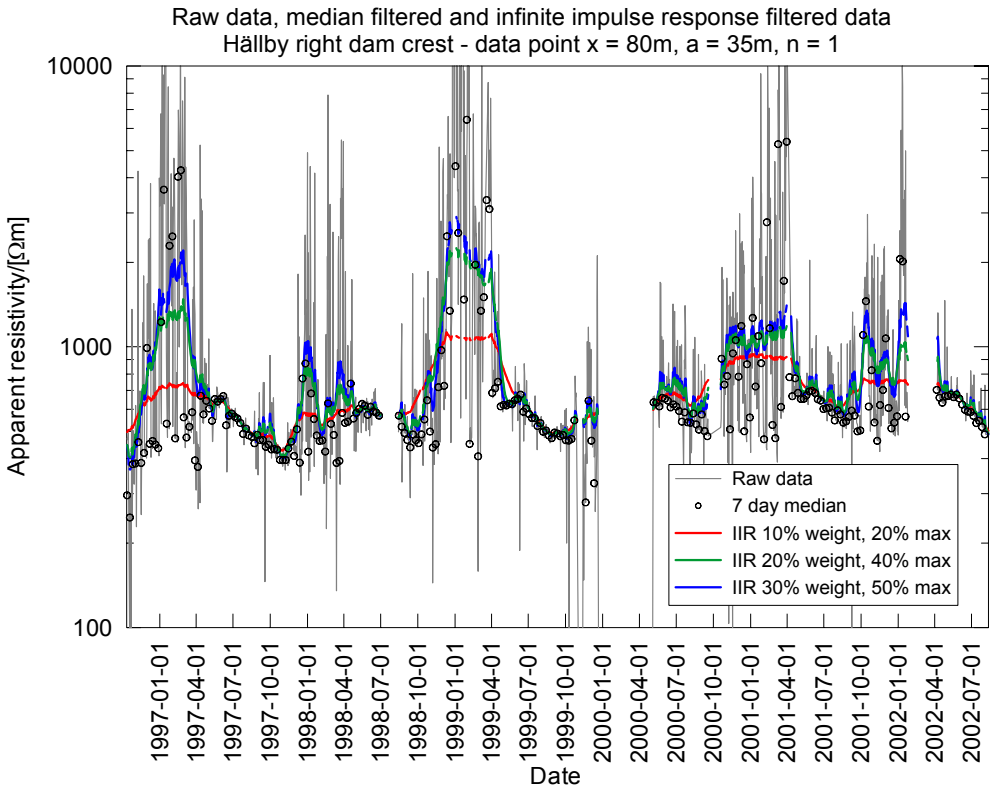

Figure 6-7: Apparent resistivity vs. time measured with 35 m a-spacing Wenner array with midpoint at section 80 m on Hällby right dam crest.

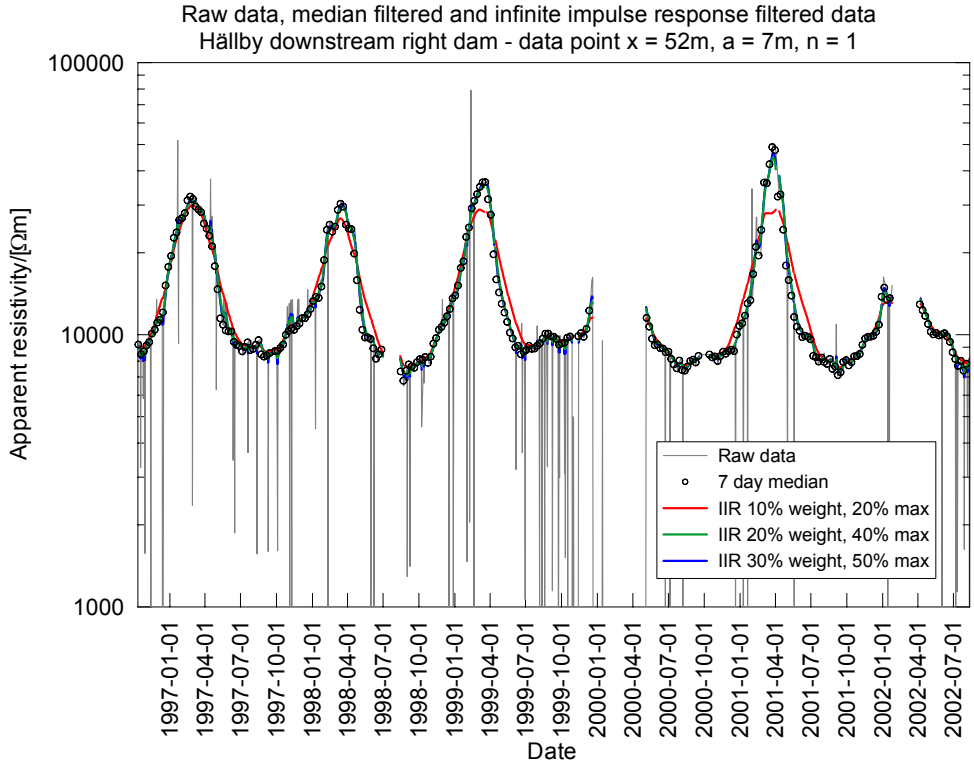

Figure 6-8: Apparent resistivity vs. time measured with 7 m a-spacing Wenner array with midpoint at section 52 m downstream Hällby right dam.

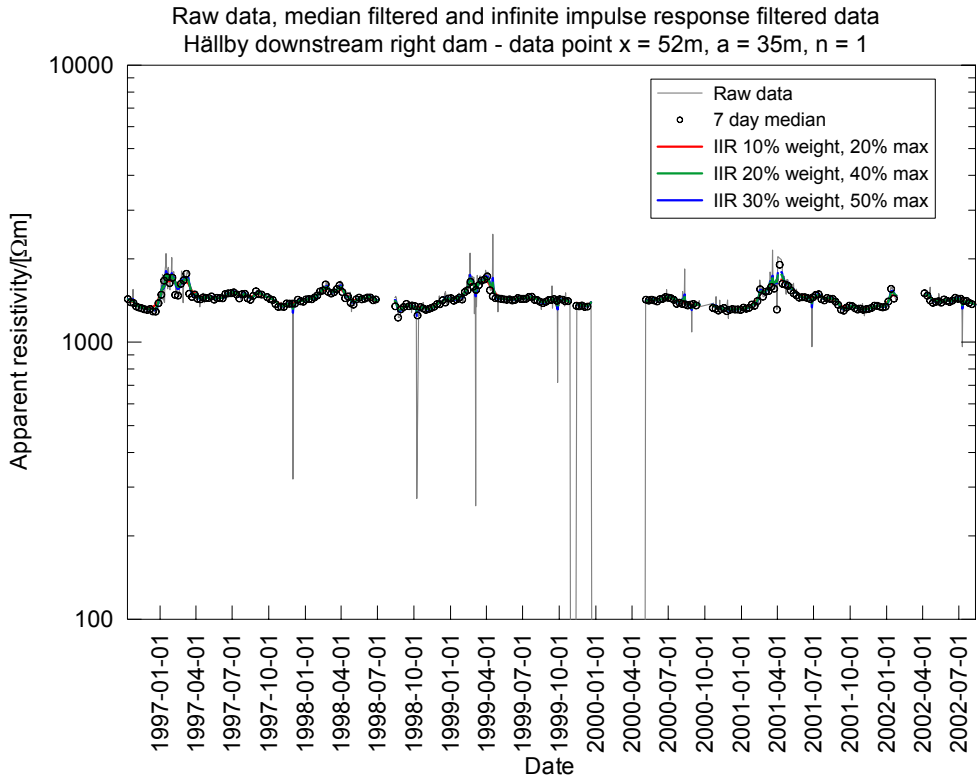

Figure 6-9: Apparent resistivity vs. time measured with 35 m a-spacing Wenner array with midpoint at section 52 m downstream Hällby right dam.

6.5 Inverted data

Routines for inversion of resistivity data at Hällby and principles behind inversion in general are described in Chapter 5. Inversion is necessary to interpret true subsurface resistivity as apparent resistivities (raw data) give a distorted picture due to different sensistivity patterns depending on the array.

As we have seen the resistivity in the dams varies in a cyclic manner over the year. Therefore a method of analysing data over periods of one year suggests itself. If a standard year is defined it is possible to identify deviations and put up limits within which variation is considered harmless. One difficulty with this method is that it is easier said than done to identify and define the normal year and allowed variation, as it requires long data series.

As mentioned in chapter 5 the inversion of long series of repeated measurements may be carried out using time-lapse inversion routines. There are in principal two ways of conducting them. The first one is using a reference data set, which is constantly the same over the whole period. This data set could typically be chosen as the all time median for the complete time interval. However, a loss of data mostly during winters as well as time interval not consisting of complete periods for shorter time sequences might affect the reference data set. The second method, which is also carried out here,

uses a sliding damped reference data set as a time-lapse reference. This reference data set is filtered with the same type of filter but significantly stronger low-pass filtering.
One part of the continuous evaluation from the monitoring program is to present the mean or median inverted model section and the distribution of the relative variation $(\rho_{max} - \rho_{min}) / \rho_{median}$. Figure 6-10 shows the median inverted models from the period 1997-09-24 – 2003-03-30 on the left dam crest, using the Wenner-Schlumberger array and L_1-type inversion. Resistivity data with a seven-day interval from the IIR filter routine was used as input. A plot of the relative variation, shown in Figure 6-11 for the same set of data, points out the distribution of the variation in inverted resistivities along the dam.

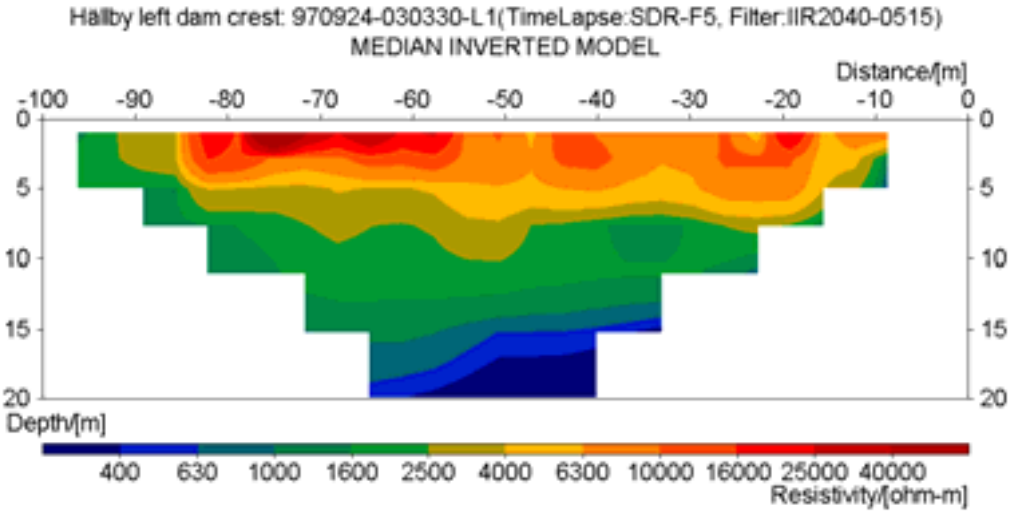

Figure 6-10: Median resistivity distribution at Hällby left dam crest over the period 970924-030330. Data was filtered with an infinite impulse response (IIR) filter before L1-inversion. A sliding damped reference (SDR) value is used for the time-lapse inversion method.

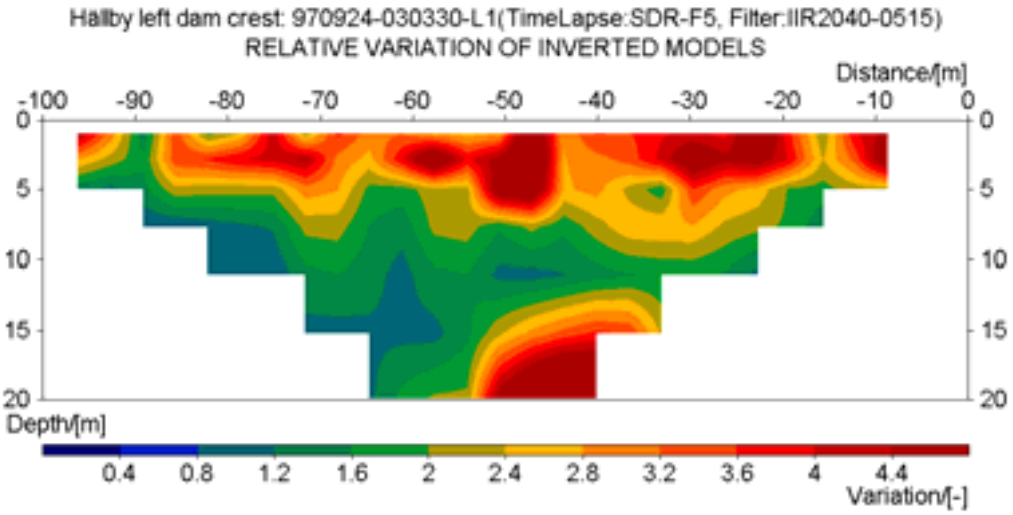

Figure 6-11: Distribution of relative variation in resistivity at Hällby left dam crest over the period 970924-030330. Data was filtered with an infinite impulse response (IIR) filter before L1-inversion. A sliding damped reference (SDR) value is used for the time-lapse inversion method.

If the noise reduction routines works poorly it is possible that extreme values pass the filtering and that will affect the relative variation significantly. Furthermore, when plotting the relative variation one particular extreme value in the raw data affects not only one point in the plot, but also the nearby zone as the inversion routine aims at minimizing the total error.

In Figure 6-12 and Figure 6-13 the median models and the relative variation respectively for the right dam crest are shown. Earlier studies show bad data quality for the right dam crest (Johansson et al. 2000), which is still evidenced by the distorted inverted median models. The variation on the right dam also gives a messy impression that confirms prior doubts about the usefulness of the measurements on the right dam crest. However, applying the IIR filter leads to a significant improvement and shows that even if data looks doubtful at first glance important and useful information may be present.

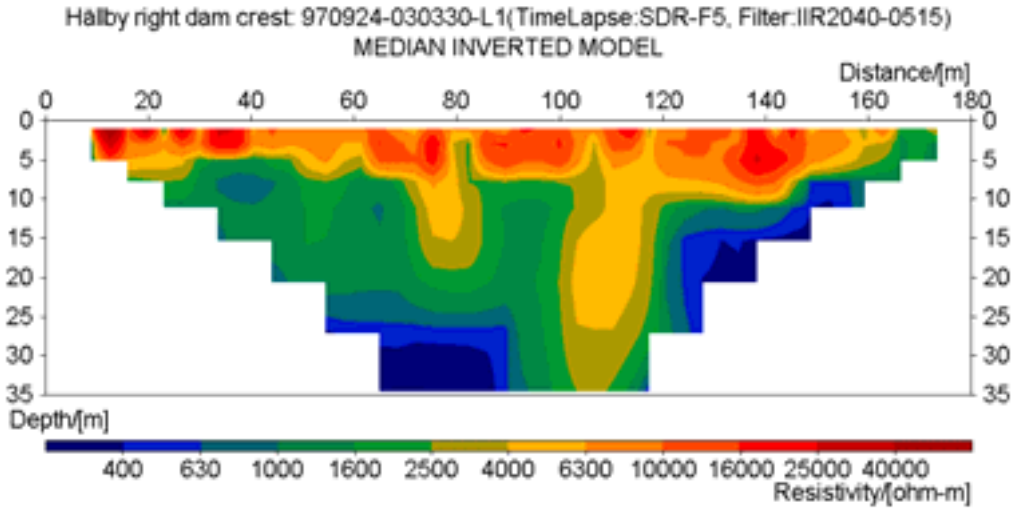

Figure 6-12: Median resistivity distribution at Hällby right dam crest over the period 970924-030330. Data was filtered with an infinite impulse response (IIR) filter before L1-inversion. A sliding damped reference (SDR) value is used for the time-lapse inversion method.

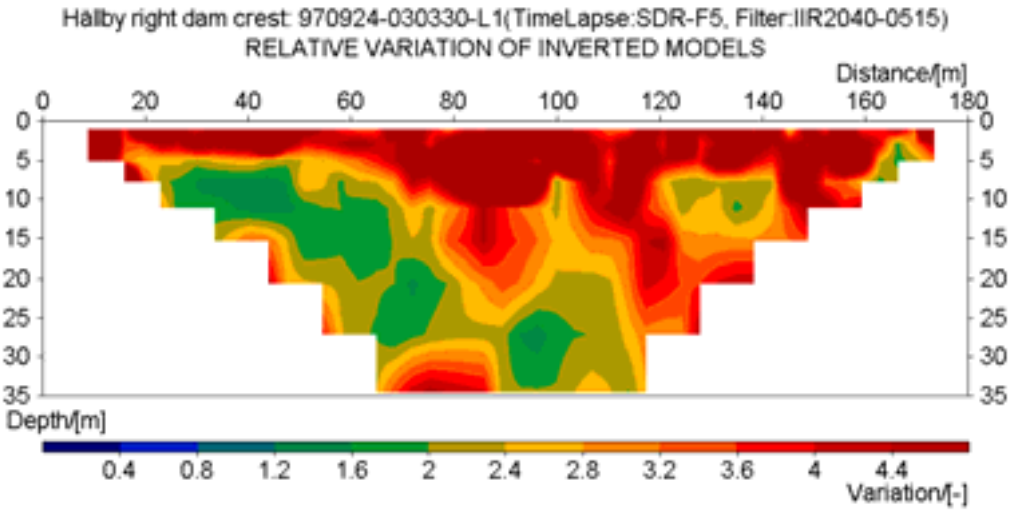

Figure 6-13: Figure 6-14: Distribution of relative variation in resistivity at Hällby right dam crest over the period 970924-030330. Data was filtered with an infinite impulse response (IIR) filter before L1-inversion. A sliding damped reference (SDR) value is used for the time-lapse inversion.

Downstream the right dam the data quality has been acceptable. The median inverted models from the four years are similar and no long-term changes are detectable (Figure 6-15). The relative variation sections exhibit a similar pattern over the period (Figure 6-16). The variations have increased during the last year compared to a very stable period the year before.

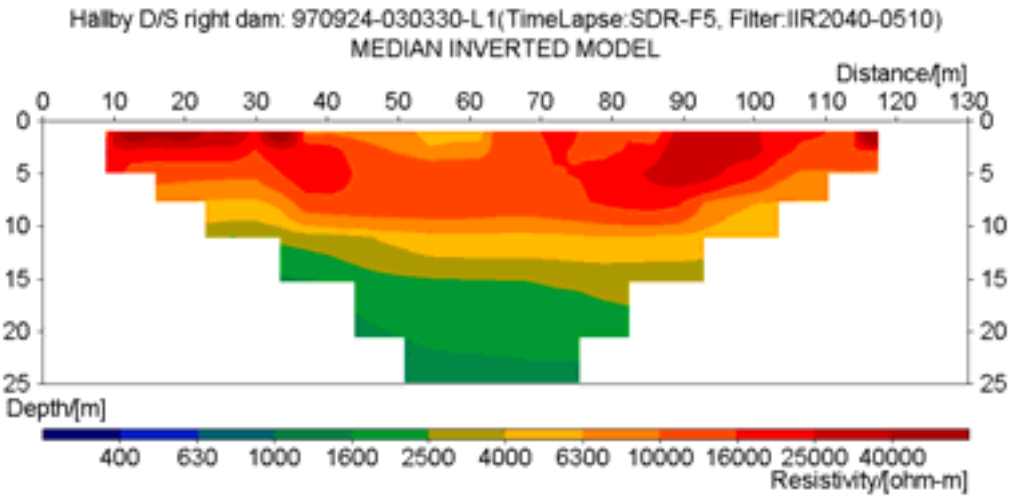

Figure 6-15: Median resistivity distribution downstream Hällby right dam over the period 970924-030330. Data was filtered with an infinite impulse response (IIR) filter before L1-inversion. A sliding damped reference (SDR) value is used for the time-lapse inversion method.

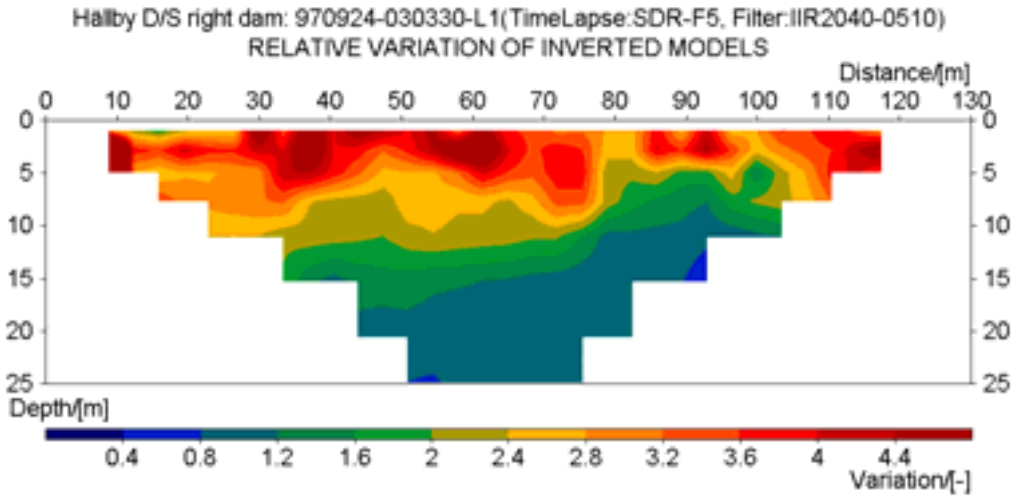

Figure 6-16: Figure 6-17: Distribution of relative variation in resistivity downstream Hällby right dam over the period 970924-030330. Data was filtered with an infinite impulse response (IIR) filter before L1-inversion. A sliding damped reference (SDR) value is used for the time-lapse inversion method.

It is clear that the relative variation is a rough measure and a very simple statistical tool. However, for the purpose of quickly analysing the complete model section it is considered useful. Besides, it has the advantage of not being too sensitive to the fact that data is missing, mostly during the high resistive winter periods. The complete model section serves only as an overall inspection and more detailed examinations should also be carried out. One example of such is to analyse the change in resistivity over time in a certain point of the model section. Inverted Wenner-Schlumberger data from all depths at sections –-40.25, -43.75 and –64.75 metres on the left dam crest have been plotted versus time for the (Figure 6-18, Figure 6-19 Figure 6-21). In Figure 6-20 the inverted data is presented for all chainages using measurements at the largest depth 19.9m on the left dam.

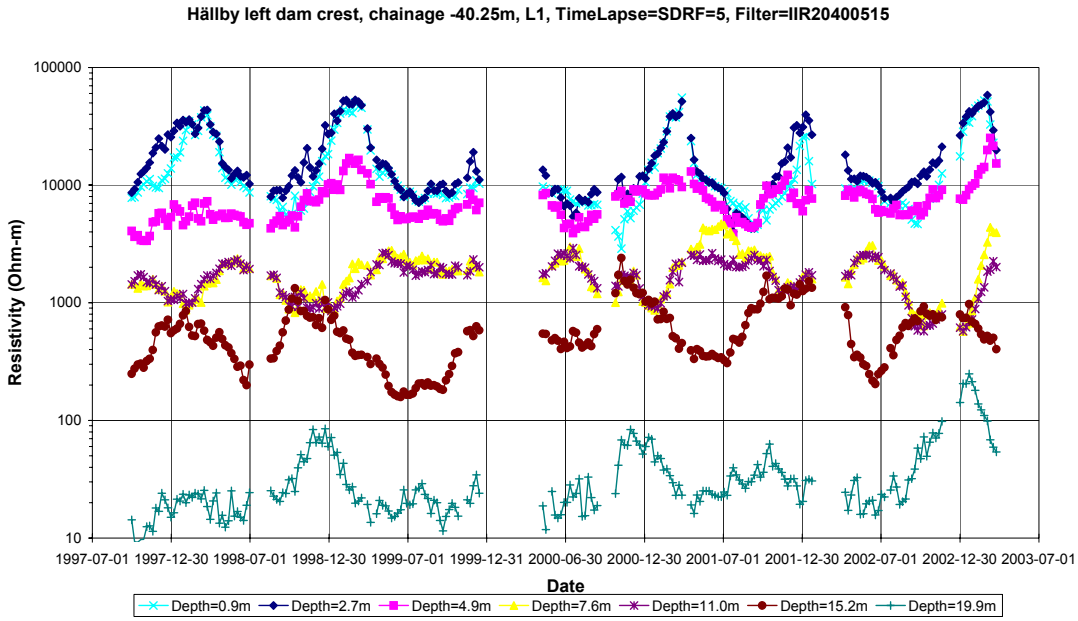

Figure 6-18: Time series of L1-inverted filtered (IIR), time-lapse inverted data from Hällby left dam, chainage –40.25m at seven different depths.

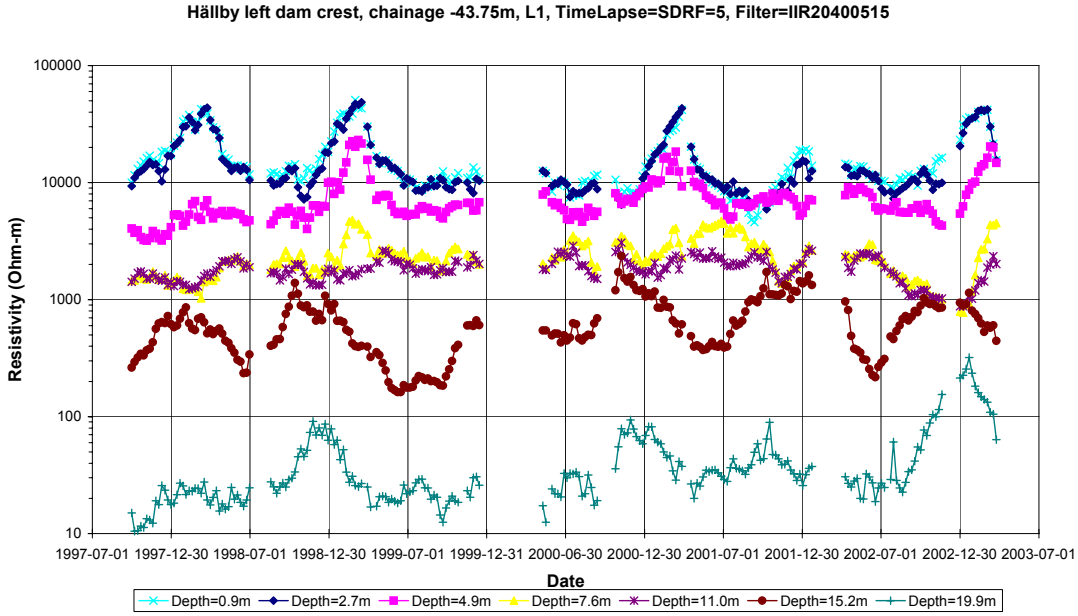

Figure 6-19: Time series of L1-inverted filtered (IIR), time-lapse inverted data from Hällby left dam, chainage –43.75m at seven different depths.

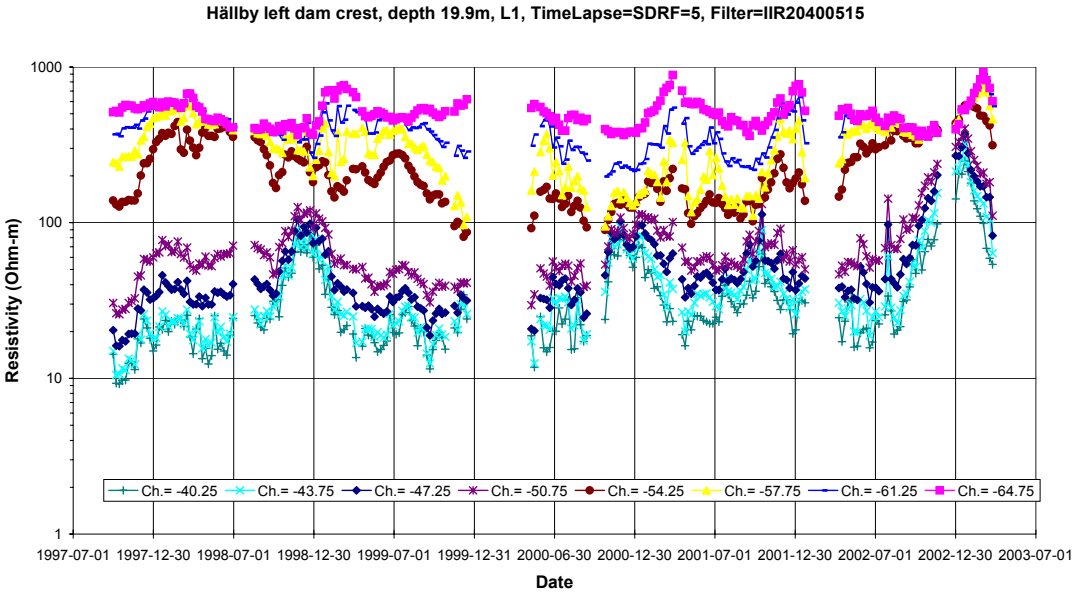

Figure 6-20: Time series of L1-inverted filtered (IIR), time-lapse inverted data from Hällby left dam at 19.9m depth for different chainages along the dam. .

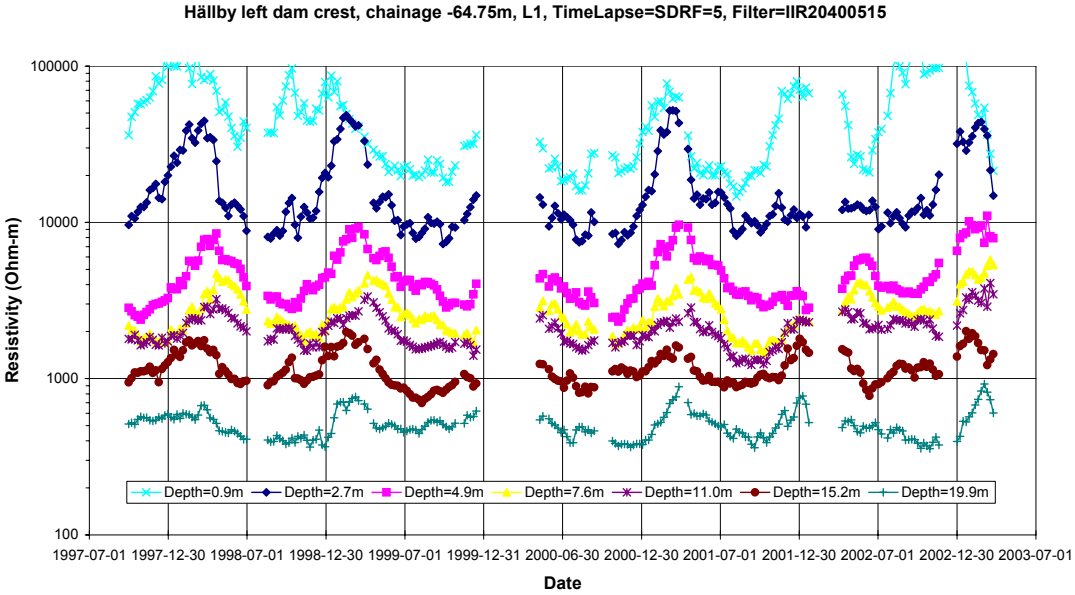

Figure 6-21: Time series of L1-inverted filtered (IIR), time-lapse inverted data from Hällby left dam, chainage –64.75m at seven different depths.

The rough evaluation technique described here involves first looking at the whole inverted model sections using the median and the relative variation as very simple statistical tools and then check the zones that turn out to be interesting in more detail. Applying this technique on the left dam leads us to investigate further what happens at the high variation zone at large depths around chainage –40 to –50. We also have high relative variations at shallow depths, but that is hardly surprising as the temperature variation is highest near the surface with freezing and thus extreme variation in

resistivity during winter. A convenient way to check specific areas is to look at the complete time series. For chainages around –40 to -50 a tendency of higher resistivities with time at depth 19.9m is obvious. This could be due to special conditions during the last winter season but the fact that it is restricted to only this zone of the dam makes such explanation somewhat dubious.

To further look into this matter rawdata, i.e. apparent resistivities, was examined. For measurements using a-spacing 14 and n-factor 2.5 the apparent resistivities for chainage –42m are clearly lower and demonstrates higher variation than the neighbouring areas (Figure 6-22). Normally, an analysis like this one with apparent resistivities is not performed as apparent resistivities might disagree considerably from real resistivities given by inversion. However, in this situation it serves as an extra control.

Another check can be done by choosing another set of parameters for the inversion and thereby ruling out the option that artefacts have been added in the inversion process to generate this phenomena. Checking with the L2-norm inversion gives us the similar increase in resistivity for the investigated regions (Figure 6-23), even though the increase in this case is a bit smoother as could be expected considering the nature of the L1- and L2-norms.

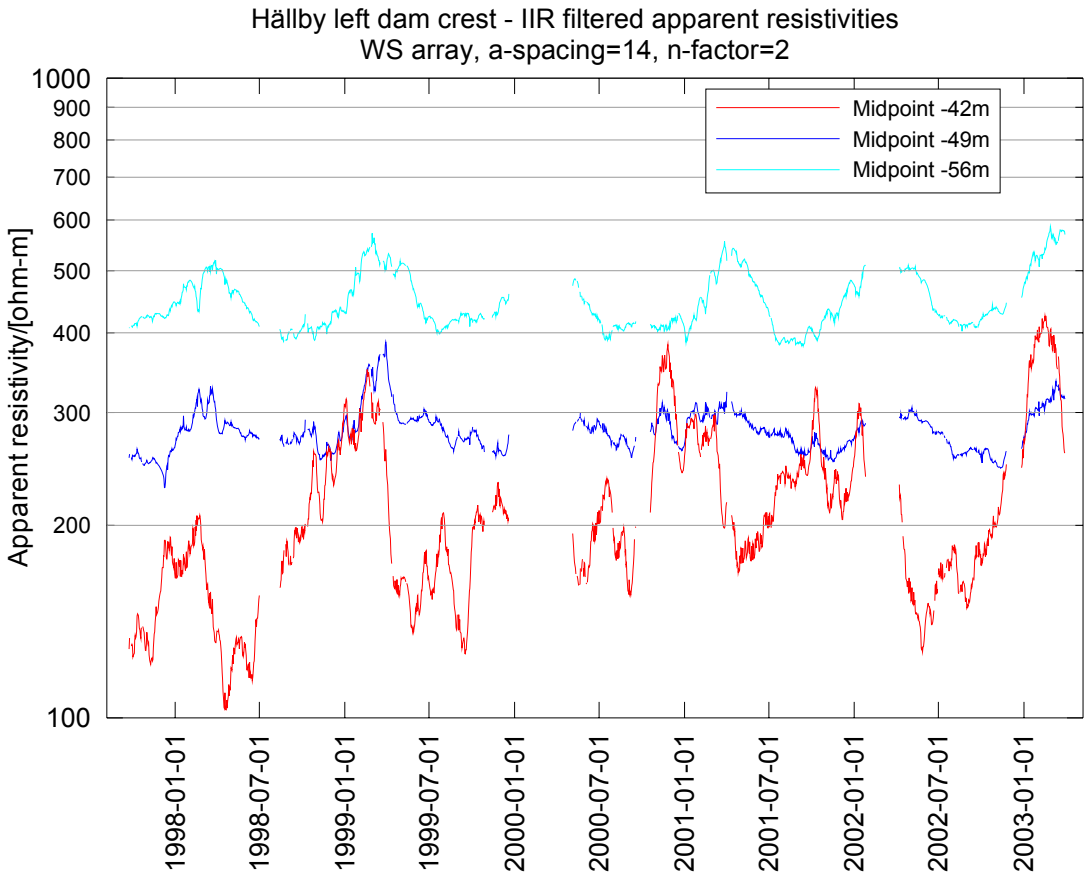

Figure 6-22: Apparent resistivity vs. time measured with 14 m a-spacing and n-factor 2.5 with Wenner-Schlumberger array with midpoints at section 42, 49 and 56 m on Hällby left dam crest.

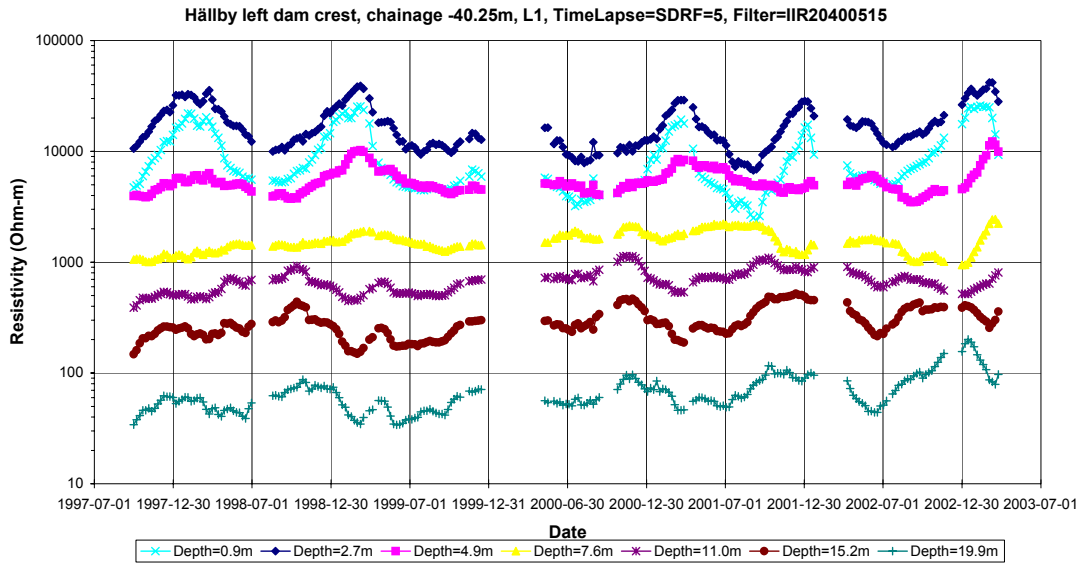

Figure 6-23: Time series of L2-inverted filtered (IIR), time-lapse inverted data from Hällby left dam, chainage –40.25m at seven different depths.

6.6 Offshore electrode layouts

Due to uncertainties regarding the positions of the upstream (offshore) electrodes careful evaluation of data from the upstream electrode layouts has not been considered meaningful before. Now however, after positioning of the electrodes a system for regular evaluation is going to be established. The existing automatic functions that process data from the dam crest and downstream layouts cannot be used for the upstream data without further development.

At this point a few sporadic examinations has been carried out, where a few data sets from isolated occasions over the year have been inverted. Twelve data sets were chosen, each representing the 15th every month during 2001. Both L_1- and L_2-type inversion was performed and the mean model and the variation coefficient for the models were calculated in order to find out about the behaviour of the variations. All models from both the left dam (Figure 6-24, Figure 6-25) and the right dam (Figure 6-26, Figure 6-27) are based upon the measurements from the Schlumberger array.

Absolute values from the mean models range typically from 1000-5000 Ωm upstream the right dam and 500-5000 Ωm upstream the left dam. At the left end of the left dam the resistivity is clearly lower.

Significant variation is seen on the left dam side in the part closest to the intake (Figure 6-24b, Figure 6-25b). Apart from this the variations are relatively small, especially when using the L_2-inversion method, but also for the L_1-norm. This indicates stable conditions, except for the area closest to the intake on the left side. A more extensive study, using a longer series of data will be needed to draw further conclusions.

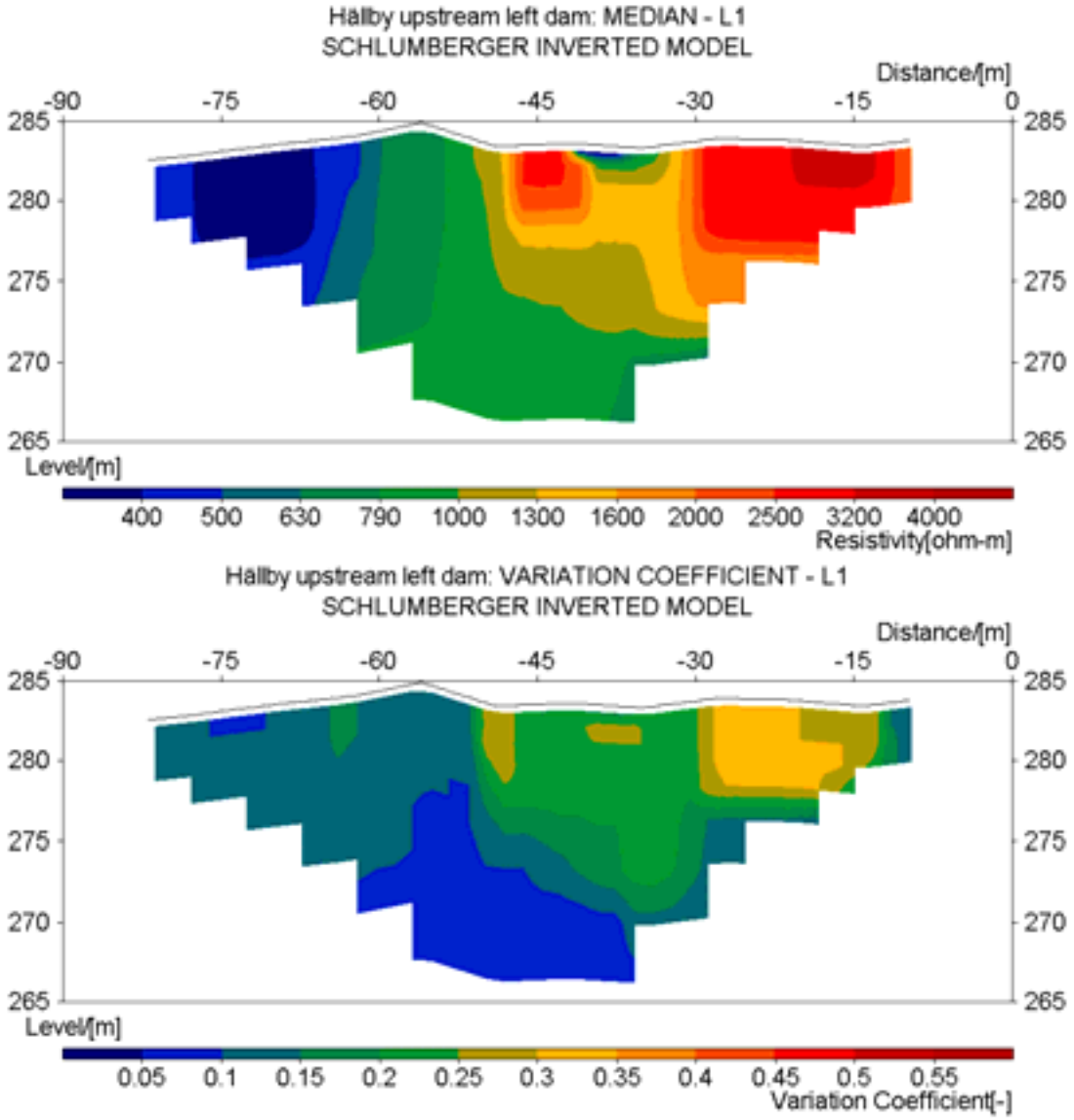

Figure 6-24: L1-inverted model using the Schlumberger array on the offshore layout upstream the left dam at Hällby. Median inverted model and variation coefficient for twelve chosen occasions from 2001 (the 15th in every month). Reservoir elevation is between 291.2–292.0 m.

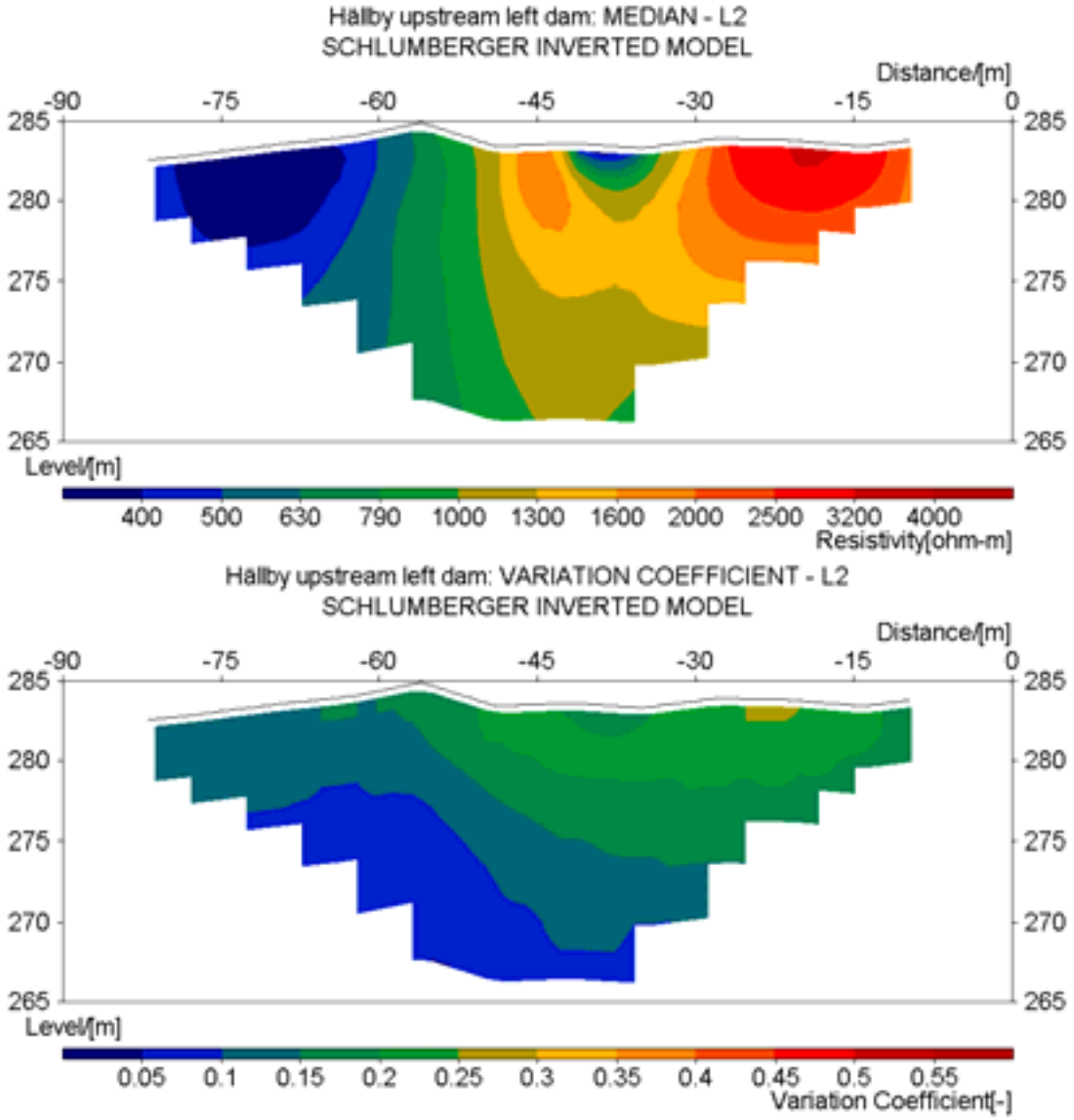

Figure 6-25: L2-inverted model using the Schlumberger array on the offshore layout upstream the left dam at Hällby. Median inverted model and variation coefficient for twelve chosen occasions from 2001 (the 15th in every month). Reservoir elevation is between 291.2–292.0 m.

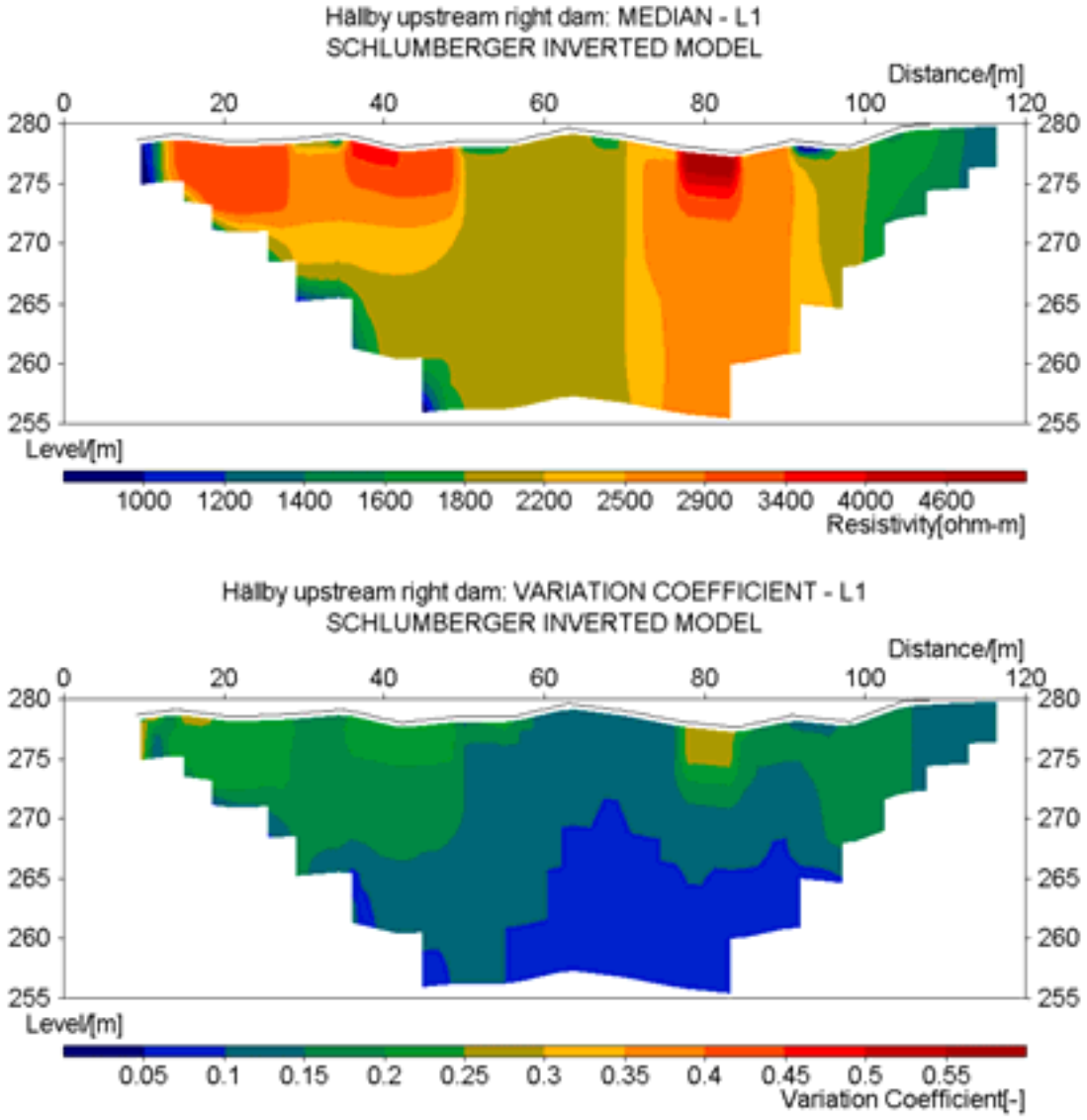

Figure 6-26: L1-inverted model using the Schlumberger array on the offshore layout upstream the right dam at Hällby. Median inverted model and variation coefficient for twelve chosen occasions from 2001 (the 15th in every month). Reservoir elevation is between 291.2–292.0 m.

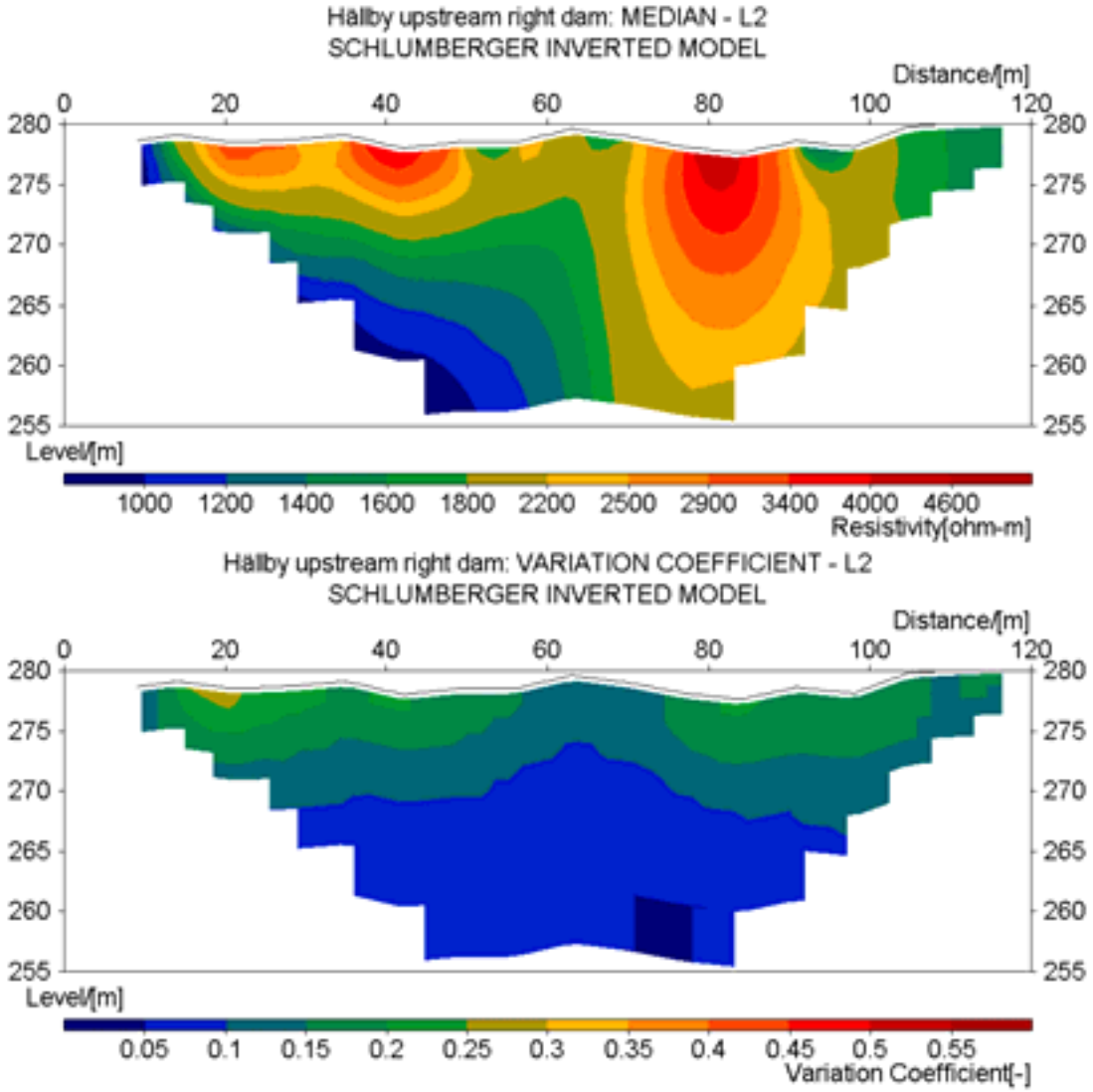

Figure 6-27: L2-inverted model using the Schlumberger array on the offshore layout upstream the right dam at Hällby. Median inverted model and variation coefficient for twelve chosen occasions from 2001 (the 15th in every month). Reservoir elevation is between 291.2–292.0 m.

6.7 Data evaluation difficulties

Work on assessing the influence of sheet piles at the connection between the dam core and the concrete structure has been initialised. Both the left dam and the right dam are constructed with two sheet piles in the connection with the concrete structure. Presence of metal objects, especially when they are of this size, affect resistivity values and makes it harder to evaluate the data in the zone where they are located. It is difficult to fully compensate for such objects in a two-dimensional model, but different techniques to sidestep the problems computationally should be usable.

Theoretical studies of non-conventional measuring arrays have commenced and will hopefully lead to better possibilities to measure not only along the dam but also across the structure using some parts of the existing layouts at the same time.

7 RESISTIVITY MONITORING AT SÄDVA

7.1 General

Monitoring at Sädva has been carried out on a daily basis since May 2001. The monitoring includes SP-data from both the main dam and the dyke. At the dyke, however, all SP-measurements are conducted only with steel electrodes. Evaluation of all results measured until late March 2003 has been carried out.

7.2 Reservoir water

Resistivity and temperature in the reservoir are measured automatically on a daily basis since August 2001. Technical problems lead to unreliable results from the resistivity probe measurements until the change of instrument in August 2002. Concerning the temperature measurements there was an offset voltage influencing the results leading to a parallel movement of the whole data set prior to August 2002 when the equipment was changed. These measured voltages have been shifted manually for the period before the change of instrument so that the temperature could be reconstructed, but it results in some uncertainty for that period. The temperature measurements from the two sensors at Sädva are shown in Figure 7-1. It can be noted that the two measured temperatures fall on top of each other for long periods, and the periods where that depart from each other may indicate either incomplete mixing of the reservoir water or that the mini power plant was not operating.

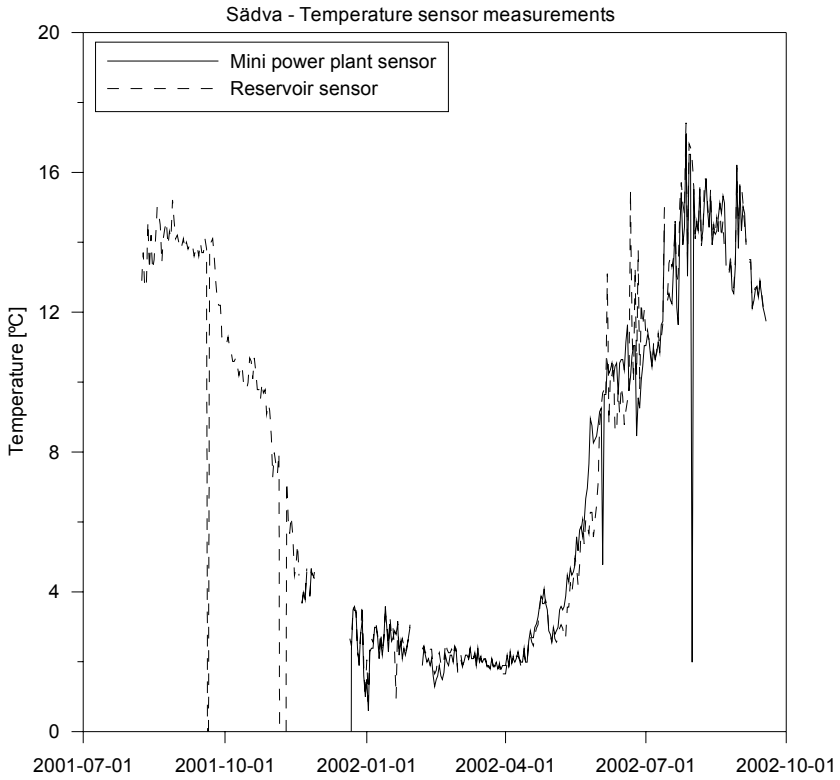

Figure 7-1: Measured temperature in the reservoir.

The Swedish University of Agricultural Sciences performs various measurements of resistivity (conductivity) along the Skellefteälven river. Slagnäs is one of the locations, situated around 100 km downstream of Sädva. Monthly measurements of water resistivity in Slagnäs since 1993 are presented in Figure 7-2.

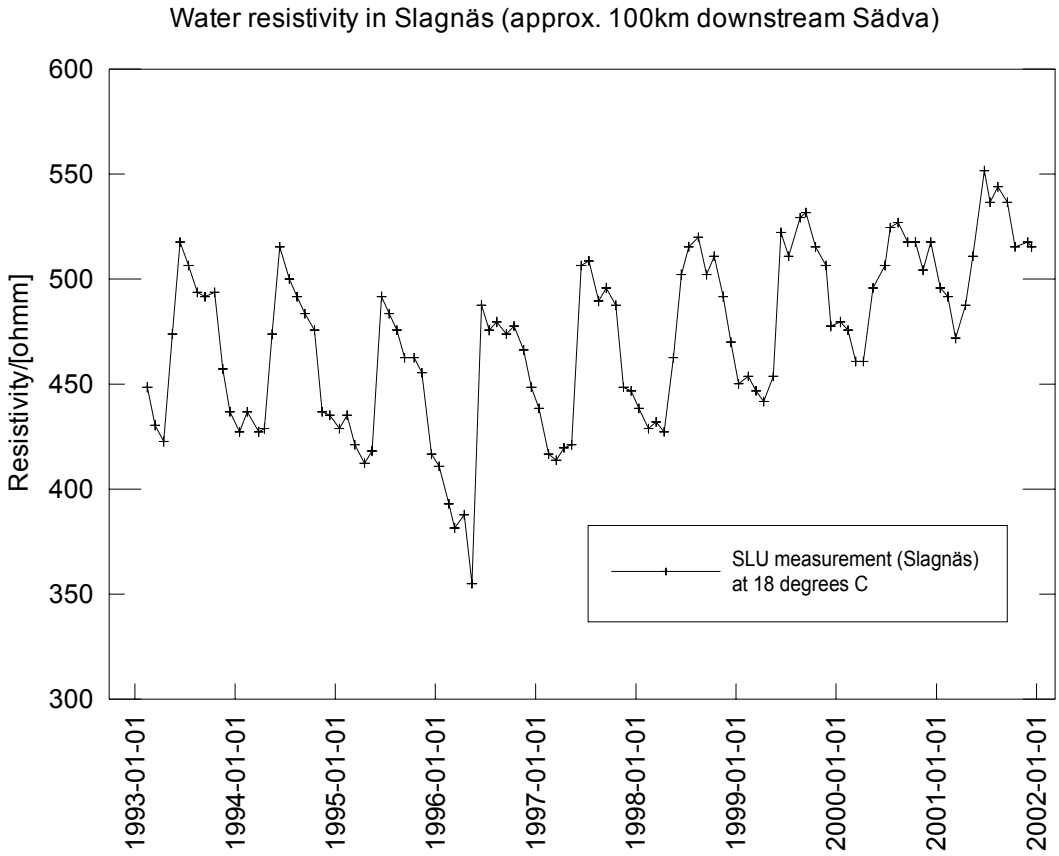

Figure 7-2: Resistivity variation in the reservoir water in Slagnäs, plotted as equivalent resistivity at 18°C.

7.3 Raw data

As has already been discussed in chapter 6 direct evaluation of raw data, i.e. apparent resistivities, is generally avoided. However, in connection with monitoring over long time series and in situations where absolute values are less important it might be useful to also evaluate apparent resistivities.

Time-series of single measurement points, representing single points in the pseudosections, have been analysed over the full monitoring period. A few examples from the main dam (Figure 7-3, Figure 7-4) and the dyke (Figure 7-5, Figure 7-6) have been selected and are presented here. All the selected examples of raw data series come from Wenner array measurements. All series include continuous daily data and extend over almost two full years even though at the end of the period the system have experienced technical problems starting about a month after the change of instrument in August 2002. The pattern with a yearly period is clearly recognizable. It is a sign of good installations and stable conditions that the monitoring system seem to perform well during the coldest season, having in mind the very harsh climate at the location.

The same IIR filtering method, which was used on the Hällby data has been applied here as well. It is clear however, that in comparison with the data from Hällby these

measurements behave more stable and the need for noise reduction methods in general is not as crucial for the Sädva measurements. These data sets, as well as the inverted profiles below, mainly constitute reference plots and serve as overall basic information about the situation of the resistivity distribution in the embankments. It is yet to early to draw any conclusions about the status of the dam from this information.

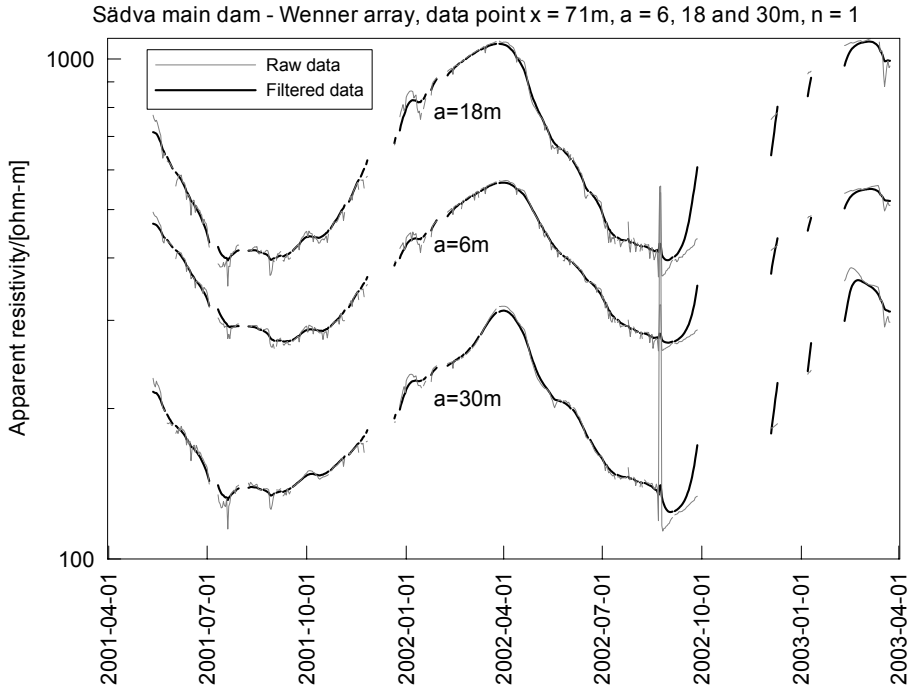

Figure 7-3: Apparent resistivity vs. time measured with 6, 18 and 30 m a-spacing Wenner array with midpoint at section 71 m on Sädva main dam.

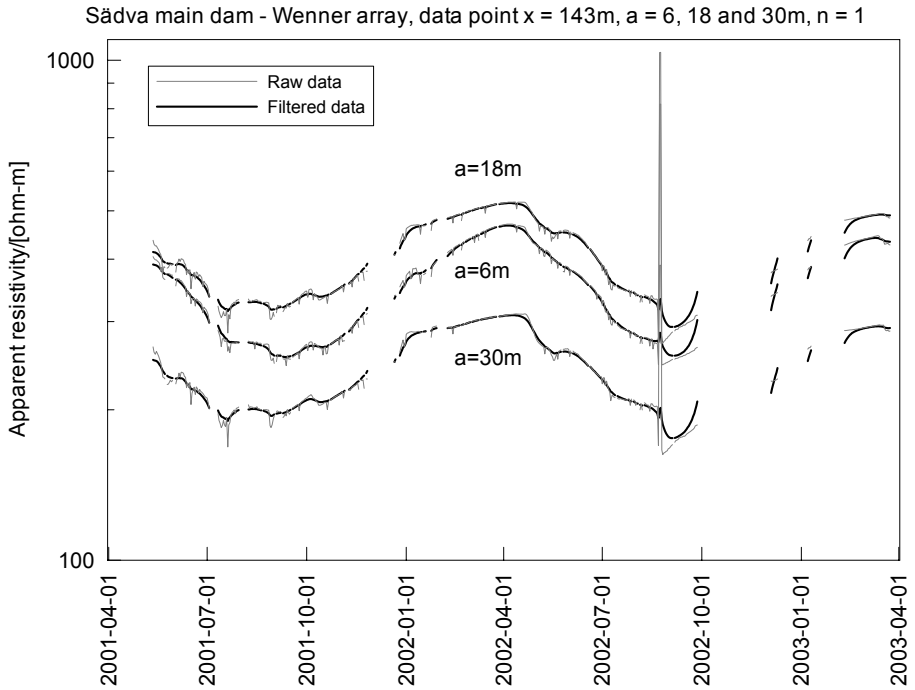

Figure 7-4: Apparent resistivity vs. time measured with 6, 18 and 30 m a-spacing Wenner array with midpoint at section 143 m on Sädva main dam.

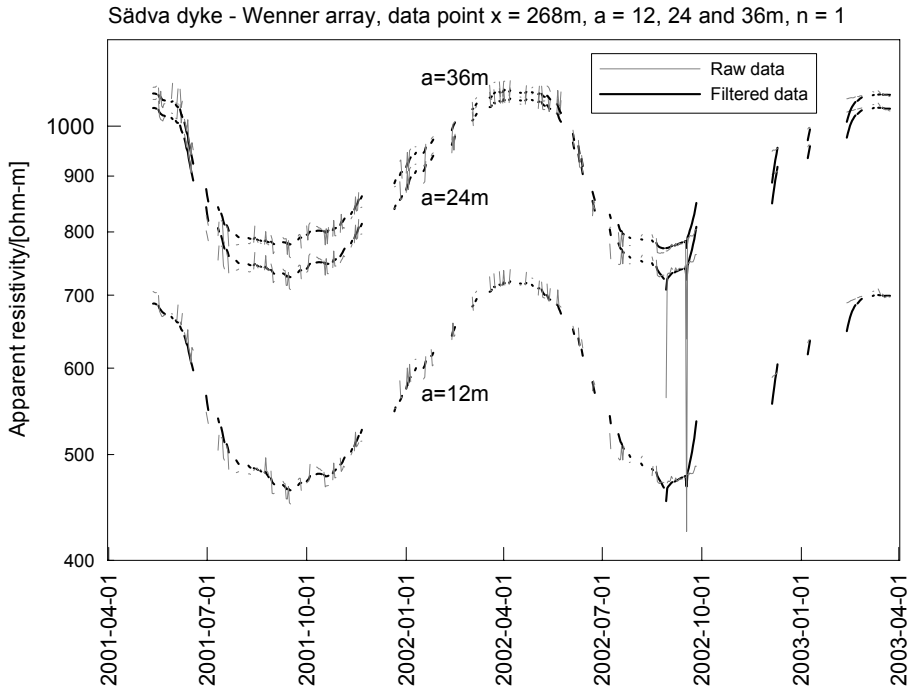

Figure 7-5: Apparent resistivity vs. time measured with 12, 24 and 36 m a-spacing Wenner array with midpoint at section 268 m on Sädva dyke.

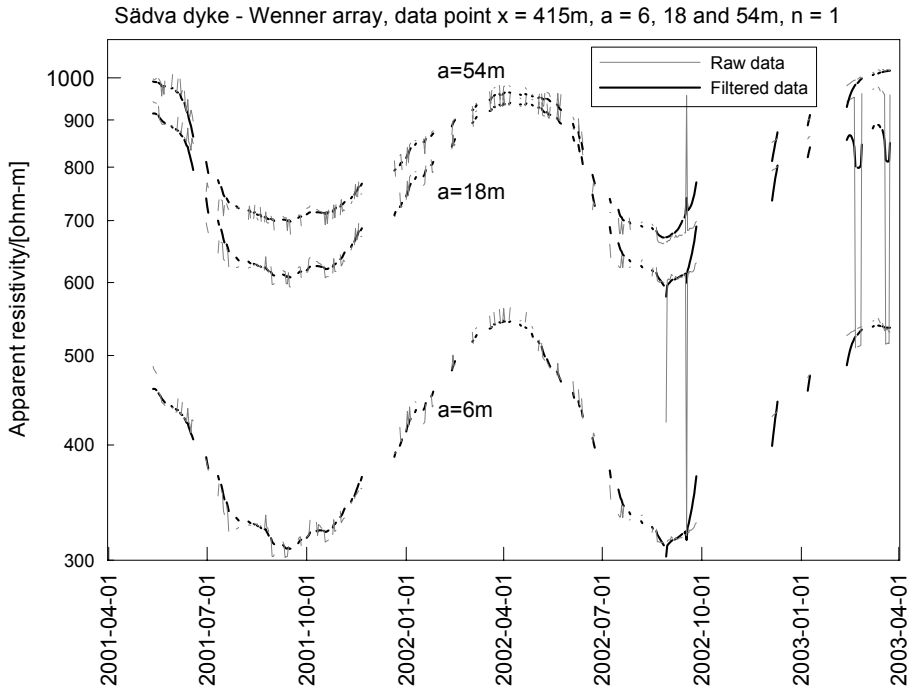

Figure 7-6: Apparent resistivity vs. time measured with 6, 18 and 54 m a-spacing Wenner array with midpoint at section 415 m on Sädva dyke.

7.4 Inverted data

The routines for inversion of resistivity data that was used for Hällby were also applied for Sädva. These routines as well as principles behind inversion in general are described in Chapter 5.

As was discussed in chapter 7.3 we have seen a cyclic resistivity variation over the year. To be able to distinguish changes in the dam structure from resistivity monitoring the yearly variation should preferably be clearly identified. As this is the first two years of continuous monitoring at Sädva and some periods lack data, it is hard to say anything about abnormal variations, but still the information is very useful to get general information about the geoelectric situation in the embankments.

Medium time-lapse inverted models from Wenner monitoring data over the period from May 2001 to March 2003 from the main dam and the dyke is presented here (Figure 7-7, Figure 7-8). Resistivity data from the IIR filtering routine was used as input, and the inversion was made using a slightly stronger filtered sliding damped reference data set. For both the dyke and the main dam sections the bedrock level is indicated in the figures. As regards the dyke, also the foundation level is indicated. It is partly founded on moraine and therefore the foundation level partly does not coincide with the bedrock level. Observe that due to the fact that section 0 metres starts at the spillway the profiles from both the main dam and the dyke are - contrary to praxis - seen looking upstream.

The mostly moderate variation in resistivity distribution in the main dam indicates rather homogeneous conditions. The most distinguished zone in the main dam is the high resistivity region in the left part of the dam. These high resistivities might be caused by internal structures such as concrete objects. Absolute values of resistivity within the dyke itself are in the same range as it is for the main dam. Below the foundation level, or rather the bedrock level, the resistivities are naturally increasing. A very distinct low resistivity zone is located below bedrock level with its centre around at section 450 metres. This is interpreted as a variation in rock type or rock quality of the underlying rock.

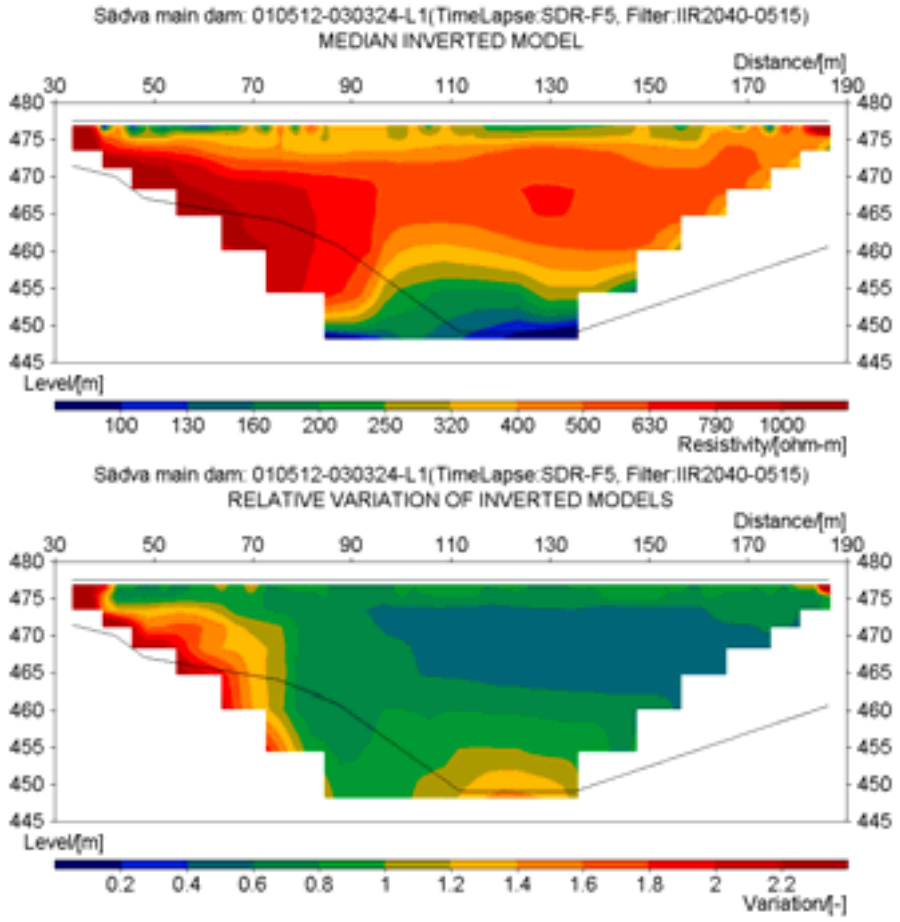

Figure 7-7: Wenner median time-lapse inverted resistivity data (above) and relative variation (below) from Sädva main dam using the L1-norm over the period 2001-05-12 – 2003-03-24. The solid line represents the bedrock level.

The relative variation for the same arrays over the same period (Figure 7-7, Figure 7-8), points out the distribution of the variation in inverted resistivities along the dam. The inverted models seem to be very stable over time. Compared to the layouts at Hällby the variations here are definitely lower with nearly all zones of the embankments having a relative variation less than two over the period. The main reason for this is probably the fact that the electrodes at Sädva are better protected against freezing in the winter and therefore the extremely high resistivities experienced at Hällby during the cold season are naturally avoided. On the main dam the variation is rather low apart from the

leftmost region where a larger variation is evident. One explanation for this variation may be a larger temperature variation in and around the concrete structure at the end of the embankment dam. On the dyke the variations are mostly relatively small, with the most prominent exception around 430-450 metres along the dam where a deep zone of larger variation is clearly indicated. Some shallow zones of higher variation are also visible in the leftmost part of the section.

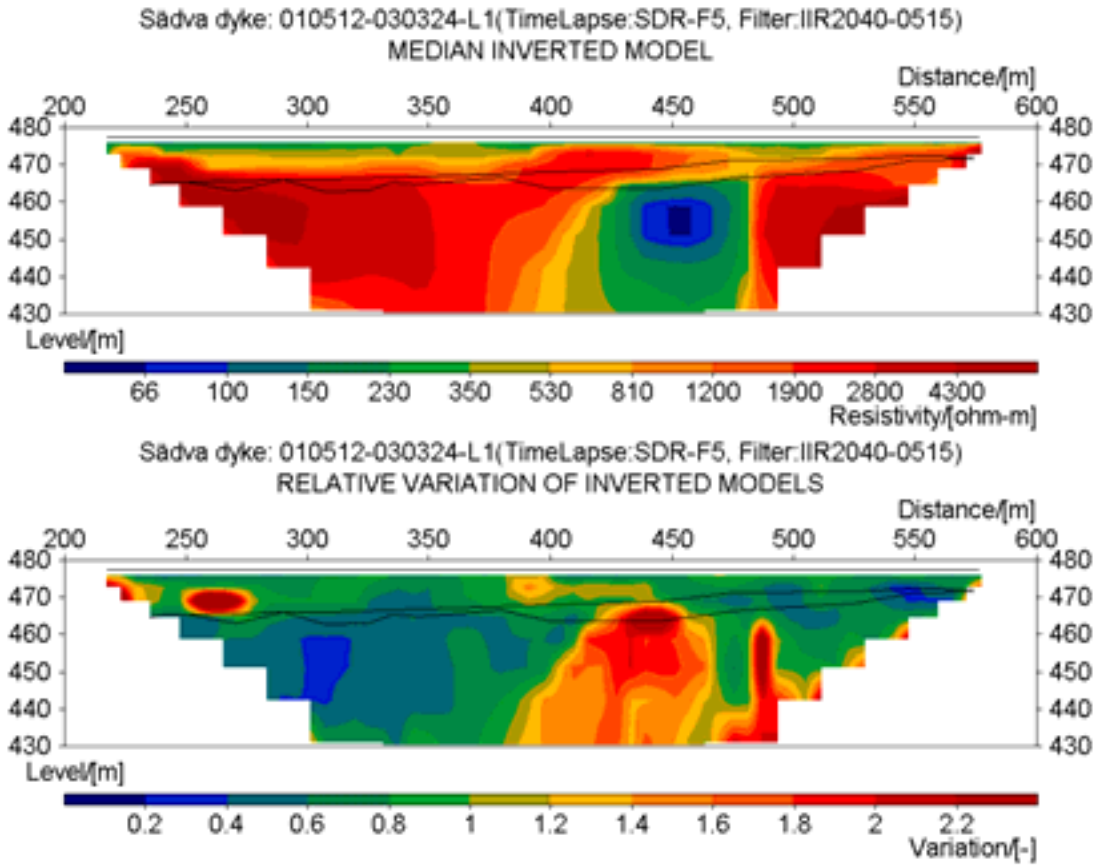

Figure 7-8: Wenner median time-lapse inverted resistivity data (above) and relative variation (below) from Sädva dyke using the L1-norm over the period 2001-05-12 – 2003-03-24. The solid lines represent the foundation level and the bedrock level.

The homogeneous conditions in the main dam are also evident when checking the time series for all depths at chainage 135.5 metres (Figure 7-9). The appearance is typical for most chainages on the main dam with the characteristic yearly variation. All depths inside the dam structure demonstrate similar conditions, whereas for the largest depth, which is below the foundation level of the dam, the resistivities are clearly lower.

On the dyke the data collected are not as dense in time due to problems with the monitoring system. From the start and onwards the system has frequently quit before the full program was carried out and the monitoring of the dyke has deliberately been placed at the end of the daily monitoring sequence. Chainage at 481 metres was selected for the time series as the inverted models sections indicated a large variation in that region (Figure 7-10). The time series gives a disorganized impression partly because the

lack of density in data. Moreover, only the two shallowest depths are located within the embankment as the dam height decreases towards the end of the dyke. A longer time monitoring period is probably required to fully understand the variation behaviour at large depth in the foundation of the dyke.

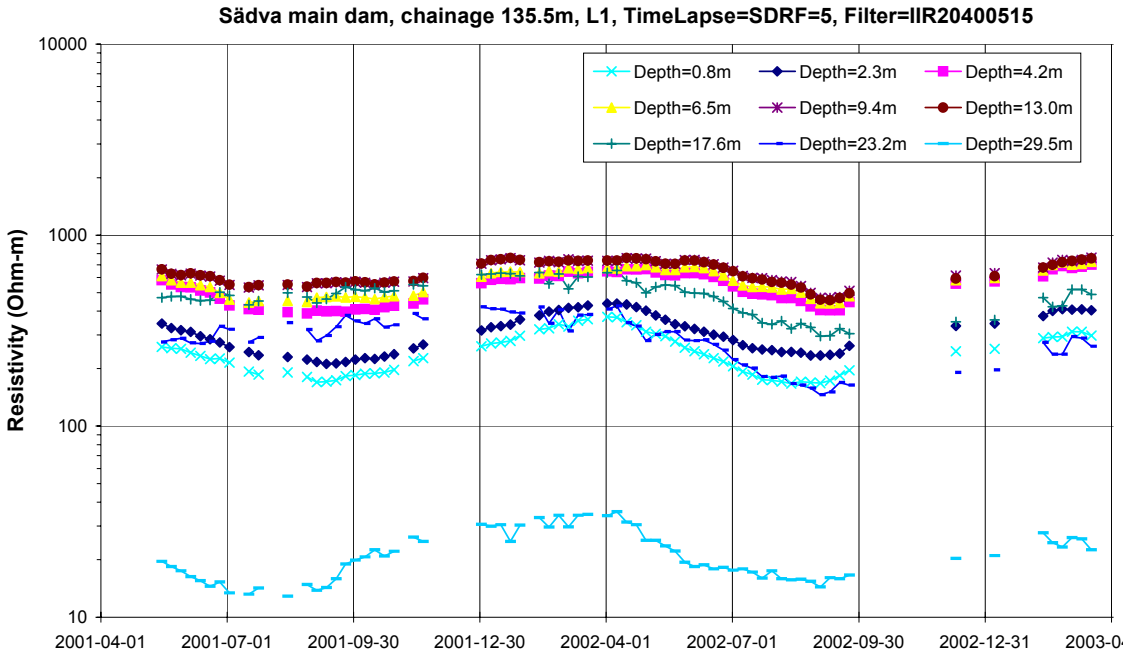

Figure 7-9: Time series of L1-inverted filtered (IIR), time-lapse inverted data from Sädva main dam, chainage 135.5m at nine different depths.

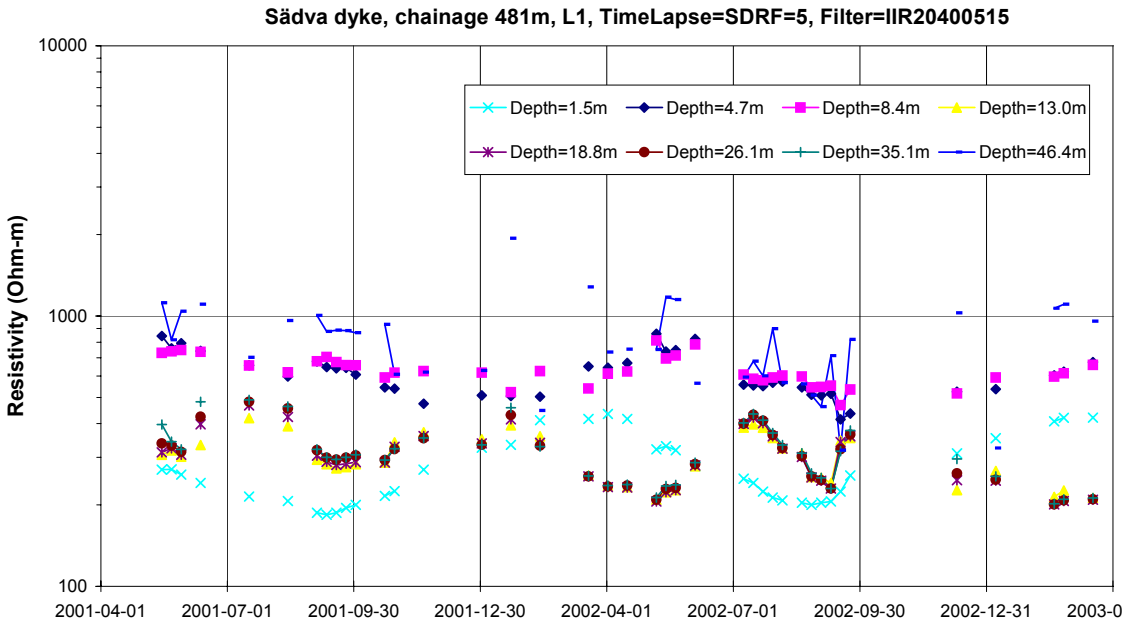

Figure 7-10: Time series of L1-inverted filtered (IIR), time-lapse inverted data from Sädva dyke, chainage 481m at eight different depths.

8 ANALYSIS OF ERRORS IN RESISTIVITY DATA

8.1 Introduction

A study of the occurrence and character of noise in resistivity data, and its influence on the inverse modelling results, has been carried out. Data from the monitored dams as well as from other sites was used in the study, and the study is being presented in a scientific paper (Zhou and Dahlin 2003). A short summary of the study is given below.

Electrode spacing errors and errors correlated to the magnitude of the observed potential are two key factors that affect the data quality for DC resistivity imaging measurements. The properties of the data observation errors and their effects on the imaging results were investigated through theoretical considerations and analyses of real data sets. The measurement errors studied were classified into two kinds of measurement errors, electrode spacing error and observed potential errors, which are the main factors in calculating the apparent resistivity or resistance for 2D resistivity imaging.

8.2 Spacing errors

The results show that the off-line spacing error is much smaller than the in-line spacing error, and that the magnitudes of errors in measured data due to spacing errors depend on different electrode configurations. For example, 10% in-line spacing errors may have over 20 % effect on the values for dipole-dipole, Wenner-β and γ-array data, whereas the other electrode arrays give smaller errors (Figure 8-1). The different electrode arrays in 2D resistivity imaging survey have different spreading patterns of the error effect, which radiate from erroneous electrodes with the magnitude decreasing with increased electrode spacing. Artefacts, close to the erroneous electrodes, appear in the inverted models due to in-line spacing errors, especially with dipole-dipole, Wenner-β and γ-array surveys. Similar artefacts or distorted images also may occur due to the small fixed 3D variations near the electrodes.

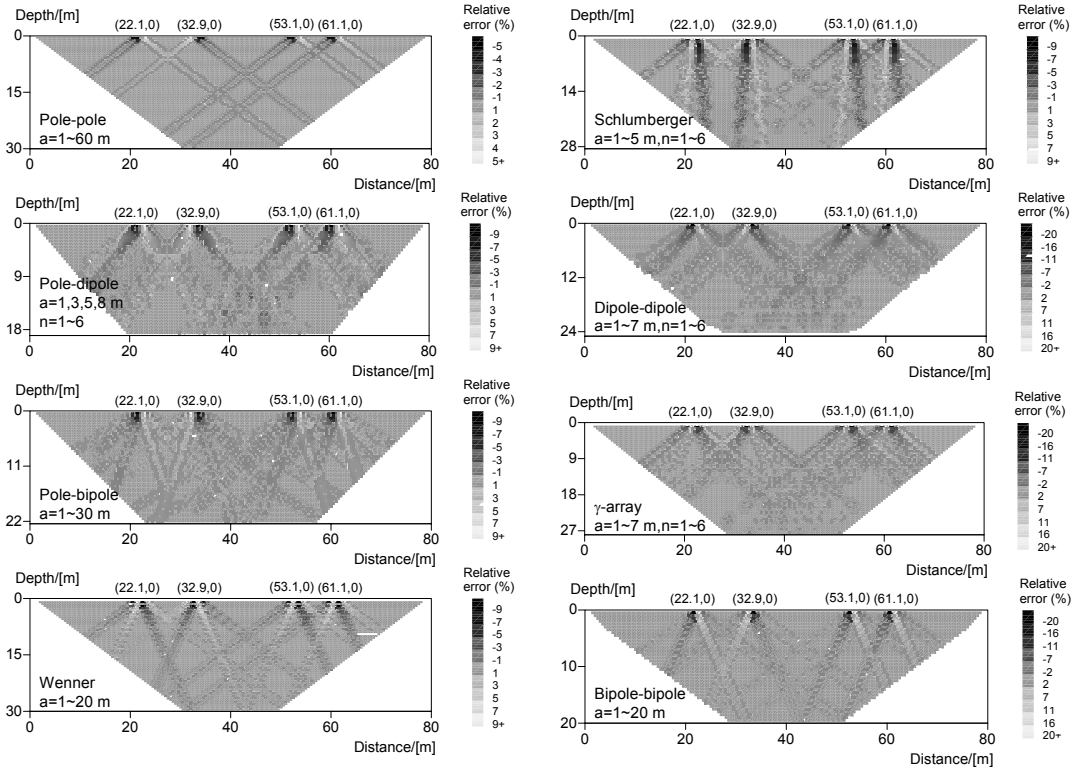

Figure 8-1: Pseudosections of the in-line spacing errors due to the wrong positions of four electrodes. 10 % spacing errors were assumed here, which may cause over 20 % resultant effect on the dipole-dipole, Wenner-β and g-array data.

8.3 Observed potential errors

The data quality, or the observed potential error, can be estimated by normal and reciprocal measurements, which can be efficiently fulfilled using an automatic data acquisition system for all data points. Visualisation of the absolute relative errors calculated by the normal and reciprocal potential readings, by means of logarithmic plot (see example in Figure 8-2) and error pseudosections, is very useful to quantitatively and spatially evaluate the data quality. The data quality may also be characterised by the mean value, standard deviation, regression function and the spatial distribution of the possible observation outliers. The visualisation may directly reflect the working status of the instrument, electrode contact resistant problems, background noise of the site and disturbing sources of the potential outliers in an imaging measurement. The analysis of the potential errors for different sites and different electrode configurations shows that the potential error increases in a power number with the decrease of the measured potential, which reaffirms the fact that the potential error depends on the strength of the measured signal and varies with sites, times and electrode configurations. The potential signal strength depends on electrode arrays and practical geological models. Generally speaking, Wenner, pole-pole and Schlumberger measurements have relative stronger potential signal than dipole-dipole and pole-dipole. It may be simply proved by comparison of the inverse geometric factor of the electrode arrays.

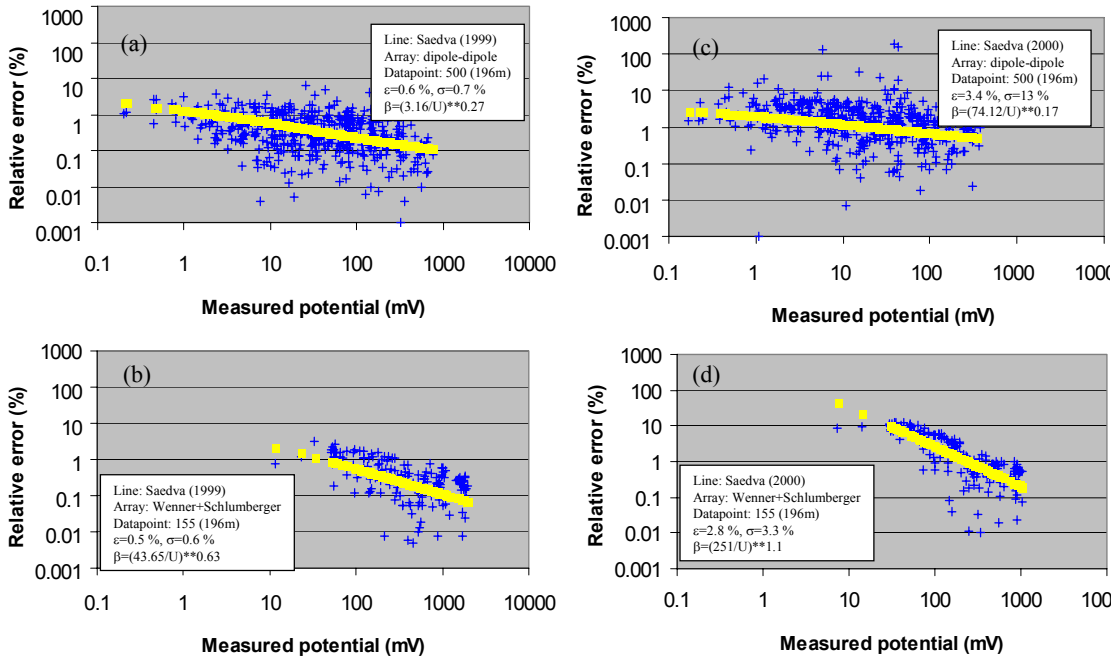

Figure 8-2: Logarithmical plots of the potential errors from normal and reciprocal measurements at Sädva dam northern Sweden. (a) Dipole-dipole survey in 1999, (b) Wenner+Schlumberger survey in 1999, (c) dipole-dipole survey in 2000, (d) Wenner+Schlumberger survey in 2000.

Power net transients, background telluric variation and instrument malfunction are possible sources that may cause the large errors present as outliers deviating from this function. The fact that the outliers are often correlated to high contact resistances for some electrodes used in a measurement is reaffirmed, but it may also be caused by unsatisfactory connection between the electrode and the cable due to e.g. dirt or oxide on the connectors. They are often the main part of the errors affecting the imaging results.

8.4 Impact on inverted models

Furthermore, a robust inversion and a smoothness-constrained inversion were applied to the investigation of the effects of the measurement errors. Using two real data sets, it was shown that the smoothness-constrained least squares inversion is much more sensitive to the potential errors than the robust inversion, but the two inversion schemes produce very similar models with a high data quality. The examples also show that artifacts or distorted images correlate with the distribution zones of the outliers in the error pseudosection. The robust inversion is quite insensitive to the outliers of data, and with high data quality, i.e. all the potential errors obtained by normal and reciprocal measurements are less than 5%, the two inversion schemes produce very similar image except more ‘blocky’ and slightly better data misfit with the robust inversion. The common features of the inverted models from the two inversion schemes and the sections having high data quality can be expected to give a reliable image of the site.

8.5 Discussion

Spacing errors should normally be a minor problem in resistivity monitoring using permanently installed electrodes, provided the installation of electrodes has been carried out with suitable quality assurance, but may become a significant if this is not the case. With permanently installed electrodes the spacing errors will be constant in time, but their impact on the data may vary as a result of variation in the near surface resistivity. However, if monitoring is carried out without permanent electrodes, i.e. electrodes are put in place for each measurement at some time interval, the influence of spacing errors can become a very important source of noise.

The observed potential errors will in dam applications largely be a function of the electrode contact resistances, since high contact resistances does not allow the transmission of sufficient current with associated low signal levels. Furthermore, if the contact electrode resistance is high it can lead to coupling problems between the current and potential lines in the electrode cables, which may result in very severe data quality problems (outliers). High contact resistances are generally most problematic in the winter when freezing of the dam crest is prevalent, resulting in orders of magnitude higher resistivities in near surface part of the dam. This has been very clearly illustrated by the difference in data quality attained for the dam crest measurements at Hällby and Sädva respectively, where as pointed out earlier the electrode installation on the right dam crest of the former needs to be improved in order to get an acceptable data quality.

Using real data sets, it was shown that the smoothness-constrained least squares inversion is much more sensitive to the potential errors, whereas the robust inversion is quite insensitive to the outliers of data, as expected. The two inversion schemes produce very similar models with a high data quality, except more ‘blocky’ and slightly better data misfit with the robust inversion. It can be recommended to try using both approaches in real situations, and the difference between the results be used as an indicator on the data quality.

9 2D NUMERICAL COMPARISON OF ELECTRODE ARRAYS

9.1 Introduction

A comparison between 10 different electrode arrays was carried out using numerical forward and inverse modelling. The results have been used as a base for modifying the measurement protocols for Sädva. The results are presented in a scientific paper (Dahlin and Zhou in press), and a short summary given below.

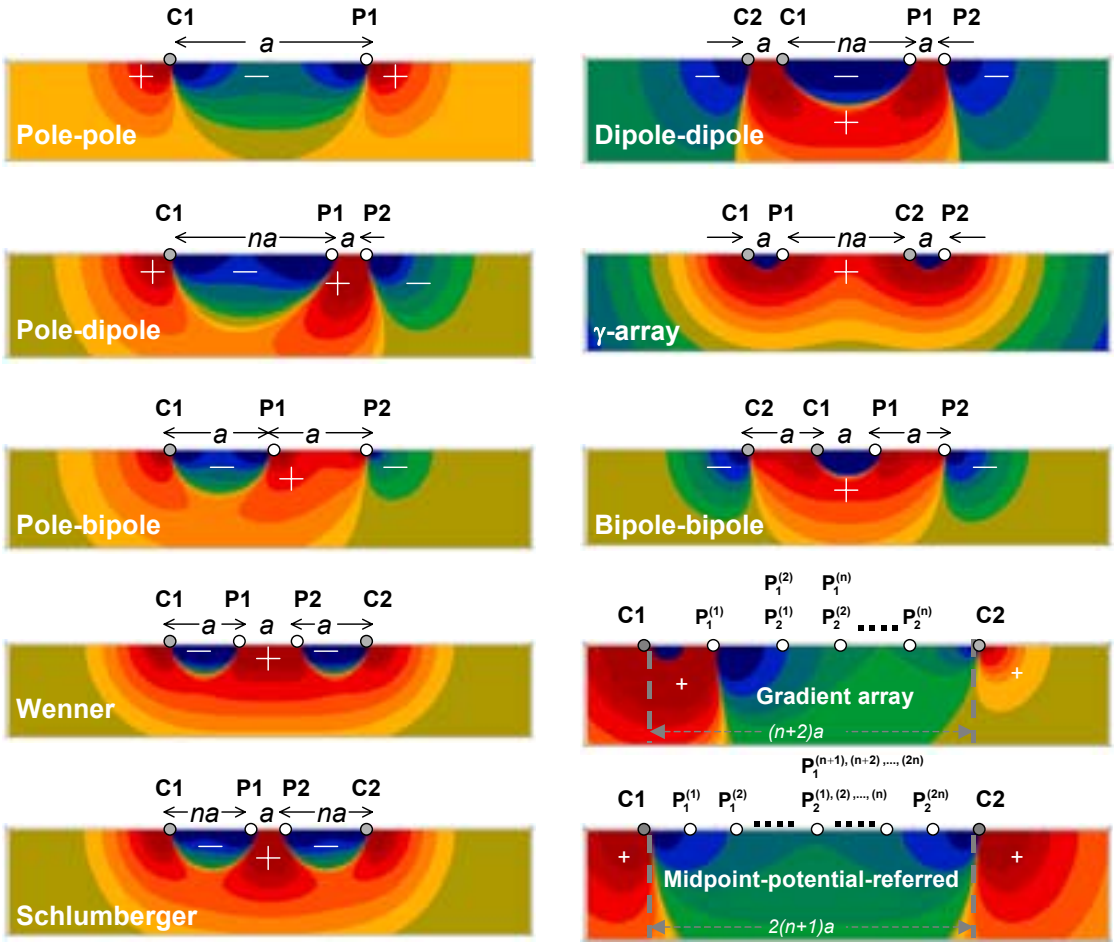

Figure 9-1: Schematic representations of electrode arrays and their sensitivity patterns of 2D resistivity survey. C1 and C2 are positive and negative current electrodes. P1 and P2 are two potential electrodes. The italic letters a and n are the array parameters that control the spacing and maximum separation of the arrays in a multi-electrode layout. For the gradient array and midpoint-potential-referred array the background shows the sensitivity pattern for the first potential electrode pair.

In two-dimensional (2D) electrical imaging, the data acquisition is done by scanning the electrode layout with several different electrode separations (*a*) along a line of some tens of electrodes (see e.g. Dahlin 1996). If applicable for the electrode array in question different n-factors are also used (Figure 9-1).

Table 9-1: Examples of surveying schemes for 2D resistivity imaging based on 81-electrodes layout.

Configuration	Survey 1	Survey 2	Survey 3
Pole-pole	a=1~60 m, scanning for each electrode, data points: 3030.	a=1~60 m, scanning for every two electrode, data points: 1530.	a=1, 3, 5, ..., 59 m, scanning for every two electrode, data points: 765
Pole-dipole	a=1, 3, 5, 8 m, n=1~6, forward & reverse scanning for each electrode, data points: 2970	a=1, 3, 5, 8 m, n=1~6, forward & reverse scanning for every two electrodes, data points: 1500	a=1 m, n=1, 2, 3; a=3 m, n=2, 3, 4; a=5 m, n=3, 4, 5; a=8 m, n=4, 5, 6; forward & reverse scanning for every two electrodes, data points: 716.
Pole-bipole	a=1~30 m, scanning for each electrode, data points: 3000.	a=1~30 m, scanning for every two electrodes, data points: 1530.	a=1, 3,..., 29 m, scanning for every two electrodes, data points: 780
Wenner			a=1~20 m, scanning for each electrode, data points: 990.
Schlumberger		a=1~5 m, n=1~6; scanning for each electrode, data points: 1710.	a=1 m, n=1, 2, 3; a=2 m, n=2, 3, 4;a=3 m, n=3, 4, 5; a=4 m, n=4, 5, 6; scanning for each electrode, data points: 780.
Dipole-dipole	a=1~7 m, n=1~6; scanning for each electrode, data points: 2478.	a=1~7 m, n=1~6; scanning for every two electrodes, data points: 1254.	a=1~7 m, n=1, 3, 4, 6; scanning for every two electrodes, data points: 836.
Wenner-β			a=1~20 m, scanning for each electrode, data points: 990.
g-array	a=1~7 m, n=1~6; scanning for each electrode, data points: 2478.	a=1~7 m, n=1~6; scanning for every two electrodes, data points: 1254.	a=1~7 m, n=1, 3, 4, 6; scanning for every two electrodes, data points: 836.
Gradient array	a=1, n=15, 30, 58; scanning for each electrode, data points: 3648	a=1, n=15, 30, 58; scanning for every two electrode, data points: 1861.	a=1, n=13; a=2, n=13; a=3, n=18; scanning for every two electrode, data points: 965.
Midpoint-potential-referred	a=1, n=9, 19, 29; scanning for each electrode, data points: 3874	a=1, n=9, 19, 29; scanning for every two electrode, data points: 1994	a=1, n=6; a=2, n=6; a=3, n=9; scanning for every two electrode, data points: 930.

The behaviour of the ten electrode arrays for imaging five synthetic models, intended to reflect some geological structures in practice, was investigated numerically. The arrays analysed include pole-pole (PP), pole-dipole (PD), pole-bipole (PB), Wenner (WN), Schlumberger (SC), dipole-dipole (DD), Wenner-β (BB), g-array (GM), gradient (GD) and mid-point-potential-referred array (MPR). Figure 9-1 shows the electrode configuration of each array type, and the sensitivity function of each array. The sensitivity function, or Frechet derivative, shows the relative contribution of different parts of the subsurface, and is a key factor in the resolution capability of an electrode array. The sensitivity function shown here was calculated for homogeneous earth, and it modifies with changes in the resistivity distribution of the ground.

9.2 Modelling approach

Five synthetic geological models intended to simulate a buried channel, high resistive and low resistive narrow dykes, dipping blocks and covered waste ponds were used to examine the surveying efficiencies (anomaly effects, signal-noise ratios) and the imaging capabilities of these arrays.

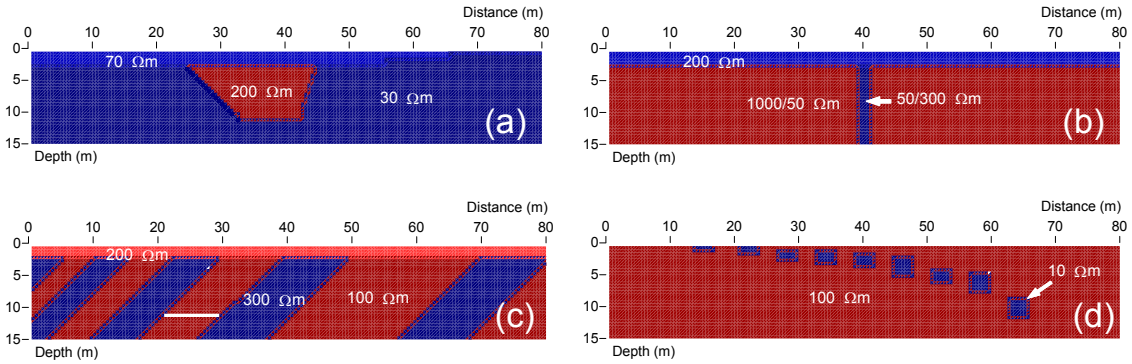

Figure 9-2: Synthetic models for numerical imaging experiments. (a) A simplified model of an old river channel in a clay environment covered by silty sediments, (b) a dyke model that represents a fractured or weathered zone in crystalline rock under a cover of coarse-grained sediment, a model with same geometry but high resistive dyke was also used, (c) dipping blocks with different widths that was intended to simulate a sedimentary rocks under a layer of till, (d) a waste pond model simulating a field site in southern Sweden.

Also, the importance of the data density and noise sensitivities of these electrode configurations were investigated using the robust inversion and smoothness-constrained least-squares inversion for the four synthetic models. The different surveying schemes with three different data density levels is summarised in Table 9-1. Two commonly used inverse schemes—robust (L_1-norm) inversion and smoothness-constrained least squares (L_2-norm) inversion—were applied to this work and a comprehensive comparison of the ten electrode arrays for 2D resistivity imaging was made. The comparison was conducted in the following aspects: resolution for the different geological models, imaging quality with different data densities and sensitivity to noise levels.

Anomaly effect, developed by Militer et al. (1979), is commonly used to evaluate the effectiveness of resistivity measurements of an electrode array. From the imaging point of view, an effective survey should have a significant value of the anomaly effect, which is desirably larger than the background noise. A 2.5D resistivity modelling software (Zhou and Greenhalgh, 2000) was used to calculate the anomaly effects of the electrode arrays on the five synthetic models, calculated as the mean values of the absolute anomaly effects by the potentials generated with and without the geological targets (buried channel, narrow dykes, dipping blocks and waste ponds) respectively. Figure 9-3 gives the results for all the eight electrodes and three surveying schemes. From these diagrams, one can see that the anomaly effects of the arrays vary with the geological models, i.e. PP has the smallest values of the anomaly effect on the buried

channel and waste pond structures (see Figure 9-3 a, d), but on the dyke and dipping block models it gives the largest values among these arrays (see Figure 9-3 b, c). On the dyke model WN, SC and GM present much lower anomaly effects than other arrays (see Figure 9-3 b), but on the other three models they offer approximate values to the ones of PD and PB. One also can see that the three surveying schemes in Table 9-1 do not significantly affect the average anomaly effect on the four geological models.

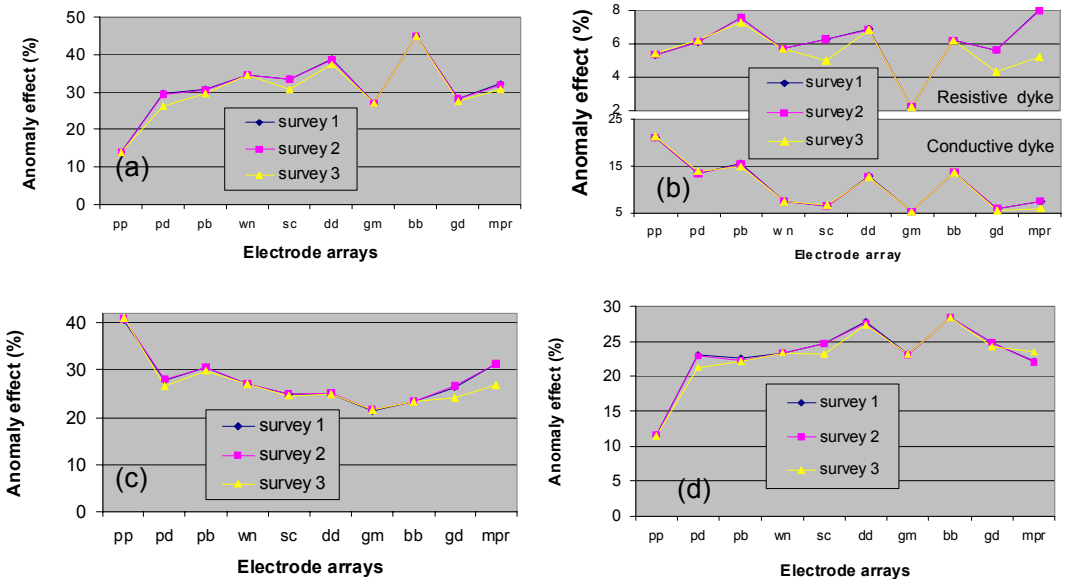

Figure 9-3: Average anomaly effects of imaging surveys on the five geological models tested. This shows that the anomaly effect of an electrode array varies with geological models, and the three surveying schemes in Table 8-1 have nearly the same average anomaly effects.

According to the anomaly effects (Figure 9-3) and the possible noise contaminations (see section 7), we estimated the signal-noise ratios of the imaging surveys for these electrode configurations and synthetic geological models. Figure 9-4 gives the comparison of the signal-noise ratios of the electrode arrays. From this figure, we can see that except the case of the narrow conductive dyke GM and WN have relative high signal-noise ratios, PD and DD give relative low signal-noise ratios in observations, and PP presents high values for the narrow dyke and buried dipping blocks and low values for the buried channel and waste ponds. However, in practice PP may have lower signal-noise ratio due to noise picked up by the potential reference electrode.

In addition, it should be mentioned that these electrode arrays apart from having different effects of spacing errors or small geological disturbances, which was not included in the synthetic noise applied here, they have different sensitivities to 3D effects. The sensitivity to 3D effects is being evaluated in an on-going study within this project as outlined in section 10.

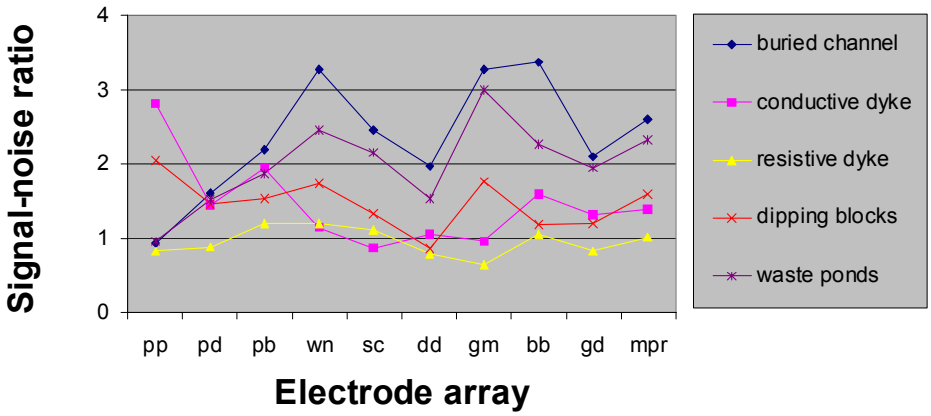

Figure 9-4: Synthetic signal-noise ratios of the imaging surveys with different electrode arrays over the five geological models.

9.3 Example result: buried alluvial channel

One example of the inverted models, representing a buried alluvial channel, is shown in Figure 9-2. The lowest data density investigated, and the data were contaminated by the potential-dependent random noises ranging from a mean of 8.3 % for GM survey to 19.4 % for DD array. The model sections resulting from the robust inversion are shown in Figure 9-5. From these results, one can see that in spite of the relative low noise levels in these surveys GM and BB give poor resolution in the bottom of the buried channel (see Figure 9-5 g-h), while PD and PB, with relative high noise level, produced better resolution of the images than the others (see Figure 9-5 b-c, the triangle-shaped channel can be clearly seen). DD also yielded a good resolution for this model, but below the target there appears a shadow zone of high resistivity (see Figure 9-5 f) which shows that the deep resolution is not as good as PD or PB arrays. This may be partly due to the highest noise level (19.4 %) of all the arrays, but also a consequence of the character of the sensitivity function. Meanwhile, one can see that WN and SC did not leave a shadow zone under the channel, and SC produced a slightly better resolution of the buried channel than WN (see Figure 9-5 d-e), but neither of them mapped the triangular shape of the target as well as PD, PB and DD. This indicates that the resolutions of WN and SC, even with relative low noise contamination (10.6% and 12.6%) and high signal-to-ratio (Figure 9-6), do not achieve the same resolutions of the shape as PD, PB and DD arrays. This figure also shows that the PP array (see Figure 9-5 a) yields a reasonably good image, but it apparently did not work as well as PD, PB and SC. The resolution of PP seems inferior to that of PD, PB, DD and SC, and it is notable that the thickness of the top layer is poorly mapped. One can see that GRD and MPR both work well for imaging the buried channel, but GR maps the shape much better than MPR does. This shows that even though the S/N-ratio of GRD is much lower than MPR, the spatial resolution of GRD is better than MPR. One also can see that there are some artifacts in the shallow part of the GRD image, while MPR seems quite clear in the top layer. Actually, the artifacts must relate to the noise contamination in GRD data, which was modelled with more noise than MPR.

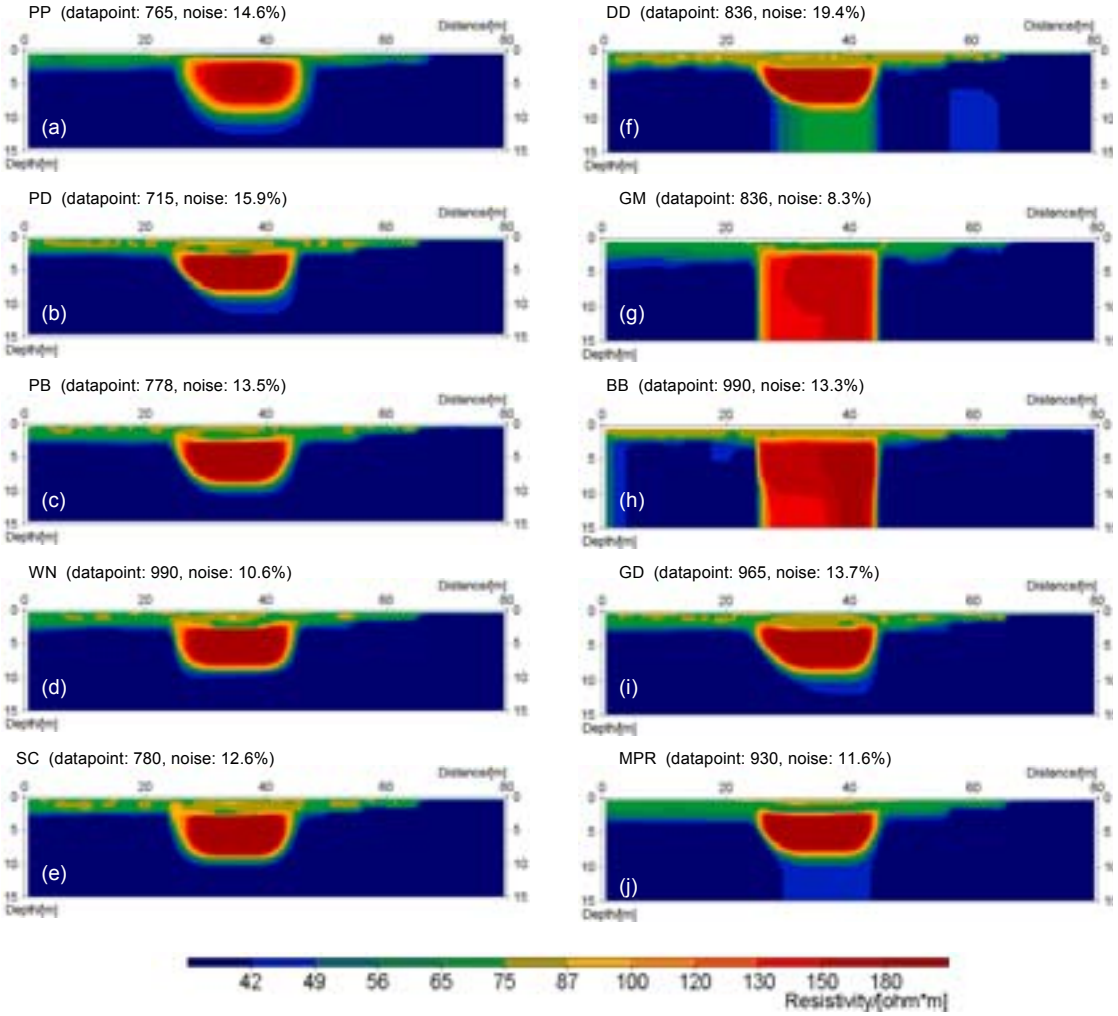

Figure 9-5: Inverted models of robust inversion for the buried channel shown in Fig. 3a. Here the data points (Survey 3) and the mean values of the potential-dependent random noise are given for the eight electrode arrays: (a) pole-pole, (b) pole-dipole, (c) pole-bipole, (d) Wenner, (e) Schlumberger, (f) dipole-dipole, (g) g-array and (h) Wenner-β, (i) gradient, (j) midpoint-potential-referred.

9.4 Data density

With the same 81-electrodes layout and the same maximum separation of electrodes, there are many options to choose imaging surveying schemes for PP, PD, PB, SC, DD and GM arrays, like the examples given in Table 10-1, which define different numbers of data points or data density. Generally, the dense data points are helpful to improve spatial resolution of imaging, especially for small targets having approximate scale to the basic spacing, and i.e. Dahlin and Loke (1997) gave an example for the resolution change with data density of WN imaging survey. They proved that it is necessary to employ small spacing or dense data in WN imaging survey for high resolution of the narrow dyke, but it can be pointed out that these results were based on experiments with lower data densities than in this work.

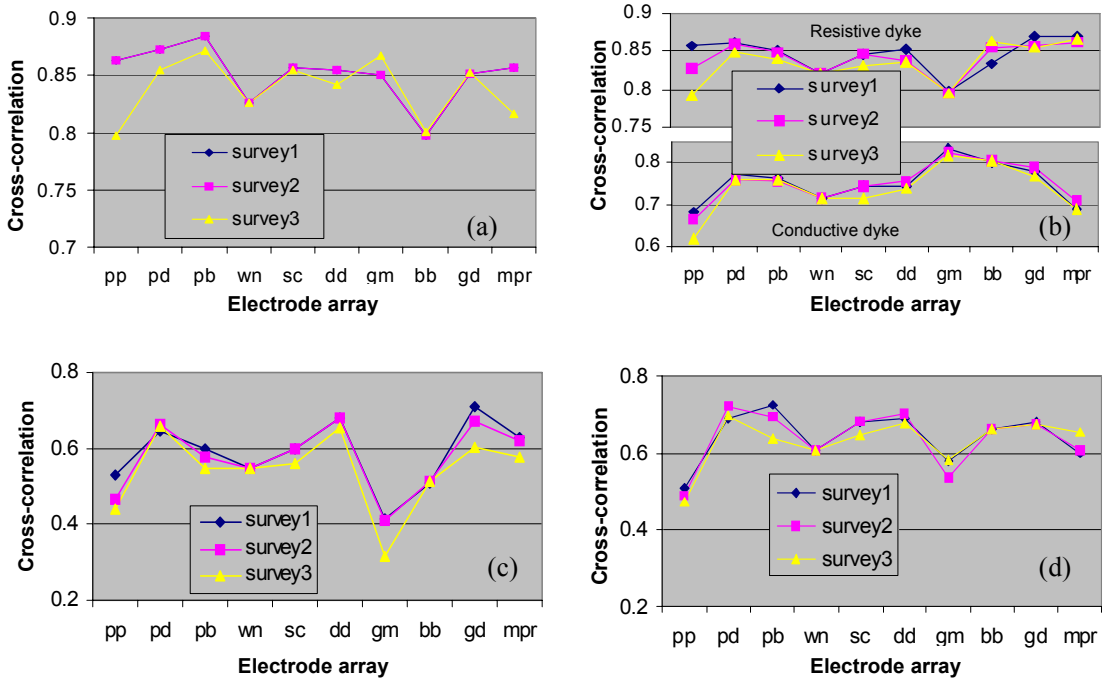

Figure 9-6: Cross-correlation curves of the robust (L1-norm) inverted models vs. the true models: (a) buried channel, (b) narrow dyke, (c) dipping blocks and (d) waste ponds. The three surveying schemes are given in Table 1.

Here, in order to detect the variations of imaging quality with the data densities of an electrode layout, or investigate an efficient surveying scheme of the arrays with a given electrode layout, we repeated all previous imaging experiments with the three surveying schemes with different data densities, Survey 1, Survey 2 and Survey 3 in Table 9-1, and calculated the cross-correlation values between the inverted models and the true models. The cross-correlation value quantitatively represents the match of two images, which may comprehensively reflect the imaging quality. Figure 9-6 and Figure 9-7 show the cross-correlation curves of the three surveying schemes against the different electrode arrays. These curves were calculated using the L_1-norm (robust) and L_2-norm (least-squares) inversion results.

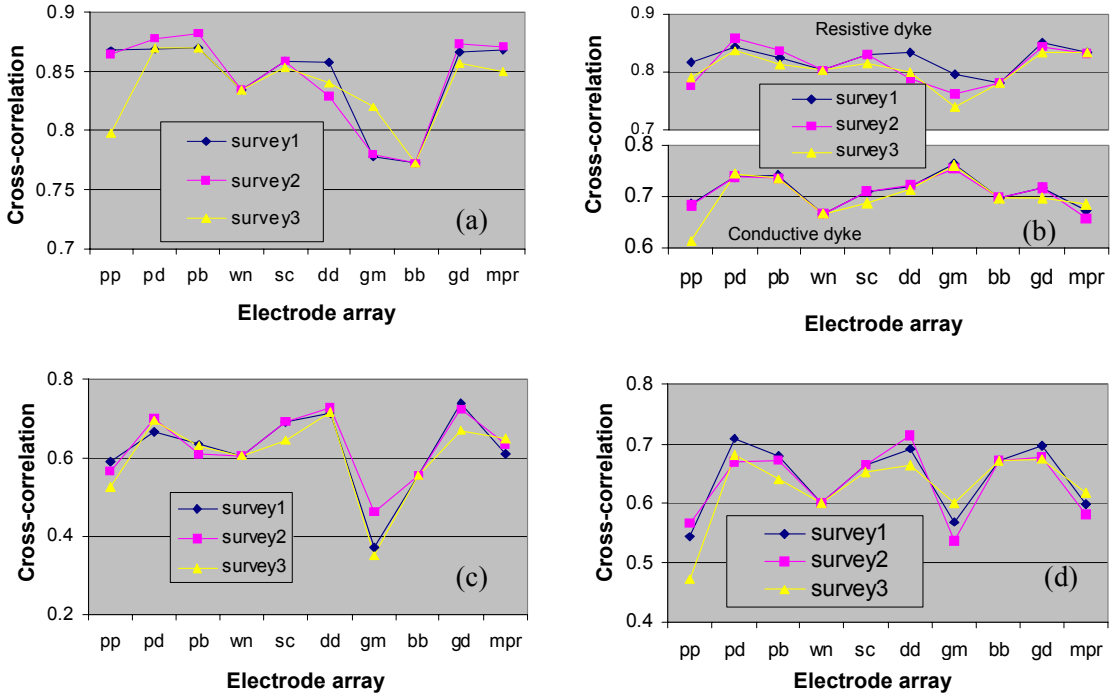

Figure 9-7: Cross-correlation curves of the least-squares (L2-norm) inverted models vs. the true models: (a) buried channel, (b) narrow dyke, (c) dipping blocks and (d) waste ponds. The three surveying schemes are given in Table 1.

Actually, Figure 9-6 and Figure 9-7 give summary views of the imaging quality of the arrays for the five models, meanwhile illustrating the variation of the imaging quality with the three surveying schemes. Comparison of the results obtained with the three surveying schemes show that they are mostly rather robust to data density variations, but that the step from Survey 3 to Survey 2 may give a significant increase in the cross-correlation value. This is particularly true for PP and GM, which are quite sensitive to data density for some models, apart from giving the poorest overall results. This means that with the same electrode layout and maximum separation of electrodes, the imaging quality of an array survey is not so sensitive to the data density within the limits tested here. In other words, the high data densities, beyond what can be achieved with WN and BB, with an electrode layout did not in all cases significantly improve the imaging quality, but it does cost much more time to acquire the highly dense data in a field with a typical multi-electrode data acquisition system. These experiments imply that an efficient imaging survey may be employed by choosing appropriate parameters n and a of the arrays, i.e. Survey 3 in Table 9-1 for PD, DD, SC and GD arrays, where they did not necessarily scan all n and a in the imaging surveys, but yielded comparative resolutions of the images with the highly dense data. Also, one can see that MPR has an imaging quality corresponding to WN, while GD may produce an image quality that is clearly competitive with PD, SC and DD.

9.5 Comparison of electrode arrays

From the above numerical simulations, the main advantages and disadvantages of these arrays for 2D resistivity imaging surveying may be summarised as follows:

9.5.1 Pole-pole

Pole-pole is a simple electrode configuration that makes it easy to automate the data-acquisition and to check data quality with reciprocity in a field, but it employs two remote electrodes that limit its applications to accessible sites. The anomaly effect and signal-to-noise ratio of the imaging survey may be relative high or low, it depends on geological models, but the theoretical noise-contamination generally stays at moderate levels comparing with other arrays. However, the imaging resolution sits a low rank among the eight electrode configurations. In addition, the remote potential electrode may pick up ambient noise, which was not included in the modelling above.

9.5.2 Pole-dipole and pole-bipole

Although having moderate anomaly effects and relatively low signal-to-noise ratios, both pole-dipole and pole-bipole can yield better spatial resolution images than PP, SC and WN. At some cost of spatial resolution, PB may obtain a somewhat better signal-to-noise ratio due to the strengthened measured signals by increasing the potential electrode spacing, which effectively reduces the noise contamination. A disadvantage is the use of one remote electrode that also limits the surveys to accessible sites, and the remote electrode complicates data quality checks via reciprocal measurements since the remote potential electrode the noise will be higher.

9.5.3 Wenner and Schlumberger

These two arrays have similar behaviours of imaging ability due to the resemblance of their electric field and measurements, with their main strength in the depth determination that is good in relation to other arrays. As a special case of SC, WN generally has less noise contamination and better signal-to-noise ratios than SC, as well as than PD, PB, DD and BB arrays (except for the narrow dyke). But the spatial resolution of WN is behind the PD, DD PB and SC surveys, while the SC survey, even with a little loss of the signal-to-noise ratio, may offer an improvement of the imaging resolution of WN. They also have the same problem that the reciprocal configuration surveys are more prone to pick up noise than the normal when controlling the data quality.

9.5.4 Dipole-dipole and Wenner-β

Generally, DD has relative high anomaly effects but more risk of noise contamination than others, so it often produces low signal-ratios in surveys comparing with BB, WN and GM. Both arrays have symmetric electrode configurations with normal and reciprocal measurements, which facilitates control of the data qualities so as to obtain a reliable and good resolution image of the surveys. However, the imaging resolution of DD is comparative to PD and better than others, particularly for location of vertical and dipping structures whereas the depth resolution is not the best. BB, a special case of DD, has a certain improvement of the signal-to-ratio of DD survey, but it more or less loses the spatial resolution of DD. Meanwhile, one should note that these two arrays are

much more sensitive to the spacing errors (Dahlin and Zhou 2001) and 3D geological bodies than other arrays (Dahlin and Loke 1997). It may be noted that the highest n-factor used in the modelling was 6, and it is often not advisable to go beyond that in real situations due to the very low signal-to-noise ratios it gives rise to.

9.5.5 Gamma

The main advantage of the Gamma array is the lowest noise contamination of the imaging survey in all the arrays, but the anomaly effects and signal-ratios are not consistently high, and the spatial resolution of the imaging is not as good as other arrays.

9.5.6 Gradient and midpoint-potential-referred

Gradient measurement and mid-point-potential-referred survey are two suitable electrode configurations for a multi-channel recording system. The numerical imaging experiments with five synthetic models show that GD scanning measurement can produce a competitive image with DD and PD, which have good spatial resolutions in resistivity imaging. MP, comparing with GD, wins a relative high S/N in survey but lose somewhat spatial resolution in the image. The resolution capability of MP catches up WN's but with more efficient data-acquisition when it applied to a multi-channel recording instrument. Both of the configurations may be employed for the practical applications. The imaging quality of the two configurations is robust to the data density. It may be a reasonable choice for the 2D resistivity imaging with a multi-channel recording system.

9.6 Conclusions

Accordingly, the numerical modelling work suggests the priorities of the PD, GD, DD and SC electrode configurations for 2D resistivity imaging survey, whose imaging qualities are relatively robust with the data densities of a multi-electrode layout. The final choice for a particular survey depends on the site conditions, field logistics, target of the survey and the equipment at hand.

At sites with noise problems DD is least suitable due to the low signal-to-noise ratio, although repeated measurements give additional possibilities to compensate for this by time based data filtering procedures. A further limitation of the DD array is that it appears to be more sensitive to 3D effects, which needs further evaluation through 3D numerical modelling. PD might be unpractical for dam monitoring installations due to difficulties in secure installation of a suitable remote electrode. Apart form this PD appears very suitable. Both SC and GD are suitable arrays for dam monitoring, but the gradient array holds a clear advantage in the better sensitivity near the ends of the electrode layout, which is often crucial in dam applications.

Good spatial resolution is strongly requested in most dam monitoring situations. Leakage zones are likelier to be horizontal than vertical (due to the construction procedure of dams), and if good resolution of the vertical change is desired DD should

be avoided. Need for depth resolution ability depends on the size of the dam and the situation.

It can be pointed out that a relatively high anomaly effect, high signal-ratio and low noise contamination does not always produce a good resolution image. This is demonstrated by the limited resolution capabilities of the PP, WN, BB and GM arrays.

10 2.5D RESISTIVITY MODELLING OF EMBANKMENT DAMS

10.1 Introduction

The study aims at improving current long term monitoring routines at two embankment dams in the north of Sweden and increase the understanding when interpreting existing data from these dams. For this purpose special software was developed as a tool for modelling resistivity distribution in earth embankment dams. The study comprises evaluation of the influence from 3D effects due to the specific dam geometry, and effects of reservoir water level and resistivity variations. Moreover a comparison between four different electrode arrays is carried out.

10.2 Software description

The software program was originally written for 2.5D resistivity/IP modelling with the finite element method and valid for calculation of potential, apparent resistivity or IP responses for a model with arbitrary geometry in the plane parallel to the electrode layout direction. Topographical modelling is possible and any electrode configurations, e.g. surface, crosshole or mise-a-la-masse off-line and in-line measurements with pole-pole, pole-dipole, dipole-dipole, Schlumberger and mixed arrays (Zhou 1998; Zhou and Greenhalgh 2000). The software was adapted to suit dam geometries by allowing an arbitrary variation in resistivity in the plane perpendicular to the electrode layout direction. The resistivities must be constant in the electrode layout direction, i.e. along the dam, and is thus assumed to have infinite extension.

10.3 Model geometry, material properties and damage types

The dam model is a rockfill embankment dam with a central moraine core and surrounding filter zones (Figure 10-1), which is by far the most common design of Swedish embankment dams. Geometry and design values are given in Table 10-1. The electrode layout is buried one meter into the top of the core at the midpoint of the cross section.

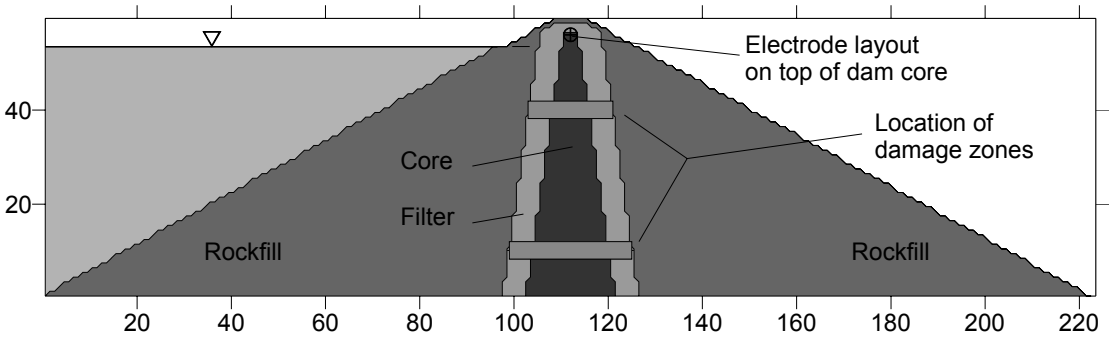

Figure 10-1. The modelled cross-section geometry. A rockfill embankment dam with a central moraine core and surrounding filter zones. The damage zones at depths 20 m and 50 m respectively are marked out but not their heights.

Electrical properties of involved materials are difficult to estimate and existing data is rare. The filter sand as well as the rockfill may be treated as an insulated matrix with all electrical conduction concentrated to the pore spaces. In this case Archie's law is applicable using porosity estimates. Regarding the core, however, the matrix can no longer be considered an insulator and other material models must be used. For this study the core resistivity was estimated from existing monitoring data from two Swedish dams (Johansson et al. 2000) together with laboratory resistivity measurements of similar moraines (Bergström 1998). Also the resistivity of the reservoir water was taken from monitoring data (Johansson et al. 2000). Electrical material properties are listed in Table 10-2.

Table 10-1. Dam geometry design parameters (se also Figure 10-1).

Dam height	60m
Crest width	8m
Upstream and downstream slopes	0.55:1
Distance: Top of core – crest	3m
Distance: Max reservoir level – crest	6m
Core width at top / bottom	4m / 20m
Filter thickness outside core: / top core	4m / 1m

Table 10-2. Electrical material properties.

Material	Resistivity [Ωm]
Core	300
Filter	2000
Upstream fill	4000
Downstream fill	20000
Reservoir water	550
Damaged core	1500

Due to software restrictions the modelled dam cross section must be identical along the whole length of the dam. Therefore it was impossible to simulate a concentrated cylindrical damage zone through the dam. Instead the damages simulated here are extended along the full dam length. As can be seen in Table 10-3, two different depths are examined. The first two types could be physically interpreted as damaged layers possibly resulting from less compaction at initial construction, whereas the final two types represent more widespread zones probably as a consequence of regional piping with a transport of fines from the core to the filter and fill.

Table 10-3. Damage types.

Damage type.	Thickness of damaged layer.	Depth from crest to centre of damaged layer.
Damage type 1. Thin seepage zone layer.	2 m	20 m
Damage type 2. Thin seepage zone layer.	2 m	50 m
Damage type 3. Large area with increased seepage.	10 m	20 m
Damage type 4. Large area with increased seepage.	10 m	50 m

A resistivity increase of five times in the core was assumed due to internal erosion. Experiments on similar moraines have shown that resistivity increases of up to 10 times due to removal of fines under water saturated conditions is likely to occur (Bergström

1998). However, this should be handled with care, as internal erosion increases porosity, affecting the resistivity in the opposite direction. The resistivity of the filter and fill was assumed not to change due to the simulated damages.

10.4 Methods and results

For all modelling situations four different electrode arrays were chosen. Those are the dipole-dipole (DD), pole-dipole (PD), Wenner-Schlumberger (WS) and gradient (GD) arrays (Figure 10-2) and they were chosen because they have shown robust imaging quality in prior modelling studies (Dahlin and Zhou 2001; Dahlin and Zhou 2002). An electrode spacing of five meters was assumed for the dam model. All combinations including a-spacings from one to seven (multiples of five) and n-factors one to six were used for the calculations, giving a total of 42 individual measurements for each array. Generally speaking the four different arrays demonstrated fairly similar responses for the different modelled situations. This was particularly true for the PD, WS and GD, which are all geometrically associated, and whose responses behaved very much in the same way. Of the four examined array the DD is the one that is to its nature somewhat different to the others, and in some situations it does seem to get responses that were different than the others. For this reason only results from DD and SC arrays will be presented here except for section 10.4.6, which deals more with comparing different arrays.

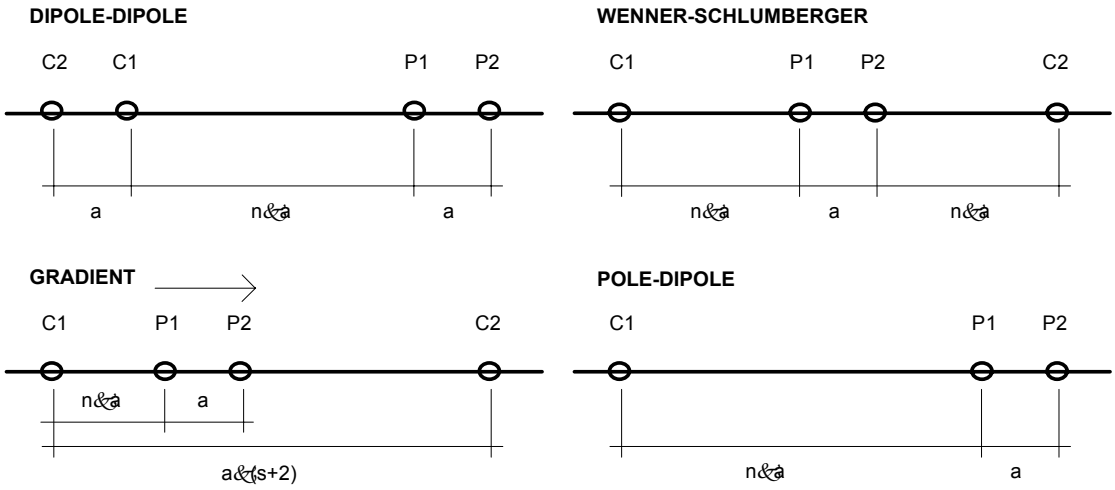

Figure 10-2. Electrode arrays used for the numerical modelling, and their geometrical factors a, n and s. For the gradient array n is derived from the shortest distance between a potential and a current electrode.

10.4.1 Three-dimensional effects

The 3D effects were examined by checking the differences between the 2.5D model response from the model cross section described in Figure 10-1 and a 1D model with the properties of the model mid section, i.e. the section with the electrode layout, extended to horizontal layers. Example results for the dipole-dipole and the Schlumberger arrays are shown in Figure 10-3.

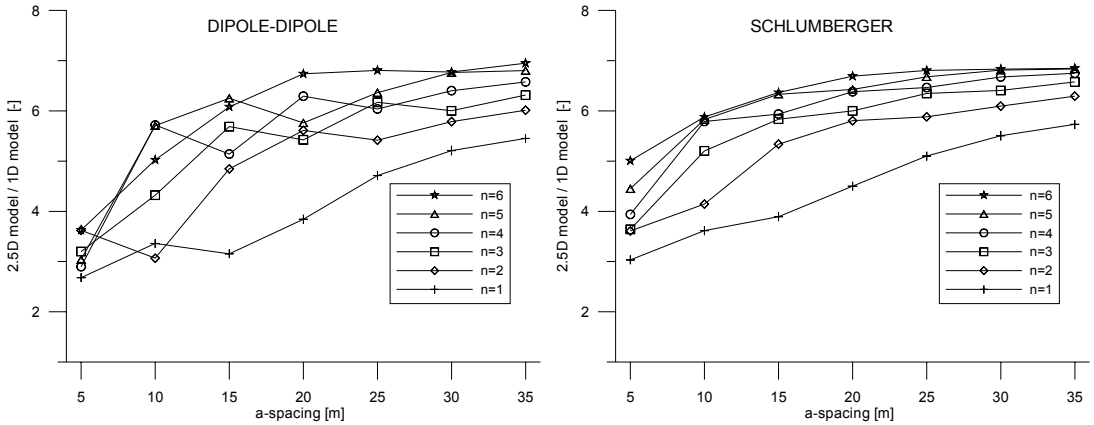

Figure 10-3. 3D effects estimated as relation between 1D and 2.5D models with assumed material properties for the modelled cross-section and reservoir. Dipole-dipole and Wenner-Schlumberger arrays with a-spacing 1-7 and n-factors 1-6.

It is obvious that a significant part of this huge 3D effect arises from the fact that the main part of the dam cross-section is rather high resistive. To evaluate the dependency of input material parameters the same evaluation was made with a constant resistivity of the whole dam cross section (and the reservoir water). The resulting 3D effect was then only related to the pure geometrical change and gave an increase in resistivity of about 30 percent for the 2.5D model (Figure 10-4).

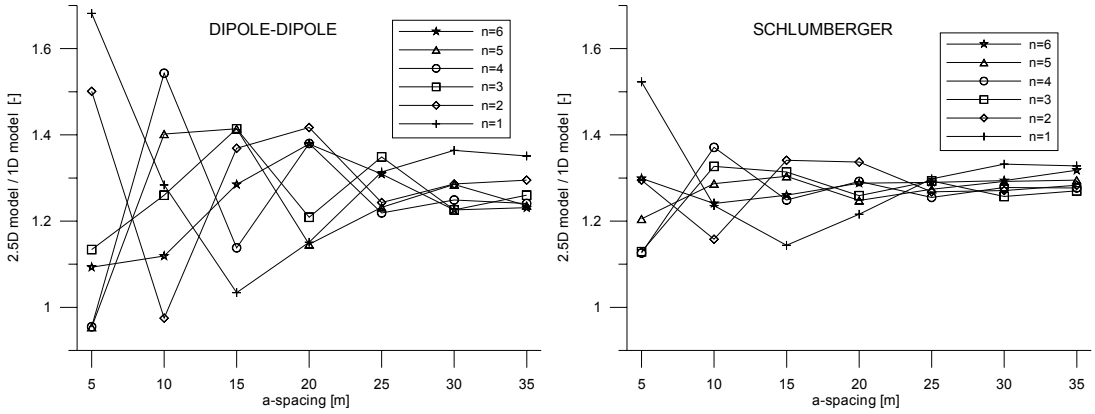

Figure 10-4. Purely geometrical 3D effects estimated as relation between 1D and 2.5D models with equal material properties in the whole cross-section and reservoir. Dipole-dipole and Wenner-Schlumberger arrays with a-spacing 1-7 and n-factors 1-6.

10.4.2 Reservoir level fluctuations

The reservoir water and its characteristics is the single most important factor when it comes to monitor resistivity inside embankment dams. Therefore it is essential to keep control of reservoir levels and to be able to foresee and estimate the effect of possible change in reservoir level on the measurements inside the dam. For this reason the effect of lowering the reservoir was examined, once again using the dam model in

Figure 10-1. Two scenarios were investigated; first an intermediate lowering of six meters from full reservoir at level +54m down to level +48m, and secondly a large lowering of 24 meters down to almost half the depth at level +30m. The calculations were made once for each depth and then output resistivities were compared with the original full reservoir model response (Figure 10-5, Figure 10-6). For the intermediate six meter lowering of the reservoir a change close to 14% were recognized for large electrode distances. For the large lowering of the reservoir the same effect was estimated moving towards approximately 40% for the largest electrode distances.

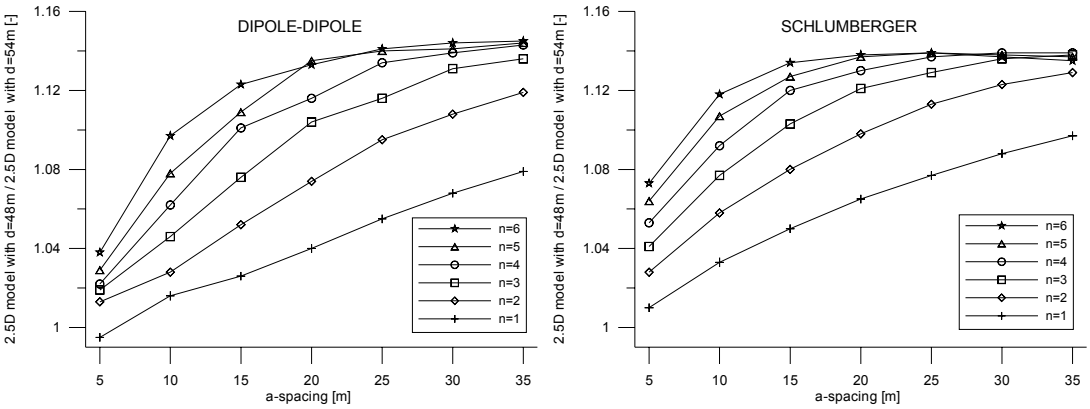

Figure 10-5. Influence on resistivity measurements along the crest from an intermediate lowering of the reservoir level from maximum level +54 m to the level +48 m. Dipole-dipole and Wenner-Schlumberger arrays with a-spacing 1-7 and n-factors 1-6.

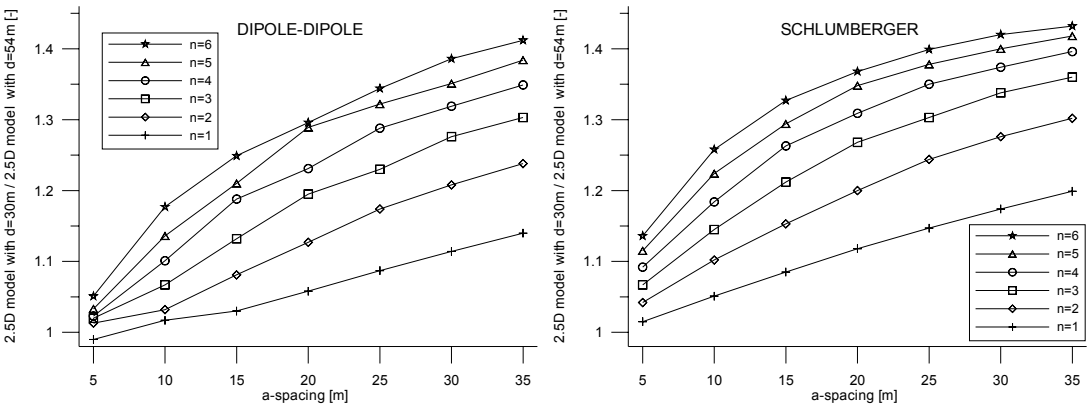

Figure 10-6. Influence on resistivity measurements along the crest from a large lowering of the reservoir level from maximum level +54 m to the level +30 m. Dipole-dipole and Wenner-Schlumberger arrays with a-spacing 1-7 and n-factors 1-6.

10.4.3 Seasonal reservoir resistivity variation

The change in characteristics of the reservoir water will as the water seeps through the dam influence on the resistivity measurements inside the dam. Long term monitoring in reservoirs at Swedish embankment dams show seasonal variation of the water resistivity typically fluctuating around 550 Ωm with peaks and lowest points at 800 Ωm and 300 Ωm respectively. A quick very rough estimation of the influence of change in reservoir

resistivity on the resistivity measurements along the dam crest was carried out using the standard model (Figure 10-1). Calculations were performed using the minimum and the maximum values for the reservoir resistivity with everything else being unchanged. Then the resistivities generated were compared with the standard model with a yearly average value of the water resistivity (Figure 10-7, Figure 10-8). The results show that only by changing the resistivity in the reservoir within the seasonal variation scheme an effect on the measurements of 10-15% above and below a standard measure might be expected. It is also clear that the effect increases with increasing electrode distances, which is expected, as a greater part of the current flow will then pass through the reservoir. Obviously, in reality the change in resistivity of the reservoir water definitely will lead to larger effects than we have seen here, as the water also affects resistivity of the materials of the dam body itself when it seeps through the dam.

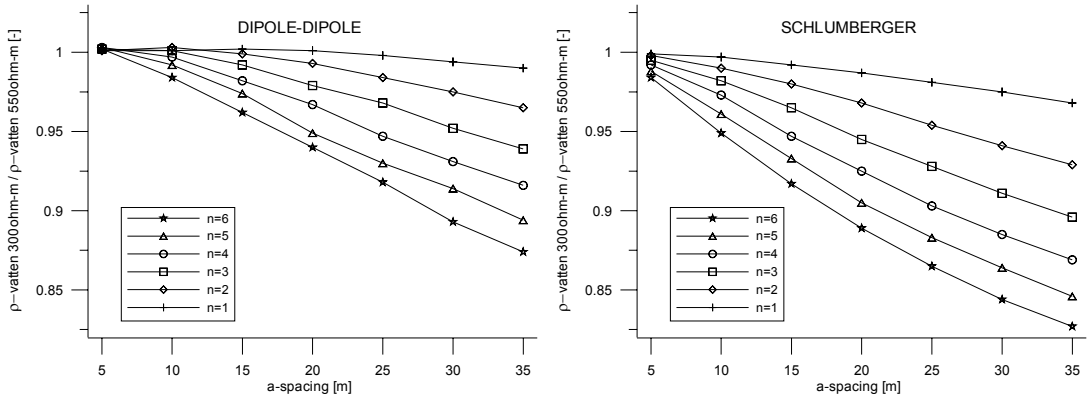

Figure 10-7. Influence on resistivity measurements along the crest from a change of the resistivity in the reservoir from 550 Ωm to 300 Ωm, symbolizing mean and minimum values from the seasonal variation. Dipole-dipole and Wenner-Schlumberger arrays with a-spacing 1-7 and n-factors 1-6.

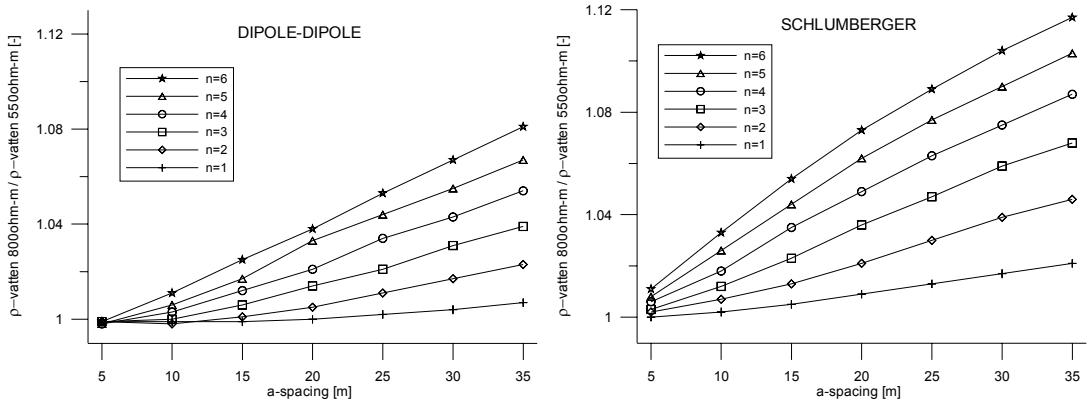

Figure 10-8. Influence on resistivity measurements along the crest from a change of the resistivity in the reservoir from 550 Ωm to 800 Ωm, symbolizing mean and maximum values from the seasonal variation. Dipole-dipole and Wenner-Schlumberger arrays with a-spacing 1-7 and n-factors 1-6.

10.4.4 Detectability of internal erosion zones

Principally there are two basic ideas behind detecting internal erosion in embankment dams with resistivity measurements. The first one uses the fact that internal erosion occurs with higher seepage flows and examines the resistivity variation scheme, i.e. phase lag and amplitude increase, and compares it with the variation in the reservoir. The second idea deals with the fact that the material properties will change as porosity increases and fines are being washed away when internal erosion occurs. In this case a permanent, or rather semi-permanent as it may heal by itself, change in resistivity characteristics of the dam core will occur in a particular zone. To be able to estimate the detectability of such changes four different internal erosion scenarios (Table 10-3) were set up and modelled using the model described in Figure 10-1.

The ability of detecting the simulated damage types was checked for each of the four chosen arrays. Anomaly effects from the simulated damage zones range from a few percent for damage type 2, small damage on large depth, and a few tenths of percent for damage type 3, large damage on shallow depth (Figure 10-9, Figure 10-10, Figure 10-11, Figure 10-12).

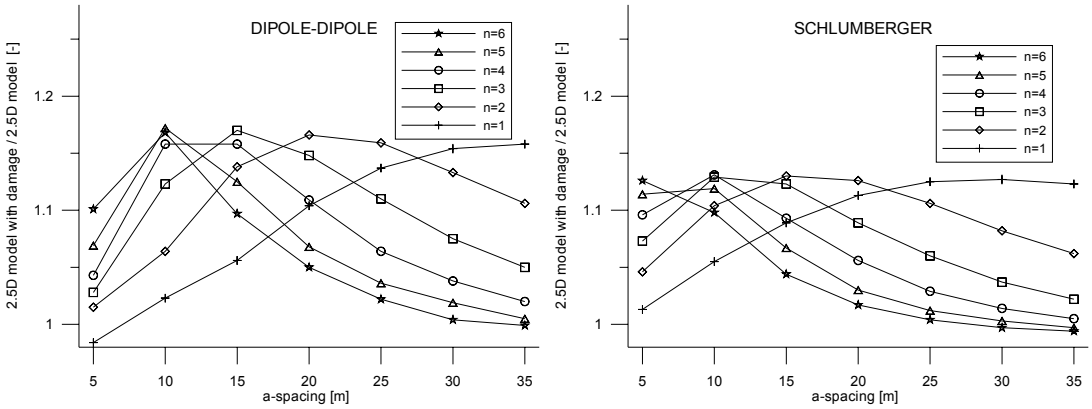

Figure 10-9. Anomaly effect from damage type 1, expressed as relation in apparent resistivities between the leaking model and the ordinary model. Dipole-dipole and Wenner-Schlumberger arrays with a-spacing 1-7 and n-factors 1-6.

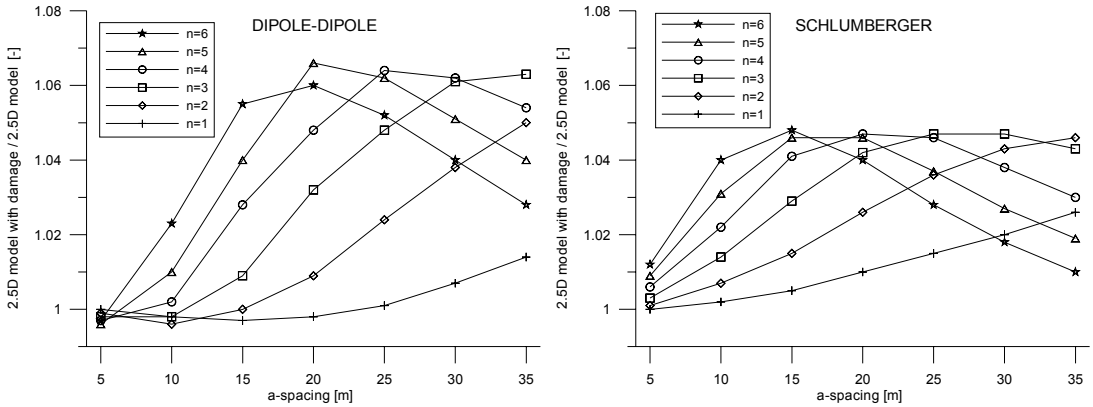

Figure 10-10. Anomaly effect from damage type 2, expressed as relation in apparent resistivities between the leaking model and the ordinary model. Dipole-dipole and Wenner-Schlumberger arrays with a-spacing 1-7 and n-factors 1-6.

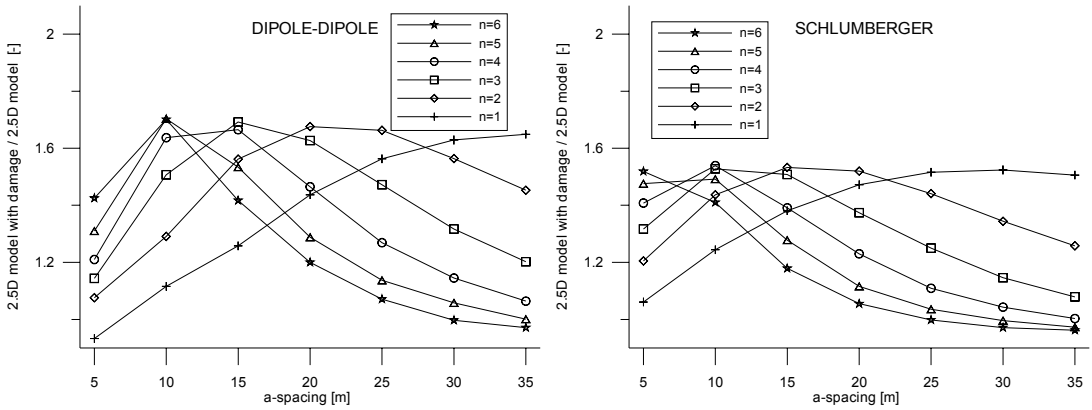

Figure 10-11. Anomaly effect from damage type 3, expressed as relation in apparent resistivities between the leaking model and the ordinary model. Dipole-dipole and Wenner-Schlumberger arrays with a-spacing 1-7 and n-factors 1-6.

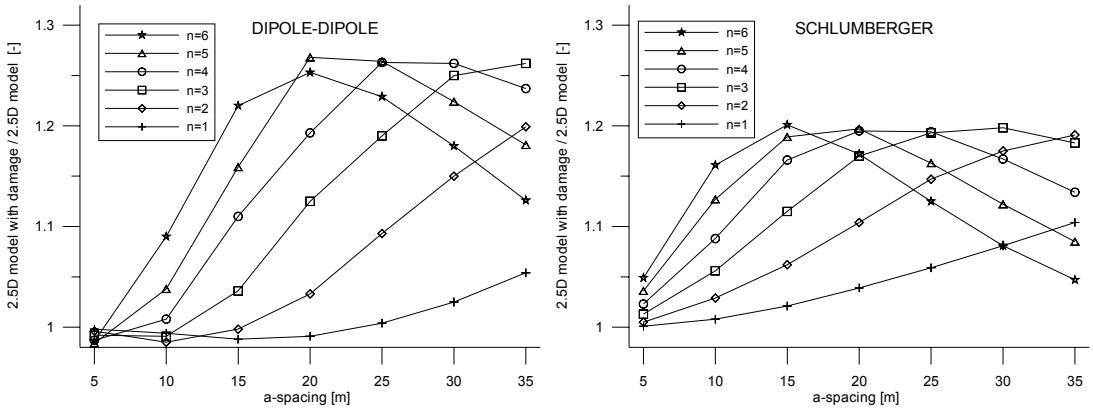

Figure 10-12. Anomaly effect from damage type 4, expressed as relation in apparent resistivities between the leaking model and the ordinary model. Dipole-dipole and Wenner-Schlumberger arrays with a-spacing 1-7 and n-factors 1-6.

10.4.5 Comparison of different layout locations

Modelling of different placement of layouts has been helpful for interpretation of data from Hällby where layouts are not only placed along the crest but also on the upstream and the downstream side. By using the standard model in Figure 10-1 together with a simulated damage zone described as type 4, large zone on large depth, in Table 10-3 the anomaly effect was calculated for four different placements of the layouts. These placements were, the upstream toe, the mid-upstream slope, the mid-downstream slope and the downstream toe. All of them are placed right beneath the surface of the dam; consequently the upstream electrodes are placed below the water table.

The results demonstrate that the four different layout placements are clearly inappropriate when it comes to detecting changes inside the core. The calculated anomaly effects are less than one percent for the layouts along the upstream and downstream toes, and for the mid-slope layouts the anomaly effect reaches one or a few percent at best. This must be regarded as clearly unsatisfying taking into account the size of the damage and the fact that a layout along the top of the core produces a clearly superior anomaly effect of around 25% for the dipole-dipole array (Figure 10-13).

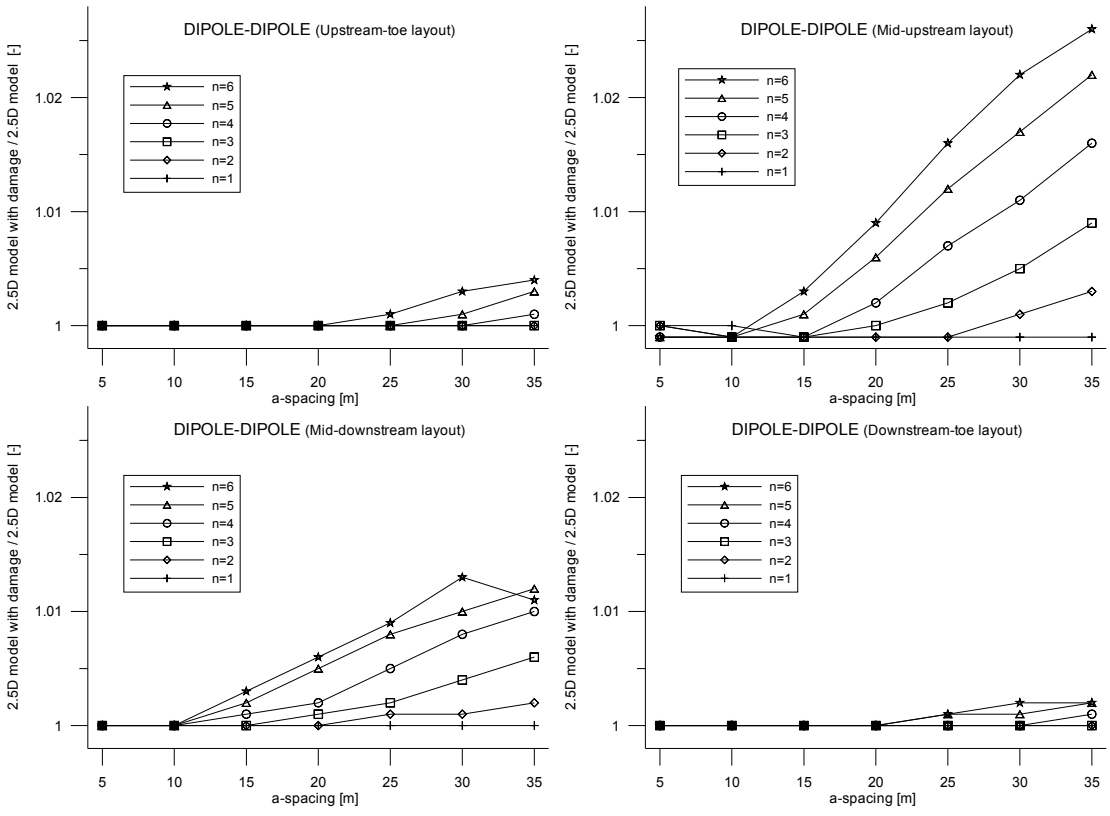

Figure 10-13. Anomaly effect from damage type 4 (large damage on large depth), expressed as relation in apparent resistivities between the leaking model and the ordinary model, using four different layout placements. Dipole-dipole array with a-spacing 1-7 and n-factors 1-6.

Obviously, the channelling effect that concentrates current flow within the conductive dam core is an important factor. However, in a real situation a possible internal erosion scenario might also bring about other effects detectable for these layouts, for instance an increased concentrated seepage close to downstream toe or in the foundation with associated temperature induced resistivity variation. In these calculations only a spatially limited change within the dam core is assumed.

10.4.6 Comparison of four different arrays

For the situations and scenarios that have been examined here, three of the four investigated arrays, GD, PD and SC, demonstrates very similar results. The fourth array, DD, differ to some extent depending on the situation. As an example the anomaly effect from damage type 1 for the four different arrays is arranged in Figure 10-14.

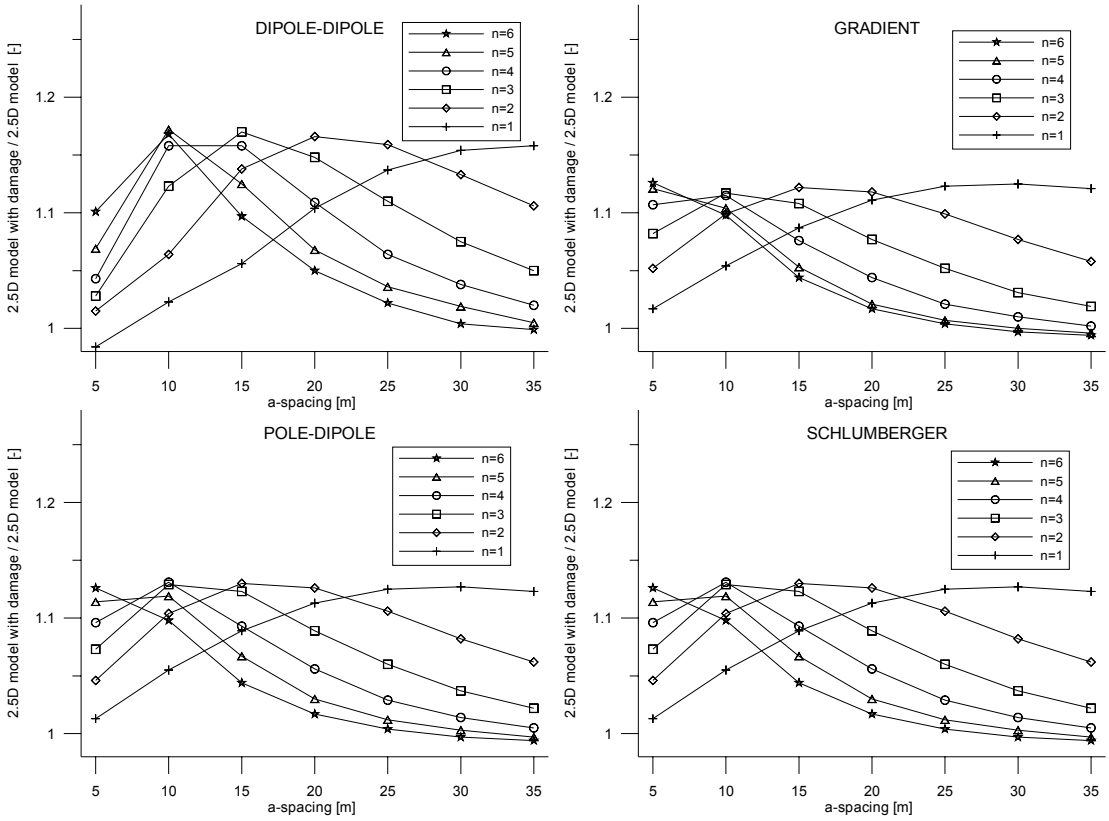

Figure 10-14. Anomaly effect from damage type 1 (smaller damage on shallow depth), expressed as relation in apparent resistivities between the leaking model and the ordinary model, using four different electrode arrays with a-spacing 1-7 and n-factors 1-6.

It is clear that when investigating constant cross-sections, i.e. no lateral changes, the differences in the design of the arrays will not fully show itself in the results. Only when examining special cases like cylindrical damages a full verification of the performance of the different arrays will be obtained. However, some basic conclusions can be drawn:

- The 3D effects are similar between all investigated arrays.
- Effect from fluctuations in reservoir levels is similar for all the investigated arrays, whereas the change in resistivity of the reservoir water seems to affect DD measurements less than the other arrays.
- All the different damage types (internal erosion scenarios) produces slightly higher anomaly effects using the DD measurements compared to the other arrays when measuring along the crest of the dam.

10.5 Discussion and conclusions

10.5.1 General

The developed software is very useful for dam resistivity modelling, as it can be used for assessing 3D effects, impact of water level changes and optimisation of electrode layouts.

The 3D effect of the dam geometry has a huge influence on the measured resistivity of the dam structure when the electrode layout is located along the dam crest. The influence is similar for all of the examined arrays and ranging typically from three to seven times the value of the standard 1D model for the geometry and material properties assumed. The effect is generally increasing with increasing current electrode distances, which could be expected as a larger earth body then is involved. The result is heavily dependent of the chosen electrical material properties, and more efforts will be put into making more precise estimations of electrical properties of the materials. However, even with a constant resistivity of the whole dam cross section the 3D effect is significant (around 30 percent) purely due to geometrical effects. The strong 3D effect also means that much of the current is concentrated in the conductive dam core, which enhances the possibilities to detect damage with electrode layouts along the dam crest.

Reservoir characteristics govern the resistivity variation pattern inside the dam. Reservoir elevation and resistivity of reservoir water is therefore crucial for interpretation of resistivity data from dam crest measurements. The resistivity measured along the dam crest is significantly influenced by fluctuations in the reservoir level. A drop in the reservoir level from 54m to 48m resulted in a change in measured resistivity of up to 14%. For the larger lowering of the reservoir down to 30m the resistivity was affected around 40%.

Anomaly effects from the simulated damage zones range from a few percent for damage type 2 and a few tenths of percent for damage type 3. Dipole-dipole has proved to give the largest anomaly effect for all of the damage types, whereas the others gave slightly lower but similar responses. However, since the dipole-dipole array is most sensitive to noise it may not necessarily be the optimal array in practical application. It should also be noted that all damage types were shaped as extended layers, and that the results may not be fully applicable to for instance a cylindrically shaped damage.

10.5.2 Conclusions for Hällby and Sädva

The performed studies have been beneficial for improving routines and increasing the understanding of the results from the monitoring programs at Hällby and Sädva.

The 3D effect is a general problem for embankment geometries but may be very much enhanced by a design with high resistive rockfill, which is the case in both Hällby and Sädva. The long-term solution is a 3D inversion code that takes care of geometrical factors, but that is not yet practically feasible. It should be mentioned that in the case of studying processes over time (monitoring) the 3D effects is of less importance.

Even if the limitation of only being able to simulate extended damage zones is a considerable drawback, it is still helpful for rough estimations of detection levels and optimisation of measurement configurations. Hopefully, this knowledge will be further developed with the near-future 3D modelling study.

Reservoir level fluctuations were not a problem when evaluating data from Hällby as they are very small and may be neglected. In Sädva however, large fluctuations occur and the results from this modelling study will be considered in the data evaluation process.

Modelling of different placement of layouts has been helpful for interpretation of data from Hällby where layouts are not only placed along the crest but also on the upstream and the downstream side.

11 SELF POTENTIAL MEASUREMENTS AT HÄLLBY

11.1 Self potential surveys

11.1.1 Survey layout

At Hällby only one survey was performed in September 2000. The reason for this was the small variation in reservoir level.

Land data was acquired along profiles, using the potential mapping method with the reference electrode situated downstream the right dam. The end points of the profiles were positioned using differential GPS measurements, and the stations along the profile were located with a tape measure. The electrodes were ordinary rugged copper-copper sulphate electrodes manufactured for the occasion. Voltages were measured using a Lawson Labs AD201 A/D-converter adapted for field use.

Offshore data was acquired through the gradient method, where a 5-metre and a 10-metre dipole were towed after a boat on the reservoir. The electrodes used were commercial, sealed, silver-silver chloride reference electrodes. They were towed at a depth of 1 metre. The location of the boat was determined by differential GPS, and the distance between the boat and the dipole was measured with a special hydro-acoustic transponder system. Dipole positions were consequently found by combining these data sets.

During the survey, the telluric activity was monitored, by registering the variation of the potential difference across two temporary crossed 50-metre dipoles placed in a field just above the left dam. Two multimeters connected to a laptop computer registered the voltages every two seconds.

11.1.2 Data processing

Telluric monitoring was performed to allow correction of the observed self-potentials. The correction was accomplished by measuring the electric field over the crossed dipoles and assuming this was valid for the whole surveyed area. Corrections to each station were then estimated by projecting the telluric electric field vector on the line connecting the base and the measuring stations and calculating the corresponding potential difference.

The offshore SP gradient values obviously depend directly on the direction of the dipole at the time of observation. Since the profiles were run in several directions the absolute value of the gradient is presented instead of pure gradients. The two data sets for the 5- and 10-metre dipoles are very similar; hence only data from the 10-metre dipole survey will be presented here.

For all maps simple kriging interpolation was used to create a regular grid of data before contouring.

11.1.3 Results

Figure 11-1 shows a contour map of the SP at Hällby. The spatial SP variation is generally calm. The only well-defined anomalies are the two positive anomalies that can be found in the innermost part of each dam. They both extend through the whole dam, from the upstream side to the downstream side. These anomalies are most probably not caused by seepage since they lack the bipolar character that generally is associated with seepage anomalies. The similarity between the anomalies on the different sides of the dam also suggests that they may be caused by sheet piles, which should be reasonably similar on the two sides.

On the right dam one can observe the expected behaviour, that SP-values become progressively more positive going downstream. On the left dam, however, there seems to be a weaker opposite trend. This is probably caused by influence on the steep topography. Topographic SP is likely the source of the negative SP-anomaly in the lower right corner of the map.

The map in Figure 11-2 show unprocessed gradient SP data. As was the case in Sädva, the gradients increase progressively as the dam is approached and there are strong gradients associated with the concrete structures in the centre of the dam.

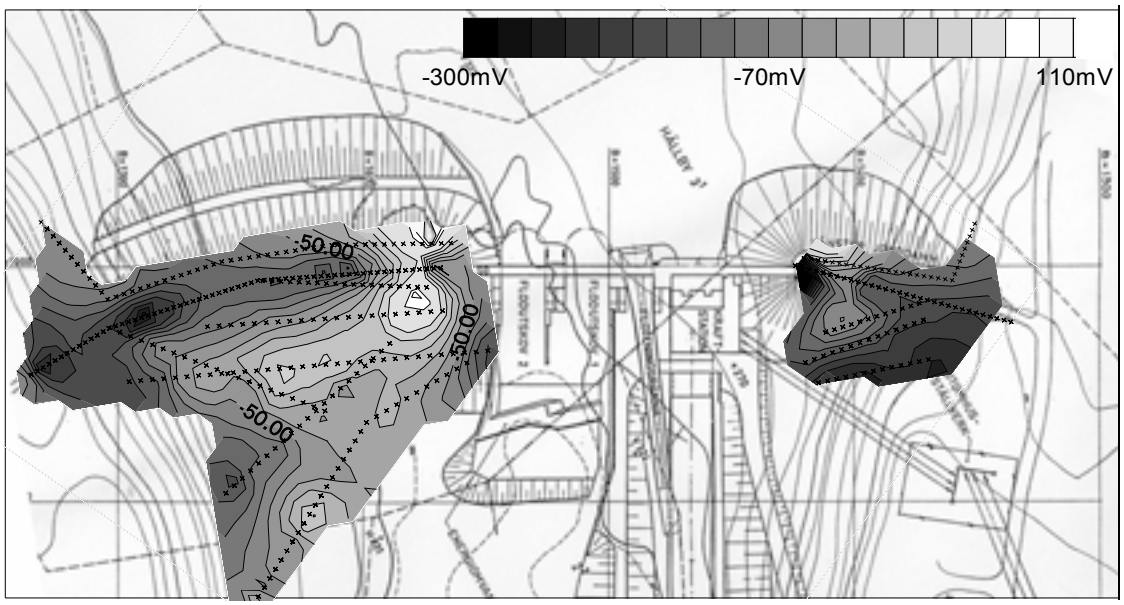

Figure 11-1: Contour map of SP data collected 000914-000917. The small black crosses show the positions of the measuring stations.

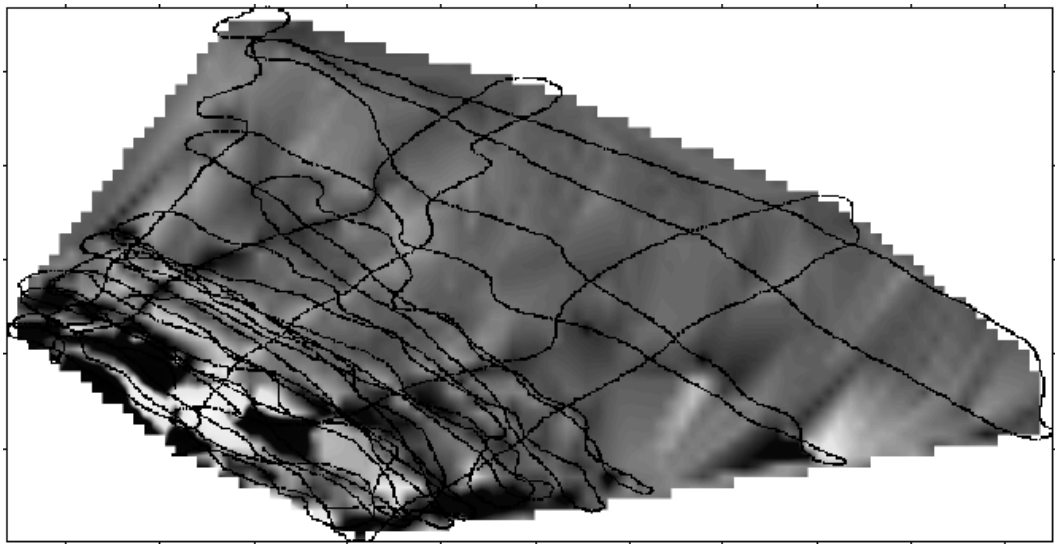

Figure 11-2: Image of offshore gradient SP-data. The image is rotated with reference to Figure 11 since positions are given in the Swedish national grid, not the local coordinate system employed at Hällby. The Dam is located in the lower left corner of the image.

11.2 Monitoring

11.2.1 Installation

SP data is collected with the same electrodes and measuring instruments as the resistivity data. The sections monitored are:

- Left dam crest
- Right dam crest
- Downstream right dam
- Upstream left dam (under water)
- Upstream right dam (under water)

11.2.2 Data processing

Raw data from all three profiles have high noise levels. It is therefore necessary to apply some filtering to the data before attempting to draw any conclusions from them. There are three distinct kinds of noise: instrument malfunction, spikes (both external and instrument generated) and random (not strictly) noise. The filtering used on all data consists of the following three discrete operations:

- Identify and remove occasions of obvious instrument malfunction (as indicated by the measured values locking at the end of the A/D converter range)
- Apply a spike removal filter
- Apply a 7-day running median filter

The implementation of the first and last filter types is quite straightforward, but the spike removal filter may warrant some more detailed description. The spike removal filter is implemented as a threshold filter based on a 25-day running median value. If a

data point deviates more than a given amount from this median value then it is replaced by a 7-day median centred on the data point.

Figure 11-3, Figure 11-4 and Figure 11-5 show time series plots of the measured SP at three selected locations. The plots illustrate the effect of the different filtering steps The bottom panes show raw data, the middle panes show data after spike removal and the top panes show data after spike removal and 7-day median filtering. In all cases the resulting data quality is acceptable. The spike at the start of the filtered time series is a filter edge effect that has consequently been removed by extending the time series before filtering and then truncating it back to the original length.

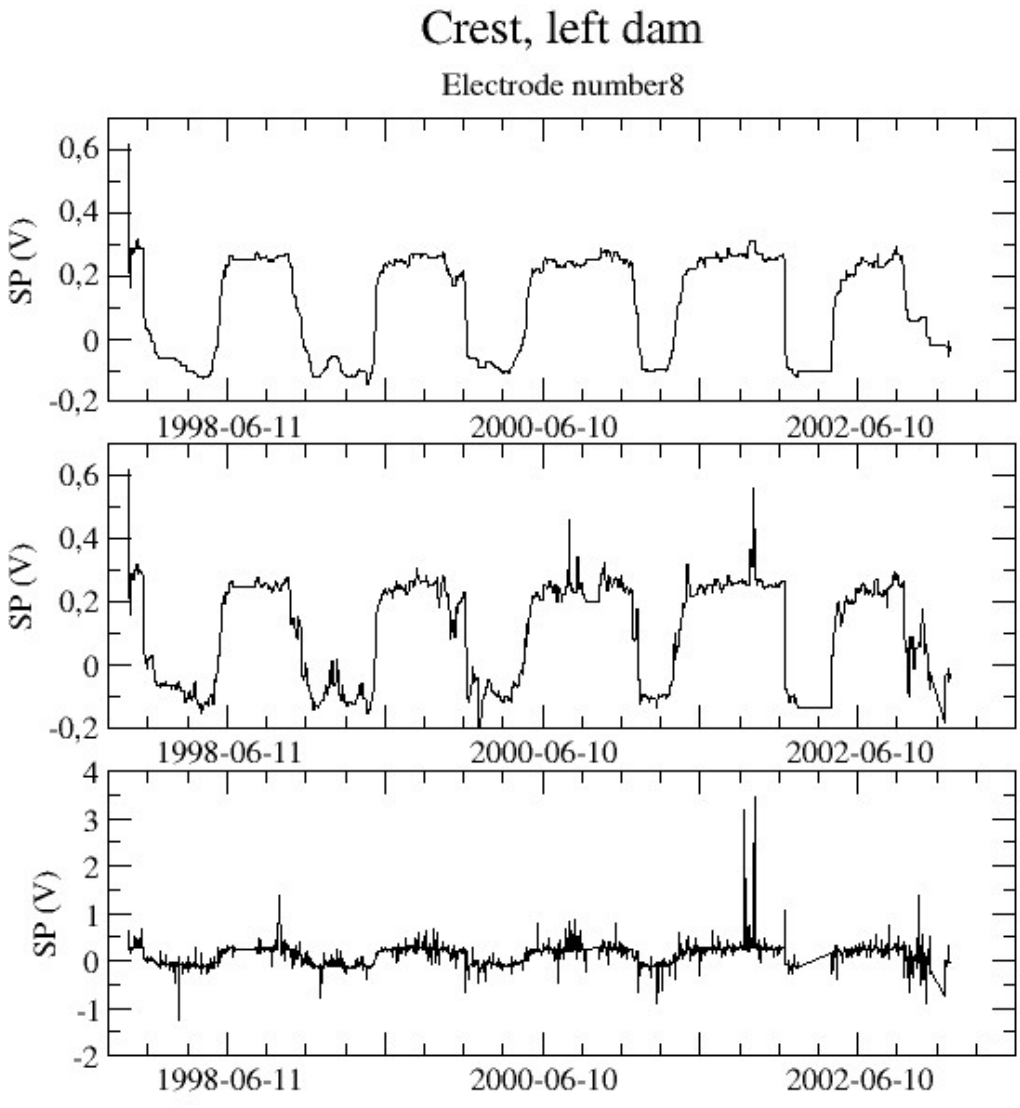

Figure 11-3: Time variation of SP for electrode 8 at the crest of the left dam. Raw data (bottom), spike removal filtered data (middle), spike removal and 7-day median filtered (top).

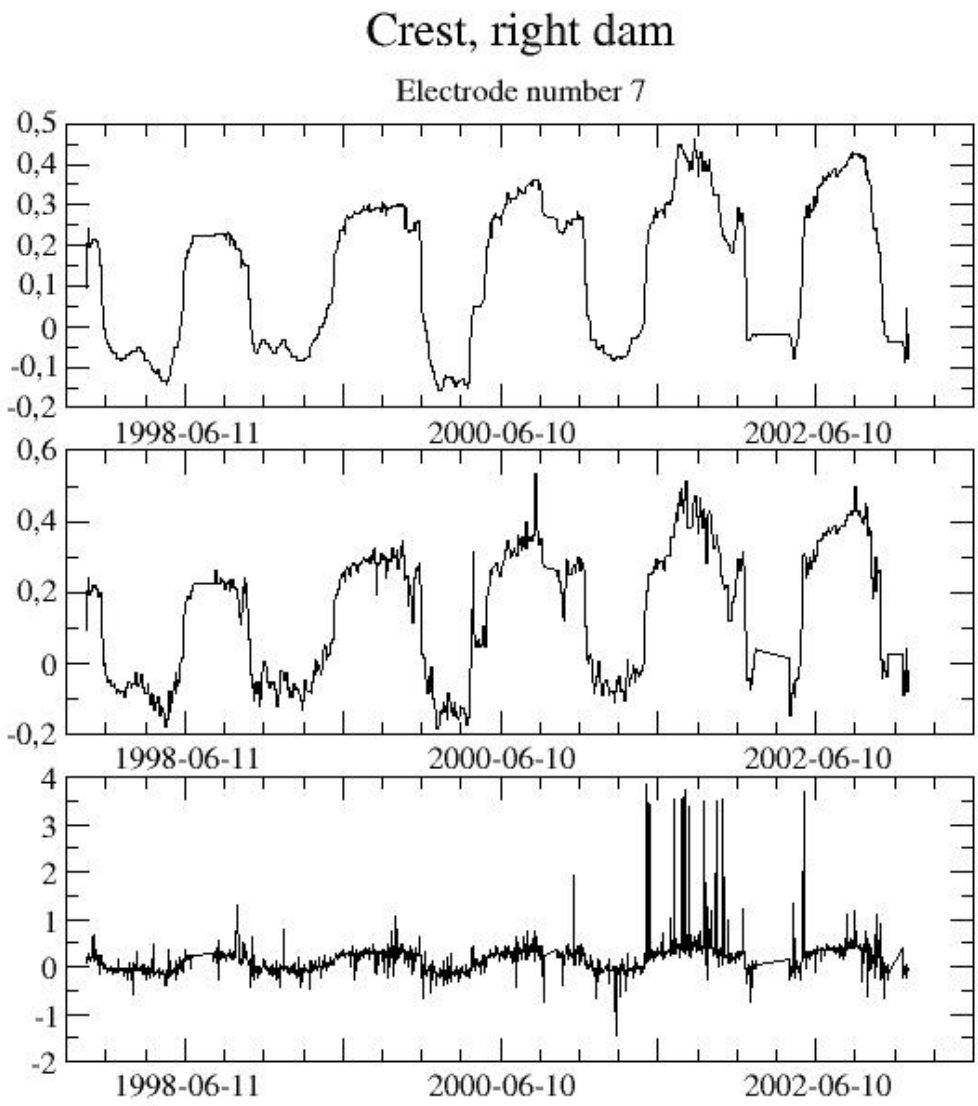

Figure 11-4: Time variation of SP for electrode 7 at the crest of the right dam. Raw data (bottom), spike removal filtered data (middle), spike removal and 7-day median filtered (top).

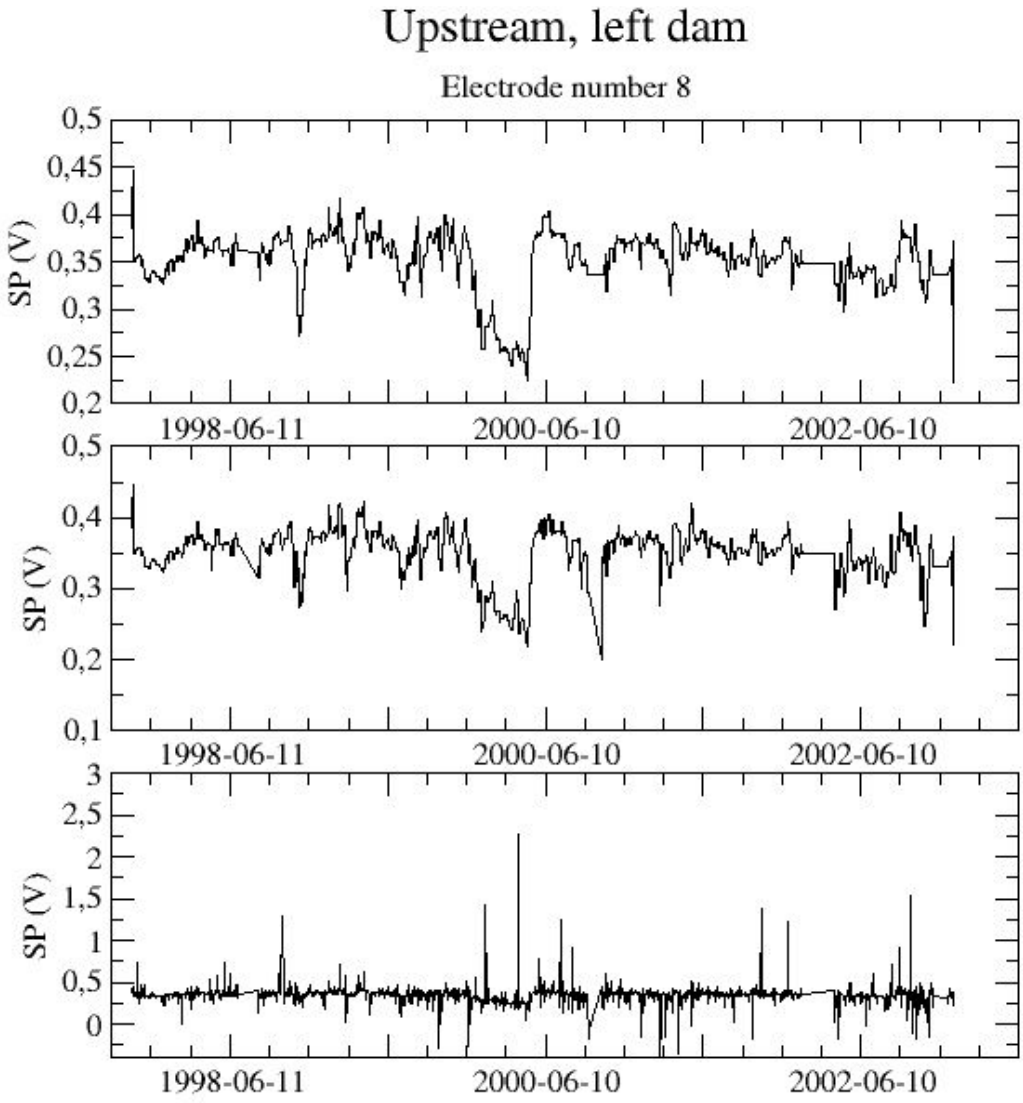

Figure 11-5: Time variation of SP for electrode 8 upstream of the left dam. Raw data (bottom), spike removal filtered data (middle), spike removal and 7-day median filtered (top).

11.2.3 Results

Self-potential data from Hällby are stable and apparently have good repeatability, although they were measured with stainless steel electrodes. Figure 11-6 and Figure 11-7 summarise the SP-data collected over the first five years of monitoring. All were median filtered over a period of a week, and have reasonably low noise levels. Clearly anomalous data indicating possible system malfunction have been edited out. The time variation is generally fairly smooth and in several of the profiles there is a clear seasonal variation of the shape of the self-potential anomaly. The general appearance of the data is, however, slightly unusual. There is a prominent, very short-wavelength component in the data. Such fast spatial variations must be associated with very shallow sources. The appearance of such sources is quite unlikely and the potential

variation is probably an effect of spurious electrode polarisation caused by electrochemical interaction between the electrodes and the ground water.

The measured anomalies are the sum of a true self-potential component and an electrode polarisation component, both of which appear to be stable and repeatable. The amplitude of the electrode polarisation potentials can be roughly estimated by comparing the amplitude of the short and long wavelength parts of the anomalies. Such an analysis indicates that the amplitude of the polarisation effect is comparable to that of the actual SP-anomaly in the land-based data. Data from the underwater profiles exhibit smaller polarisation disturbances. The reason is probably that the underwater milieu provides an electrically more stable and homogeneous environment for the electrodes. Differences in the properties of the electrodes cannot be ruled out, however.

Assuming that the polarisation effect is randomly distributed along the profile, it then follows that a smoothed version of the anomaly curve should better reflect the true SP-anomaly. From such curves it should be possible to draw at least some general conclusions on the seepage through the dam. Below the mean SP-values calculated over the whole measuring period are used for this purpose.

A comparison between Figure 11-3 and Figure 11-6 shows by way of example that there is a good correlation between SP and the apparent resistivity. When comparing the figures it is important to remember that resistivity changes cause changes in the total amplitude of SP, i.e., for a given electrode the correlation may be positive or negative depending on the polarity of the SP at that point. The resistivity shows thin maxima between late January and April that corresponds well with the minima at approximately the same period.

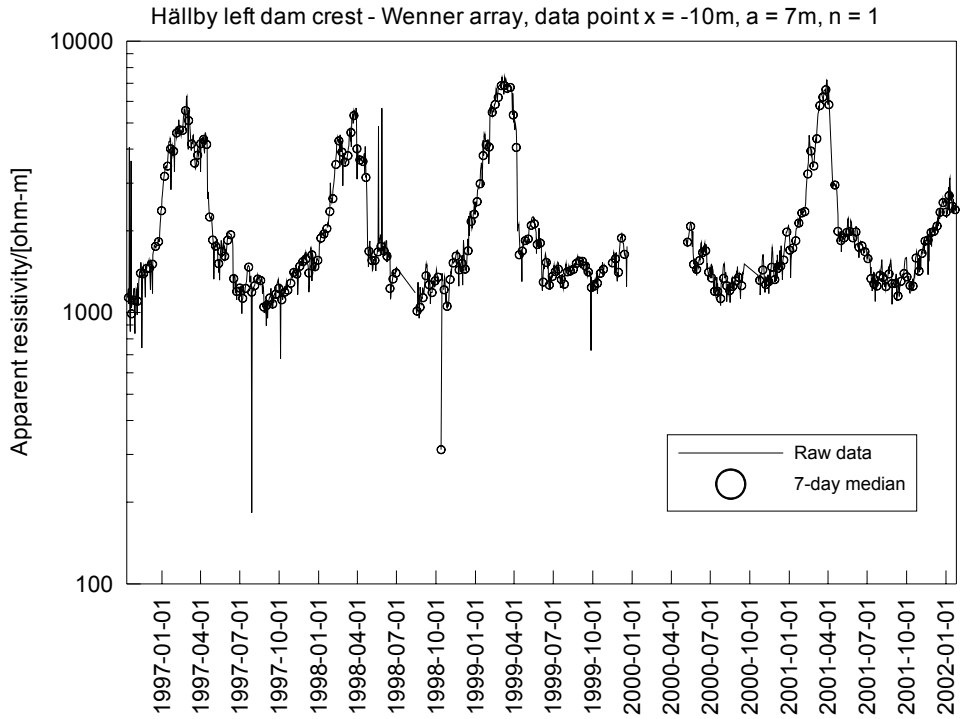

Figure 11-6: Apparent resistivity vs. time measured with 7 m a-spacing Wenner array with midpoint at section 10 m on Hällby left dam crest.

11.2.4 Left dam

On the left dam SP-recordings were made along an underwater profile on the upstream side of the dam, and along a profile at the crest of the dam. The distance along the profiles increases away from the intake.

Figure 11-6 and Figure 11-7 (fourth panel from the top) show the data acquired on the upstream profile during the measurement period. The first is a greyscale plot of the SP-values along the profile versus the date, i.e., the individual profiles constitute vertical bands in the image. The second plot is similar in format, but here the mean profile has been subtracted from all profiles, the idea being to enhance small-scale variations and to try to remove some of the erratic variation along the profiles.

The raw data plot (Figure 11-6) shows that there is a step of about 700 mV between the electrodes at sections –42 and –47 metres. Such sharp horizontal gradients are not physically plausible and indicate that the measured SP-values are probably contaminated with spurious polarisation potentials. The cause is probably a distinct change in local geological conditions, which would affect the polarisation potential of the electrodes. Subtracting the mean profile as shown in Figure 11-7 effectively removes this step and provides a more detailed image for interpretation. We see that around October 2000 there appears an increase in the residual SP at section –50 to –100 metres. This increase gradually tapers off and disappears around May 2002. Problems have been observed at this section of the dam, and it is possible that this SP variation is a reflection of those problems.

The SP data collected at the profile at the crest of the left dam are shown in the top panel of Figure 11-6 and Figure 11-7. Here the variation along the profile is calmer, but the horizontal gradients still appear unrealistically high, indicating a spurious station-to-station polarisation potential variation. In contrast to the upstream data there is a significant seasonal variation. Since the mean profile is quite flat, the residual SP does not differ significantly from the absolute SP. There is only a slight decrease in the span of the data and in the station-to-station polarisation noise.

11.2.5 Right dam

On the right dam SP-recordings were made along profiles on the upstream side of the dam, at the crest of the dam, and at the downstream side of the dam. The distance along the profiles increases away from the intake.

Figure 11-6 and Figure 11-7 (lowermost panel), show the SP-data from the upstream profile. Their characteristics agree well with those of the left dam upstream data. The polarisation noise is significant, but it is also quite effectively suppressed in the residual SP. The seasonal variation is insignificant.

The SP-data from the crest of the right dam are shown in Figure 11-6 and Figure 11-7 (second panel from top). There is a significant noise component at the beginning of the profile. This noise is significantly reduced in the residual data. The seasonal variation is weak, but clearly visible, and stronger than in either of the upstream data sets.

The downstream data, shown in Figure 11-6 and Figure 11-7 (third panel from top), are very similar in character to the data from the crest of the left dam. The seasonal variation is clearly evident. As is evident when comparing the two plots, here the removal of the mean does very little to change the character of the images.

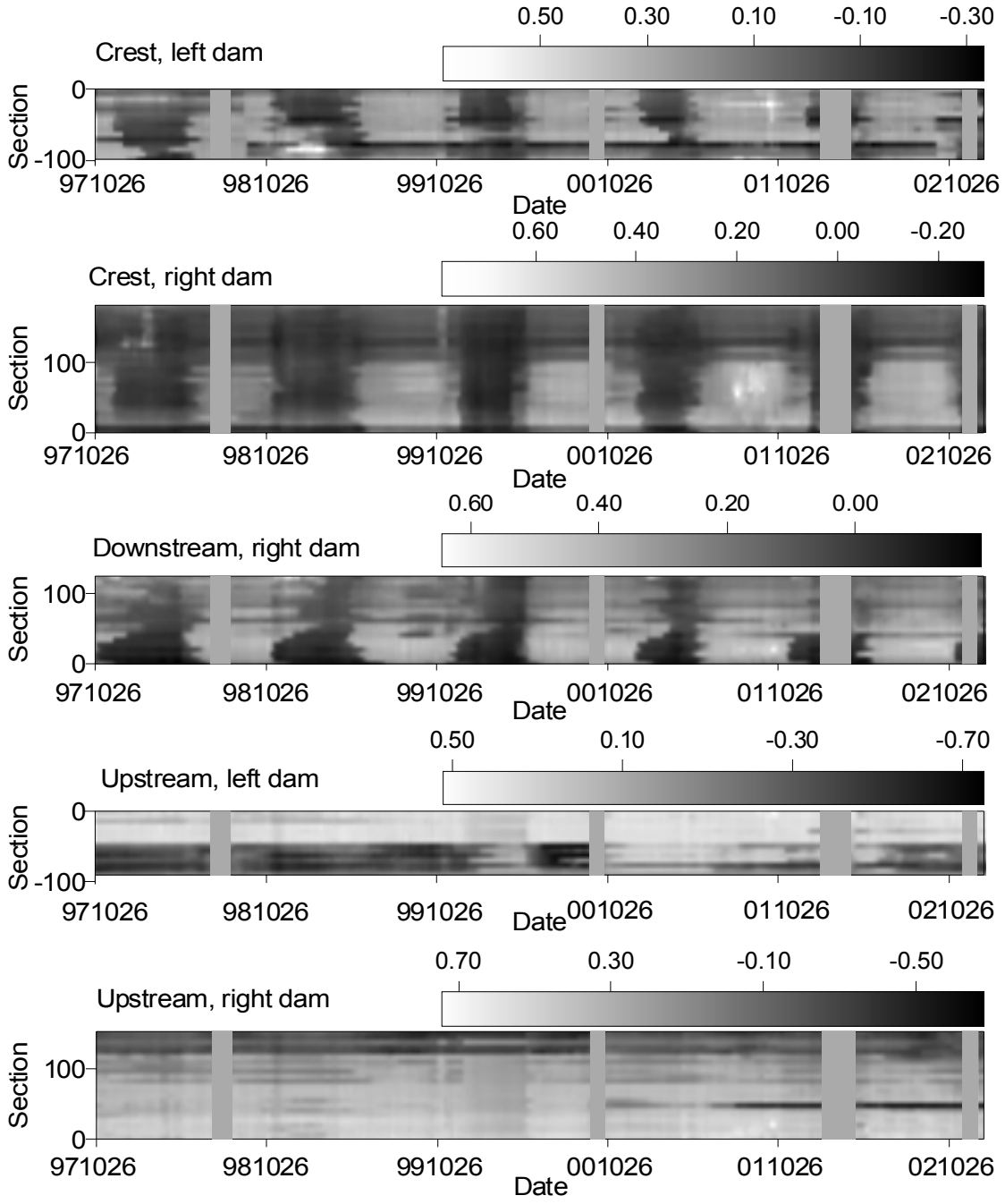

Figure 11-7: Time variation of SP at Hällby. Unprocessed data. The grey levels show SP values in Volts according to the colour bar on top of each plot. Hatched areas indicate periods of missing data.

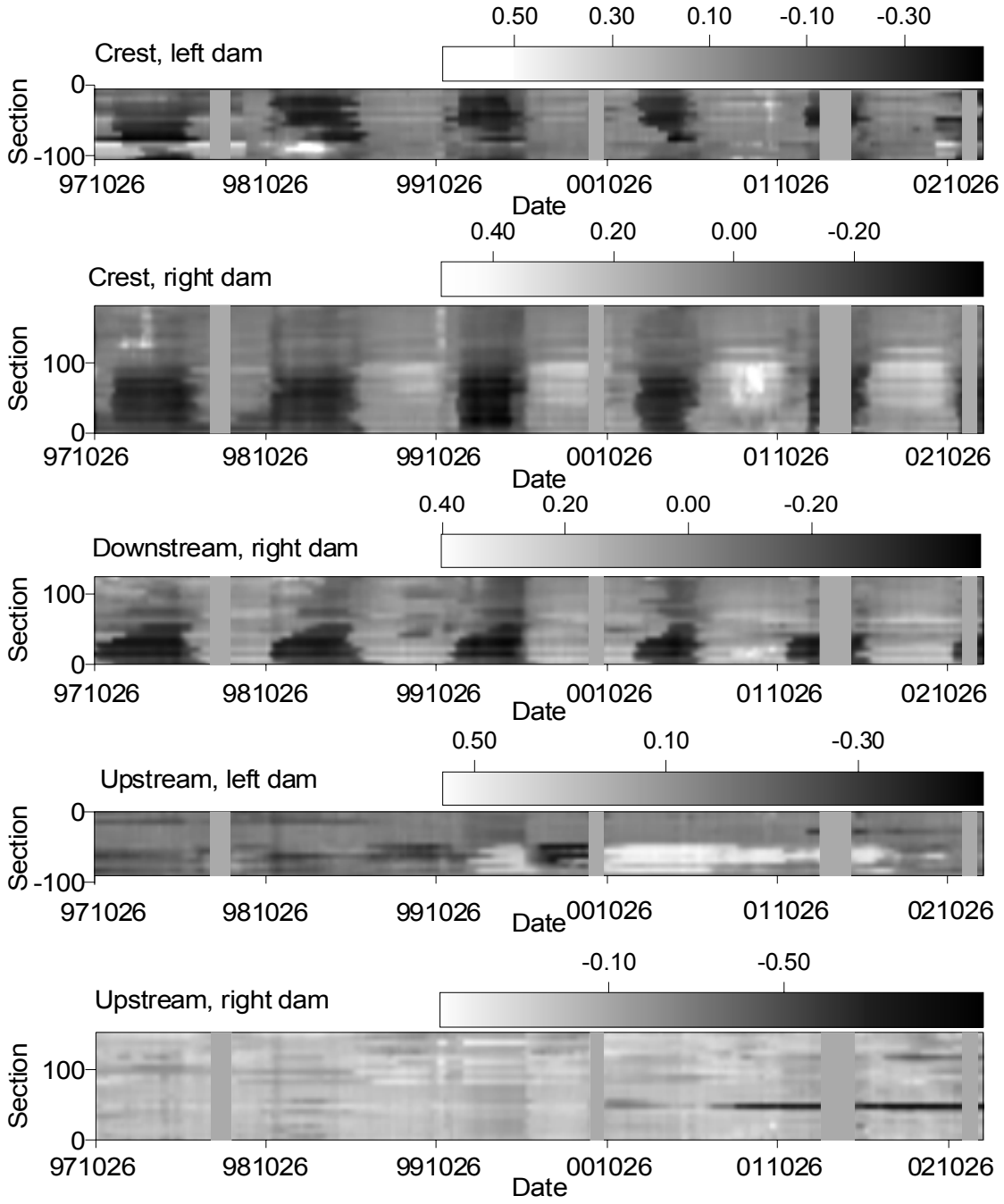

Figure 11-8: Time variation of SP at Hällby. The mean value for each electrode has been subtracted from the data. The grey levels show residual SP values in Volts according to the colour bar on top of each plot. Hatched areas indicate periods of missing data.

11.3 Conclusions

The lack of seasonal variation of the upstream anomalies indicates that there is no significant seasonal variation in the strength and location of the streaming potential sources. This agrees well with the fact that the changes in reservoir water levels are minor, less than 0.8 metres. Consequently the seasonal variation found in the land-based profiles must have another origin. Possible explanations include; changes in electrode polarisation potentials, caused by variation of the local soil properties in the vicinity of each electrode; resistivity variation caused by changes in water content, temperature and/or salinity. It has been shown by way of example that this variation is most probably caused by resistivity variation. Regardless of its origin, it is most interesting to note that this variation also shows very high repeatability. The magnitude of this seasonal variation also appears to be comparable to the magnitude of the SP-anomalies.

Even though the polarisation effects appear stable and repeatable, they are so large that it becomes necessary to try to remove them before attempting to interpret the SP-anomalies in terms of streaming potentials. A certain amount of reduction can be achieved by studying residual SP-data, but the ideal is of course to remove the noise at the source. Recent experiments at the Sädva dam, where both stainless steel and non-polarizable electrodes are installed, indicated that it might be possible to minimise the polarisation effects by applying certain depolarising measuring techniques. Subsequent investigations show, however, that this is unlikely to work in practice.

One would expect the SP to increase from the upstream area to the downstream area, as influx areas generally acquire a negative charge, and outflux areas a positive. This assumption is not really borne out by the comparison of all the profiles, shown in Figure 11-8. The reason is probably that polarisation effects offset the mean levels differently for each profile, and is a further indication of the importance of minimising these effects.

In spite of all difficulties associated with the use of polarizable electrodes one known problematic area on the left dam appears to be detectable in the offshore SP data.

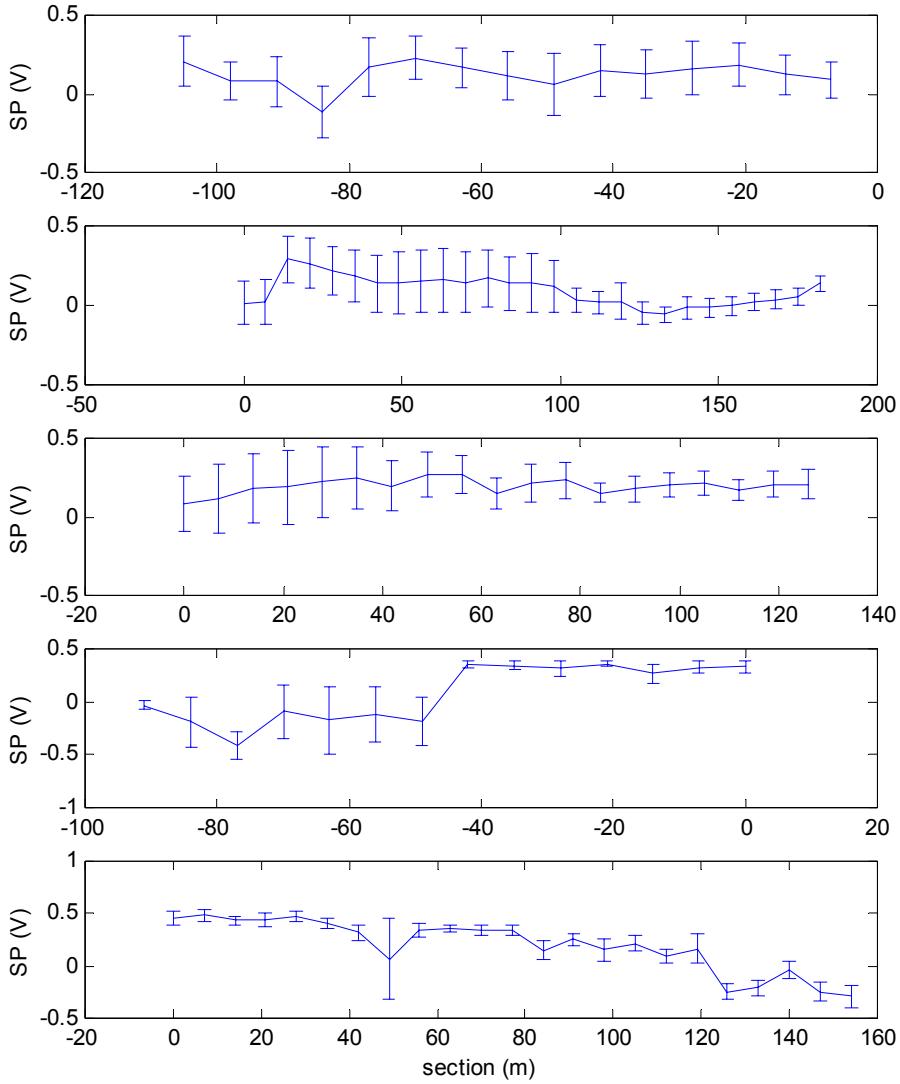

Figure 11-9: Comparison of mean SP-profiles. Left dam crest (top), right dam crest (second from top), downstream right dam (third from top), upstream left dam (second from bottom) and upstream right dam (bottom)

12 SELF POTENTIAL MEASUREMENTS AT SÄDVA

12.1 Self potential surveys

12.1.1 Survey layout

Two self-potential surveys have been carried out at Sädva, primarily to provide a baseline for the interpretation of the future monitoring data. However, the data also serve to put the spatially limited SP monitoring data on the dam into a larger context.

The first survey was done in October 2000, the second in June 2001. The first survey also included an offshore survey. The water level at the time of the first land survey was 475.5 m. During the offshore survey it was 476.5 m. Both surveys can consequently be considered high pool surveys. During the second survey the reservoir level was 463.9 m.

Land data was acquired along profiles, using the potential mapping method with the permanently installed copper-copper sulphate electrode #9 on the main dam as reference. For the first survey the end points of the profiles were positioned using differential GPS measurements, and the stations along the profile were located with a tape measure. During the second survey each station was marked on the ground and subsequently positioned with GPS. Station separation was 5 metres. The roving electrodes were ordinary rugged copper-copper sulphate electrodes manufactured for the occasion. Voltages were measured using a Lawson Labs AD201 A/D-converter adapted for field use. Data were also acquired on the permanently in-stalled copper-copper sulphate electrodes.

Offshore data was acquired through the gradient method, where a 5-metre and a 10-metre dipole were towed after a boat on the reservoir. The electrodes used were commercial, sealed, silver-silver chloride reference electrodes. They were towed at a depth of 1 metre. The location of the boat was determined by differential GPS, and the distance between the boat and the dipole was measured with a special hydro-acoustic transponder system. Dipole positions were consequently found by combining these data sets.

During the land survey, the telluric activity was monitored, by registering the variation of the potential difference across two fixed, approximately perpendicular dipoles. One dipole was located on the main dam (permanent copper-copper sulphate electrodes, dipole length 144 m.); one was located on the dyke (permanent stainless steel electrodes, dipole length 150 m.). Two high-impedance multimeters registered the voltages every two seconds.

Telluric monitoring during the offshore survey was similar, but it employed temporary installed perpendicular 50-metre dipoles, located just past the northwest end of the dyke, instead. Copper-copper sulphate electrodes were used for these.

12.1.2 Data processing

Telluric monitoring was performed to allow correction of the observed self-potentials. The amplitude of the telluric activity was, however, so small that this step was considered unnecessary. During the land survey the telluric variation never exceeded 3 mV/100m, and during the offshore survey the variation was below 10 mV/100 m.

The offshore SP gradient values obviously depend directly on the direction of the dipole at the time of observation. Since the profiles were run in several directions, we therefore calculate the absolute value of the gradient before presentation. Attempts to use numerical integration of the gradient data to yield absolute SP values proved unsuccessful, because of limitations in the accuracy of the positioning of the survey boat, caused by the intermittent loss of the real-time differential GPS corrections. The two data sets for the 5- and 10-metre dipoles are very similar; hence only data from the 10-metre dipole survey will be presented here.

For all maps simple kriging interpolation was used to create a regular grid of data before contouring.

12.1.3 Results

Figure 12-1 shows a contour map of the SP data from the first survey. Land data are absolute potentials referenced to permanent Cu-CuSO4 electrode number 9, whereas the offshore data shown are SP-gradients measured with a 10-metre dipole. The data from the permanently installed copper-copper sulphate electrodes are not included, although they agree well with data from the profile on top of the main dam. A comparison between SP measured on top of the dam crest and SP measured with the permanent Cu-CuSO4 electrodes is shown in Figure 12-2. The reason is that the permanent electrodes are buried, which means that only qualitative comparisons between the data sets are possible. The similarity verifies that both data sets apparently reflect the same subsurface structures or processes.

The map shows that the variation of the self-potentials in the area is very smooth. All notable anomalies can likely be traced to construction elements in the dam. The concrete spillway near the southwest end of the surveyed area causes a distinct positive SP anomaly that extends sideways in both directions from it. Likewise, the sharp SP gradient near the knee of the dam is associated with a buried concrete structure. The intake near the middle of the dam also shows up clearly. The large negative anomaly in the northeast corner of the area, however, is probably, at least partly, caused by the topography. The northernmost parts of the profiles that define this anomaly all go uphill and high points in the topography are often observed to be associated with negative SP anomalies.

The results of the offshore SP survey using the 10-metre dipole are shown in the contour map of Figure 12-1. The area in the vicinity of the intake to the power station was not surveyed since it was not considered safe to navigate that area. There is a general increase in the magnitude of the SP gradient towards the dam itself, much as expected. The local maximum in the middle of the map turned out to be well correlated

with a minimum in the water depth of the reservoir. This could however also be caused by concrete elements in the construction of the old dam, which is the reason for the minimum in the water depth there. The intake tower near the middle of the dam shows up clearly also in the gradient data.

Figure 12-3 shows the results of the second SP survey. The observations made about the data from the first survey generally apply here also. One notable difference is that the anomalies caused by construction elements seem to be more pronounced during this low-pool survey. A strong negative anomaly near section 350 on the dyke also shows up. Its appearance is such that it could be seepage related but this seems implausible since the reservoir level was so low that there was virtually no pressure head drop across the dyke. The anomaly is probably caused by the old dam, which intersects the dyke at approximately this position.

The contour map in Figure 12-4 shows the difference in SP between the two surveys. The main anomalies in this map are both associated with concrete elements in the dam. This shows that the assumption that anomalies caused by construction elements are more or less constant over time may not be correct. We can see, however that the negative anomaly in the northeast corner has been reduced significantly. This anomaly was assumed to be partly of topographic origin and should hence be fairly constant over time.

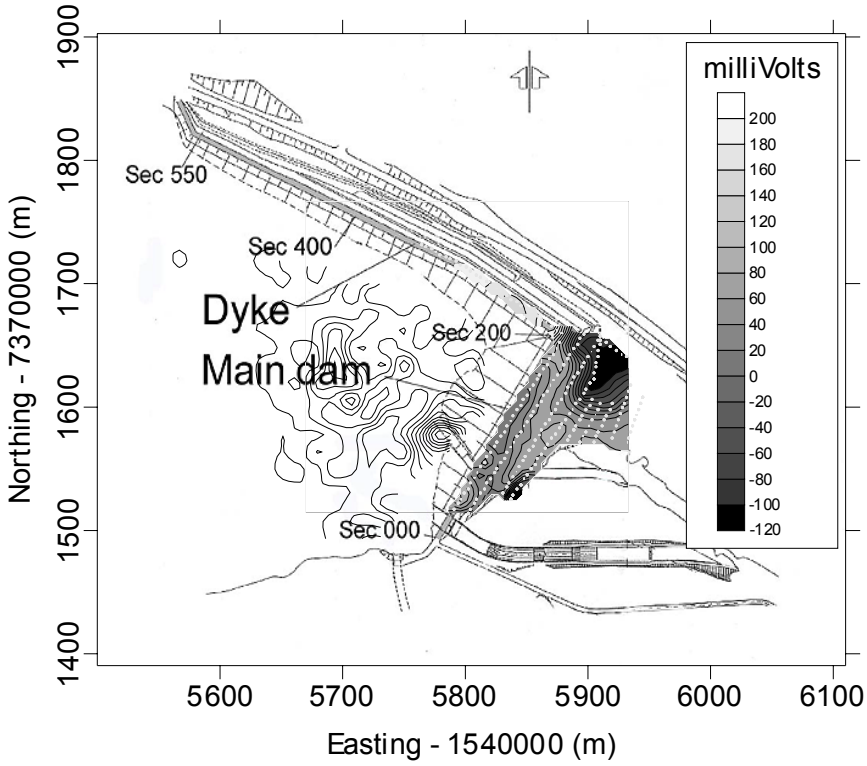

Figure 12-1: Contour map of SP data from the first survey (000920-001020). The land data are absolute potentials referenced to fixed electrode #9. The offshore data are absolute values of the SP-gradient measured with a 10-metre dipole.

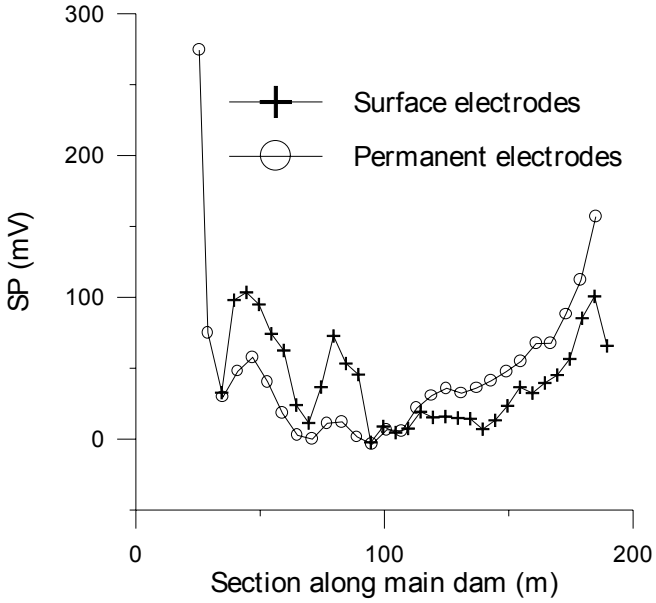

Figure 12-2: Comparison of SP data on the main dam. Open circles show measurements on the permanently installed electrodes, crosses show results of surface measurements . Both datasets were collected during the first survey.

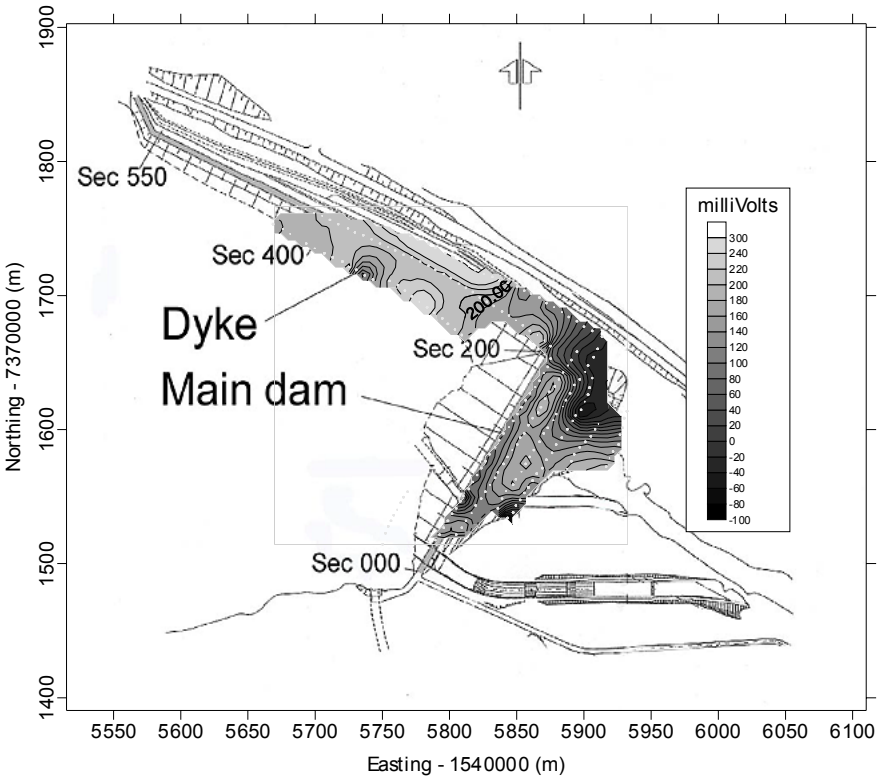

Figure 12-3: Contour map of SP data from the second survey 010601-010602. The data are absolute potentials referenced to fixed electrode #9.

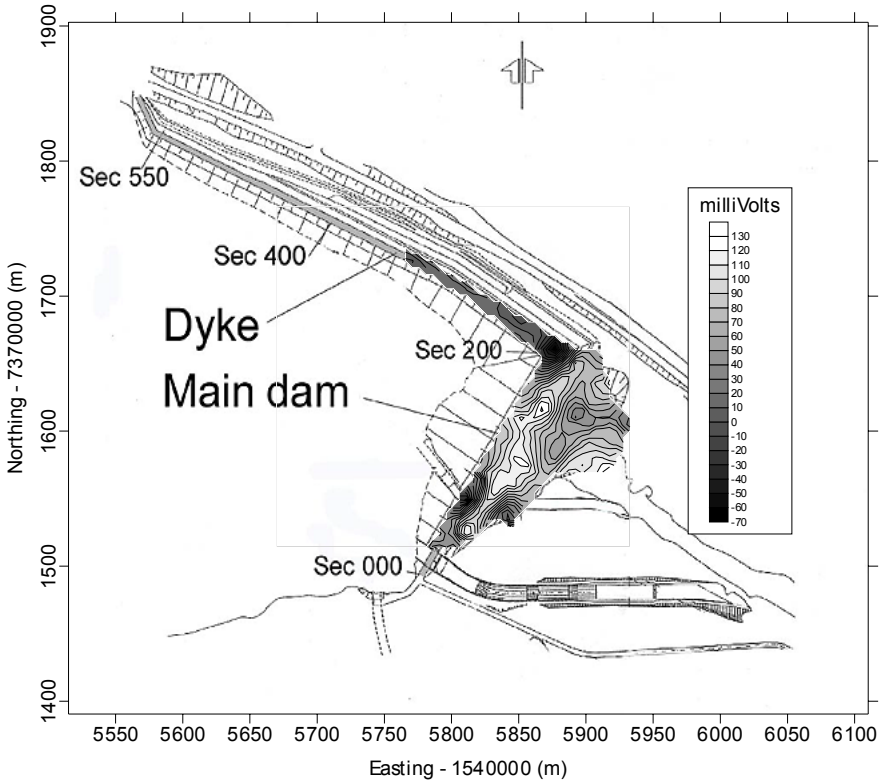

Figure 12-4: Contour map of the SP difference between the two surveys.

12.2 Monitoring

12.2.1 Installation

SP data is collected with the same measuring instruments as the resistivity data. In addition to the stainless steel electrodes used for the resistivity measurements one additional line with non-polarizing Cu-$CuSO_4$ electrodes were installed. The electrode profile locations are as follows:

- Crest of main dam (stainless steel electrodes)
- Crest of main dam (Cu-$CuSO_4$ electrodes)
- Crest of dyke (stainless steel electrodes)

All measured potentials are actually voltages referenced to non-polarizing electrode #16. The use of an electrode in the measuring area as reference causes some difficulties when one wants to study the time variation of SP. This will be discussed further in section 12.2.3.

12.2.2 Data processing

Raw data from all three profiles have high noise levels. It is therefore necessary to apply some filtering to the data before attempting to draw any conclusions from them. There

are three distinct kinds of noise: instrument malfunction, spikes (both external and instrument generated) and random (not strictly) noise. The filtering used on all data consists of the following three discrete operations:

- Identify and remove occasions of obvious instrument malfunction (as indicated by the measured values locking at the end of the A/D converter range)
- Apply a spike removal filter
- Apply a 7-day running median filter

The implementation of the first and last filter types is quite straightforward, but the spike removal filter may warrant some more detailed description. The spike removal filter is implemented as a threshold filter based on a 25-day running median value. If a data point deviates more than a given amount from this median value then it is replaced by a 7-day median centred on the data point.

There have also been some problems with the accuracy of the measuring equipment. On several occasions an exchange of the A/D converter caused a step in the measured voltages. Since one of the non-polarizing electrodes was used as reference for all measurements it was possible to correct for these instrument errors by removing the observed voltage for the short circuit connection that occurs when an electrode is used both as reference and observation electrode. This short circuit voltage should obviously be zero, but this was unfortunately not always the case. After removal of this measurement system zero offset the time series had a more continuous appearance.

Figure 12-5, Figure 12-6 and Figure 12-7 show time series plots of the SP at selected locations. The plots illustrate the effect of the different filtering steps The bottom panes show raw data, the middle panes show data after spike removal and the top panes show data after spike removal and 7-day median filtering. The spike at the start of the filtered time series is a filter edge effect that has consequently been removed by extending the time series before filtering and then truncating it back to the original length. For the Cu-$CuSO_4$ electrodes the resulting data quality is good. The time series for the stainless steel electrodes on the other hand have an irregular appearance with several random steps in the SP levels. There is also no trace of the seasonal variation that is apparent in Figure 12-5. In contrast to the results at Hällby it seems as if the stainless steel electrodes do not give reliable results at Sädva.

In order to enhance the variation of the SP the mean profiles shown in Figure 12-9 were subtracted from the maps in Figure 12-8. Figure 12-10 shows the resulting residual SP maps.

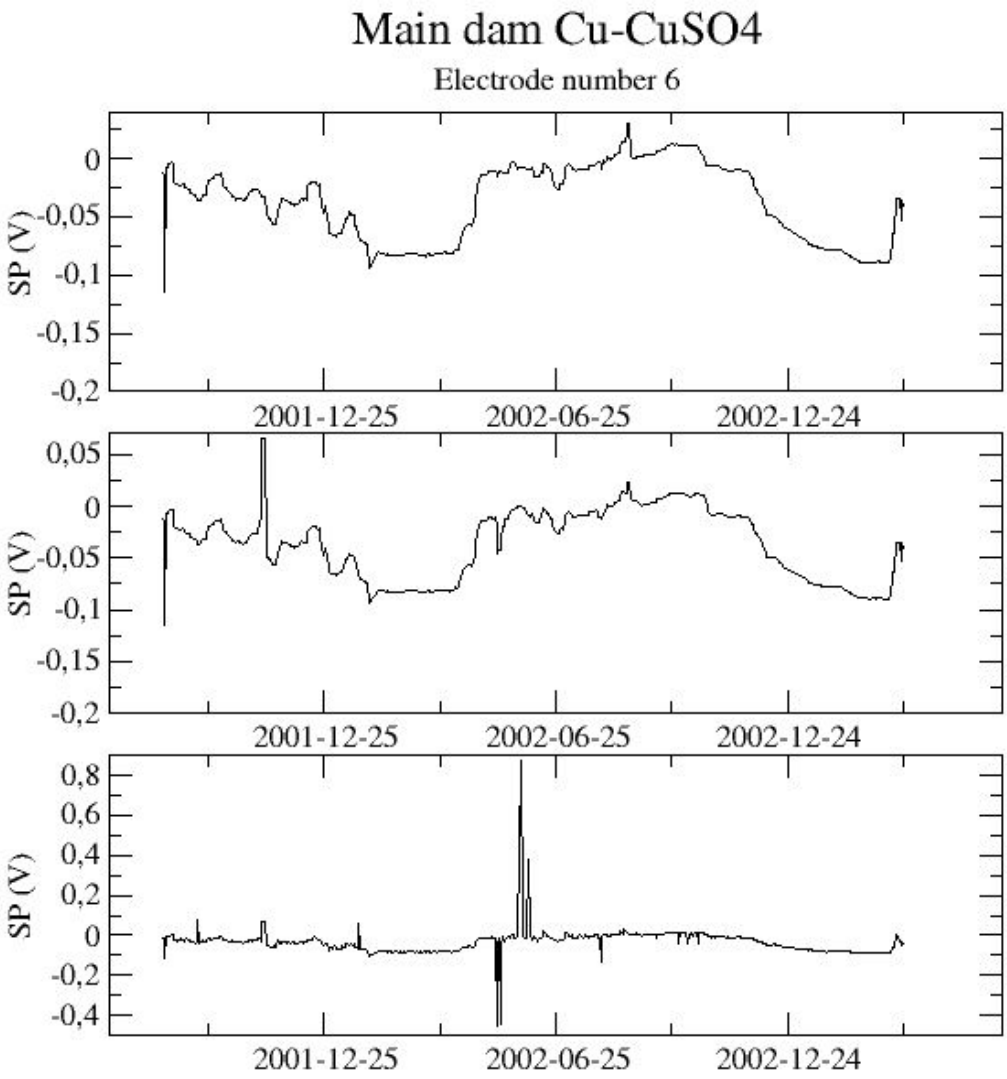

Figure 12-5: Time variation of SP for Cu-$CuSO_4$ electrode 6 at the main dam. Raw data (bottom), spike removal filtered data (middle), spike removal and 7-day median filtered (top).

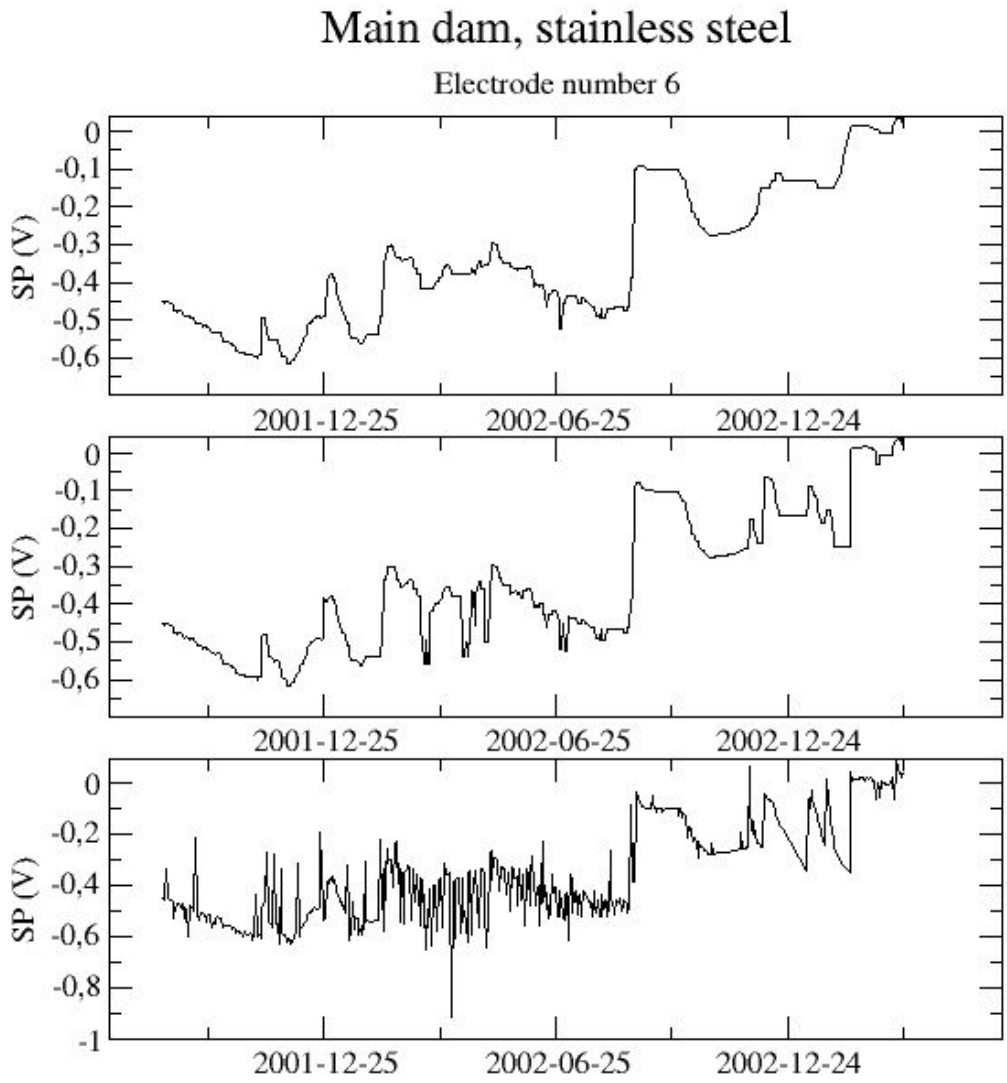

Figure 12-6: Time variation of SP for stainless steel electrode 6 at the main dam. Raw data (bottom), spike removal filtered data (middle), spike removal and 7-day median filtered (top).

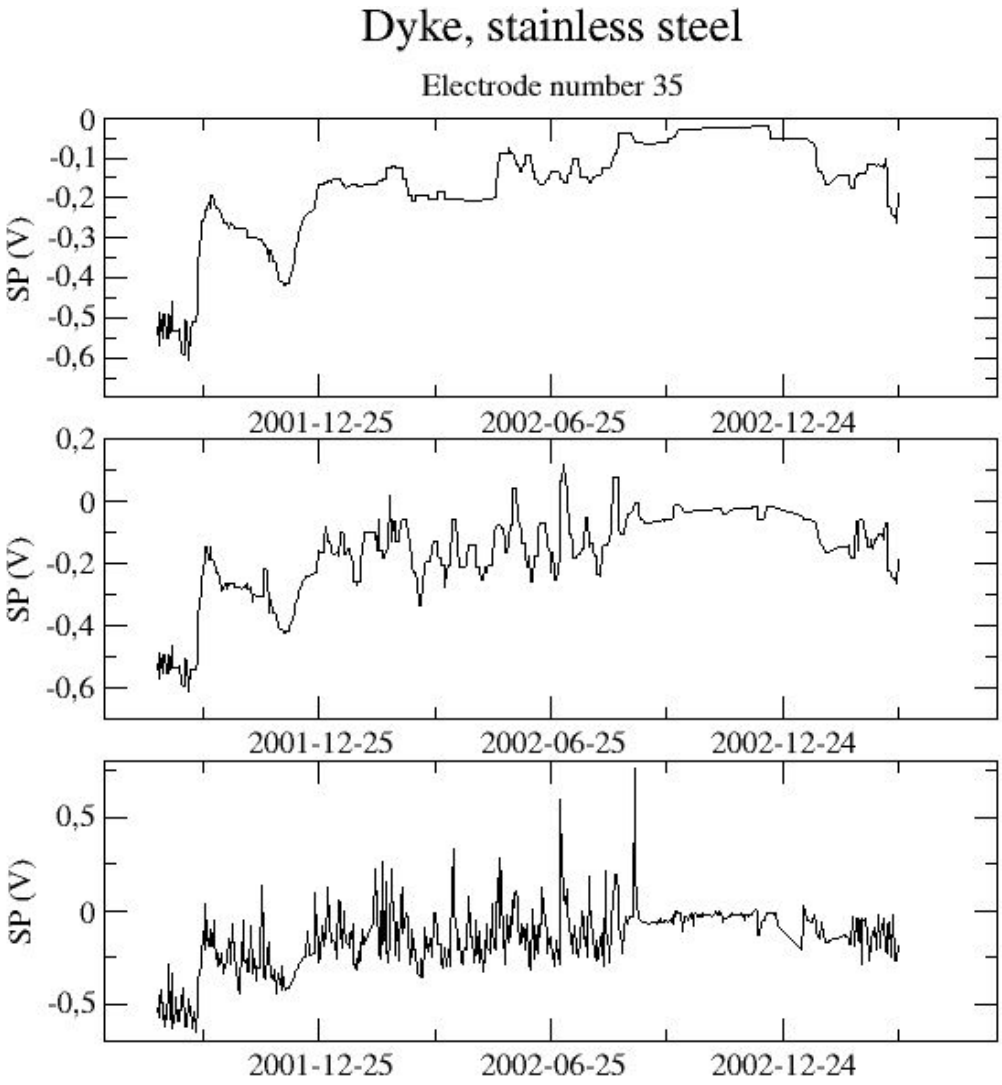

Figure 12-7: Time variation of SP for electrode 35 at the dyke. Raw data (bottom), spike removal filtered data (middle), spike removal and 7-day median filtered (top).

12.2.3 Results

Figure 12-8 and Figure 12-10 show the SP variation and the residual SP variation respectively, over the whole measuring period for all three profiles. As expected given the above observations the data measured using the stainless steel electrodes have a very noisy appearance and are not really possible to interpret. We see that subtracting the mean is quite effective in enhancing view of the temporal variation of SP by removing the spatial station-to-station variation.

The use of an electrode in the observation area as reference causes problems when one wants to study the time variation of the data. Figure 12-9 (middle pane) illustrates the problem. The Cu-$CuSO_4$ electrode located at section 113m is used as reference for all

SP measurements. It is quite obvious that the variation of the SP at each observation station increases with increasing distance from the reference. This means that the variation cannot be interpreted directly. It would be tempting to assume that areas with high station variation are anomalous also in other respects, but this is not possible with the present reference layout. In order to work efficiently with the time variation of the data is consequently necessary to employ distant reference electrodes so that the processes in the dam do not influence the potential at the reference electrode. A second very important consequence is that the seasonal variation of the background SP caused by changes in the streaming potential sources is attenuated. If we assume that the dam is more or less homogeneous then all points along the profile would have the more or less the same seasonal variation. Thus measurements with a reference on the dam will attenuate this variation, probably making the variation caused by resistivity changes dominate. This theory is corroborated by a comparison of the example given by Figure 12-5, Figure 3-3 and Figure 12-12. The SP shows weak maxima in September-October. These coincide approximately with the time of the maximum reservoir level. The sharp increase in SP that occurs in March-April does not correlate with the reservoir level, but does so with the apparent resistivity at section 83 m. The variation associated with the resistivity variation is much stronger than the one associated with the changes in water level.

The measured anomalies can be viewed as the sum of a true self-potential component and an electrode polarisation component. The polarisation component is negligible for the Cu-CuSO4 electrodes. The potentials measured on the stainless steel electrodes appear to be dominated by the polarization component, which unfortunately is not stable rendering the observed SP difficult to impossible to interpret. This is in contrast to the results at Hällby where the polarization effect is more stable. So far we have no explanation for this difference.

12.2.4 Conclusions

The total observation time is still quite short so the following conclusions must be regarded as somewhat preliminary.

The stainless steel electrodes do generally not give reliable SP measurements. This is not surprising considering the general consensus that non-polarizing electrodes should be used for SP measurements. In light of this the stable and repeatable results obtained at Hällby were unexpected, and so far we have not been able to find any explanation for this. Hence, the increased variation in the last years for part of the left dam upstream side may be indicative of a change in properties in the dam.

The non-polarizing Cu-$CuSO_4$ electrodes give reliable SP measurements although noise levels are such that quite extensive filtering is necessary.

The use of a reference electrode on the dam attenuates the seasonal variation of SP caused by changes in streaming potential source strength. The observed seasonal variation is therefore mainly caused by seasonal variation in the resistivity.

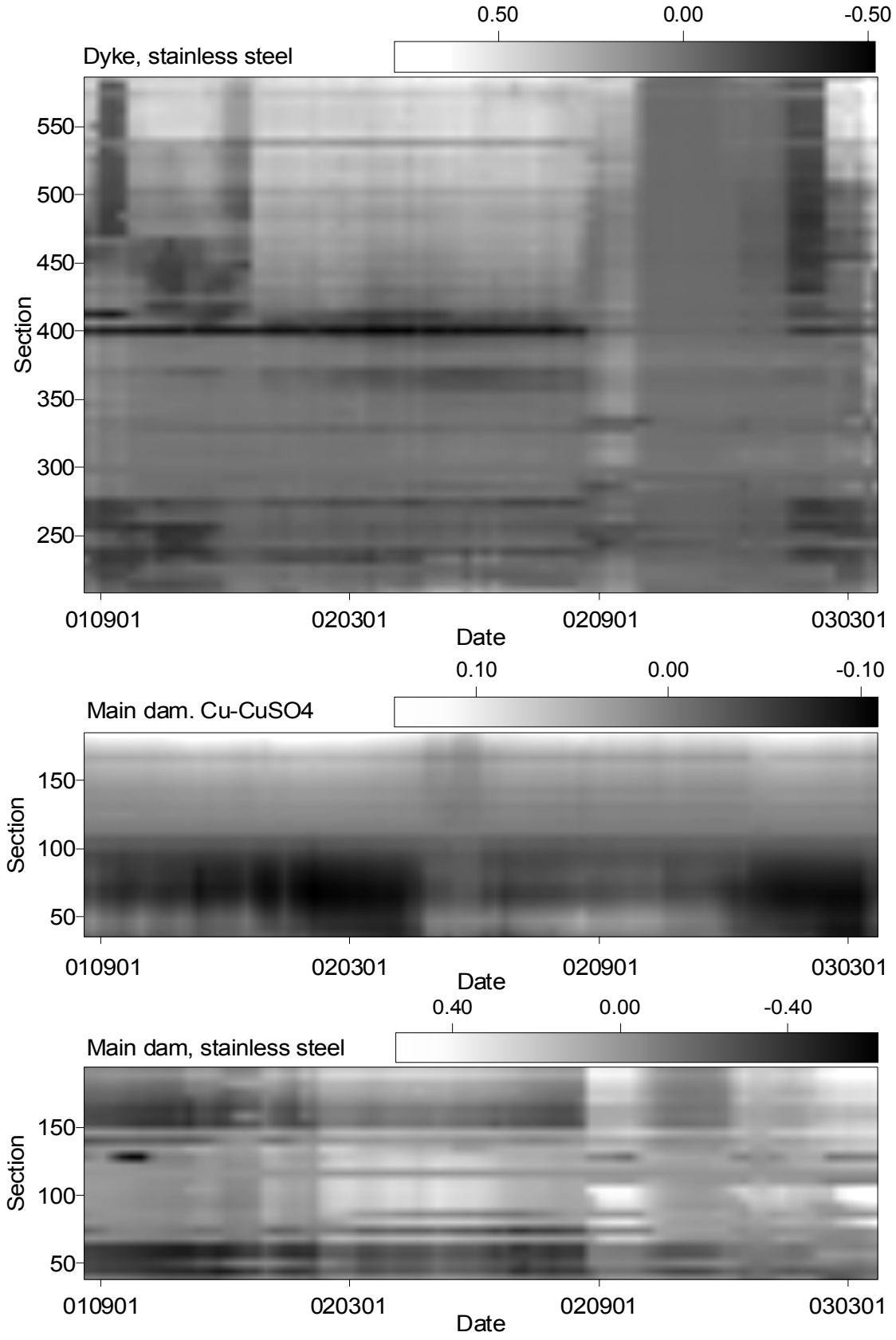

Figure 12-8: Time variation of SP at the monitored profiles at Sädva . Unprocessed data. The grey levels show SP values in Volts according to the colour bar on top of each plot.

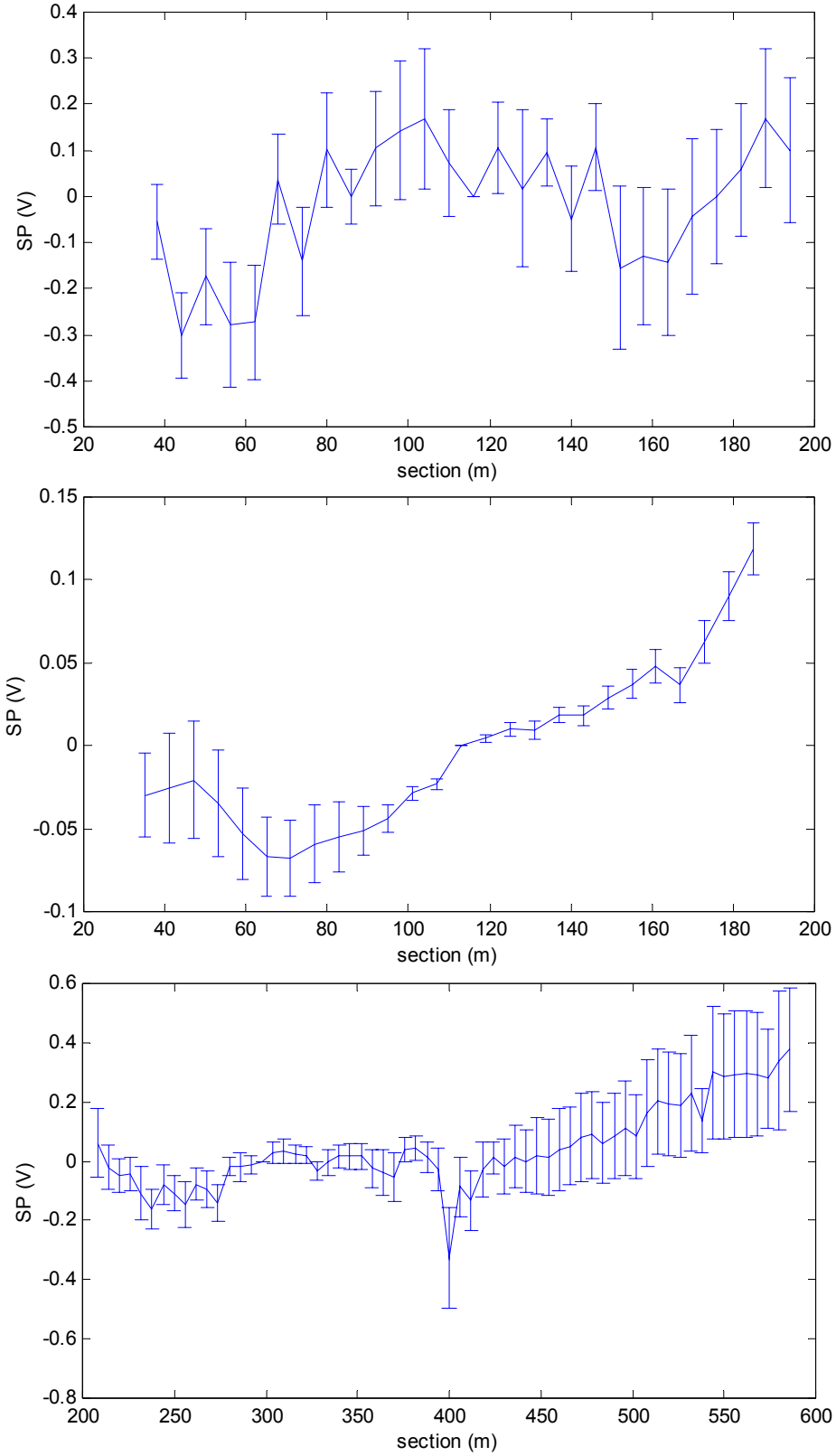

Figure 12-9: Mean SP profiles calculated between 2001-08-20 and 2003-03-24. Main dam stainless steel electrodes (top), main dam Cu-CuSO4 electrodes (middle), dyke stainless steel electrodes (bottom). The error bars show the variation (expressed as standard deviation) of the SP for each electrode.

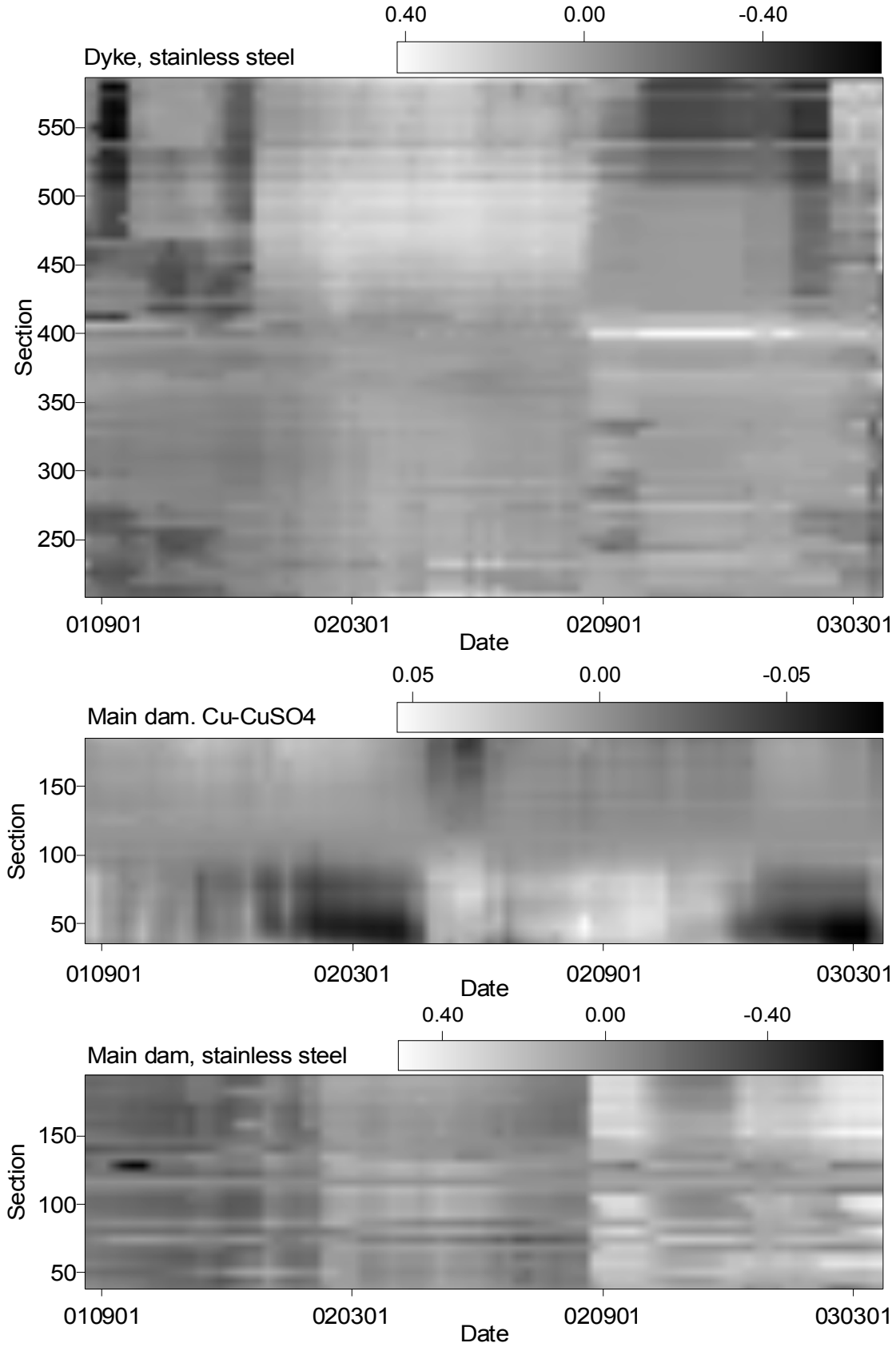

Figure 12-10: Time variation of SP with the mean profiles shown in Figure 12-9 subtracted. The grey levels show residual SP values in Volts according to the colour bar on top of each plot.

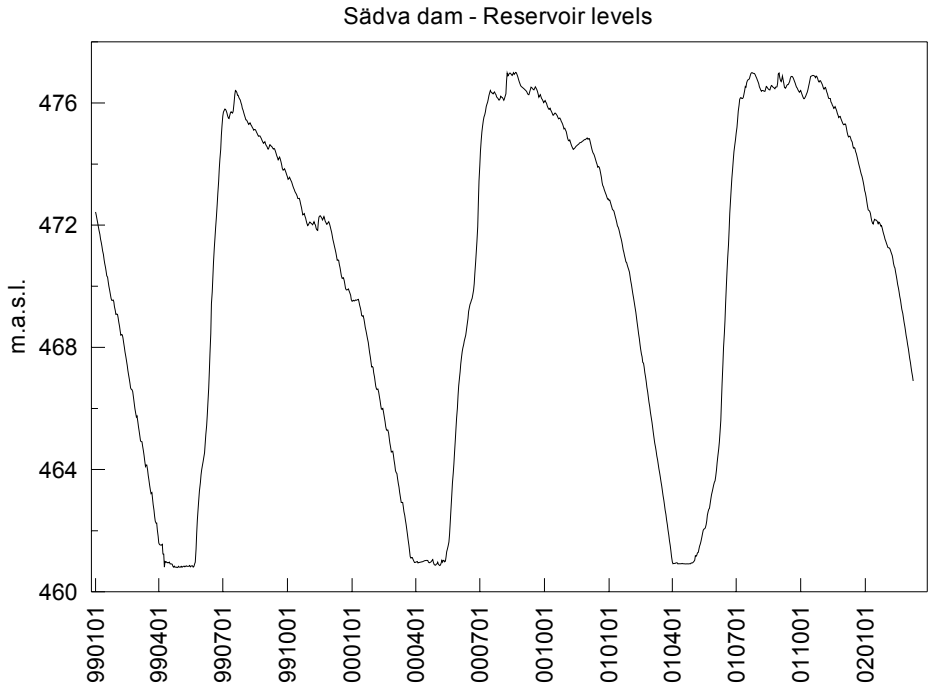

Figure 12-11: Reservoir levels at Sädva Dam.

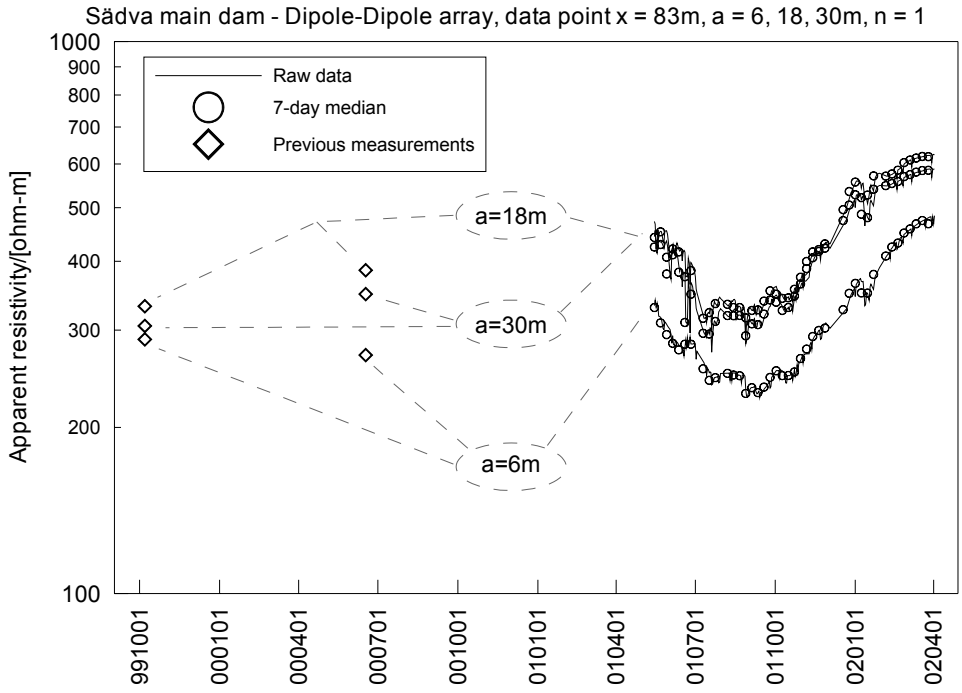

Figure 12-12: Apparent resistivity vs. time measured with 6, 18 and 30 m a-spacing Dipole-Dipole array with midpoint at section 83 m on Sädva main dam.

13 DISCUSSION

13.1 Installations and data acquisition

The data acquisition system at Hällby has made daily resistivity measurements since 1996 with only two longer breaks of 1-2 month. SP measurements were added in 1997. The monitoring equipment is reliable and is functioning well. The first break was caused by instrument malfunction, a faulty polarity switch relay in the transmitter. The reason for the two-month break in 2002 was problems with the telephone connection, which was misinterpreted as another failure and therefore unfortunately led to loss of data. Monitoring data from the layouts on the left and right dam crests and from the layout downstream the right dam is continuously evaluated and interpreted. Data from the upstream electrodes, which was previously not evaluated due to non-existing electrode positioning has now been partially analysed. Preparations for measurements using the LOE-pipes at the foundation of the left dam and the right dam have been carried out.

A system similar to the one at Hällby was chosen when the installations at Sädva were made and daily measurements have there proceeded since May 2001. At Sädva stability problems occurred that took significant time and effort to sort out. On average about every second day the system breaks before all measurements are carried out. However, the high priority measurements, which are placed first in the sequence, have an adequately complete record. The data acquisition computer and parts of the instrumentation have been replaced and a UPS has been installed to overcome this problem.

13.2 Resistivity monitoring data

The developed system for data processing analyses data statistically and controls and improves data quality. A new low pass filtering routine (IIR-filter) has been developed. It is more capable than the former running median-mean filter of removing outliers while not disturbing the natural trends. Inversion has been carried out on filtered data using a variety of inversion parameters. The L_1-norm optimisation method in combination with time-lapse inversion using a stronger filtered sliding damped reference data set has been preferred at this stage. Time-lapse inversion, which means inverting data from different points of time together, is a reasonable approach to analyse the monitoring data from embankment dams.

The data processing system appears to work well with the Sädva data using a weekly median filter as pre-conditioning before inversion. The Hällby data demands more powerful de-spiking and low-pass filtering, for which we believe we have found a way forward through the tested infinite impulse response (IIR) filtering. However, further development is required to achieve the ultimate aim to have a fully automatic system that is able to satisfactory evaluate measurements versus “normal conditions of the dam”. Next steps will include:

- Developments of a fully automatic data transfer system.
- Further development of the data filtering by applying a filter that is not infinite to its character. Using the IIR filter, a new added value at the end of the time-series may theoretically influence all earlier data and this is inconvenient, as the inversion process must then be redone.
- Implementation of automatic data inversion.
- Identifying and defining normal conditions for each dam.
- Development of an automatic analysing tool that is able to recognize normal conditions and alert when there are variations beyond those.

At Hällby the left dam crest, the right dam crest and the layout downstream the right dam have been investigated over a six and a half year period. Both raw data and inverted data have been analysed.

The left dam crest has shown noisy but acceptable data quality in prior studies and that is still the case here. Over the investigated period both the inverted data and raw data show an increase in resistivity in the region around –40 to –50 metres at large depths. This trend can be detected longer back in the investigated period, but is most evident over the last year. The changes are large enough to deserve a physical explanation. One possible reason could be an ongoing process of internal erosion where the fines in the actual part of the core are transported away giving reason to the resistivity increase. It is yet too early to draw any far-reaching conclusions though. However, the near future monitoring results from this region will be followed with especially high interest.

The right dam crest has shown poor data quality in prior studies, and also the recent data is unsatisfactory in quality. Improved installation of the electrodes along the right dam crest, i.e. to place the electrodes below the thermal insulation layer, is required for a permanent improvement of the data quality. The new filtering routines that have not been used before have significantly increased the amount of information and this shows that even with originally quite poor data quality good data handling routines may still produce important findings. Generally, at the right dam no remarkable changes are detected over time.

Downstream the right dam the data quality has been acceptable. The inverted models from the four years are similar and no long-term changes are detectable.

A few sets of data (twelve – each representing one month during 2001) from the upstream electrode layouts show very small variations for the Schlumberger array concerning both the left and the right dam. A more extensive study, using a longer series of data will be needed to draw further conclusions.

The data series from the monitoring at Sädva analysed here cover almost two years in total, although a bit scattered in time in the last part. The data quality is clearly more stable compared to Hällby, and the need of data filtering for noise reduction is much smaller. The different electrode arrays tested give similar results apart from differences

that can be explained by different 3D sensitivity patterns. Time-lapse inversion results appear to perform well, although it is too early to draw far-reaching conclusions on the dam behaviour.
The mostly moderate variation in resistivity distribution in the main dam indicates rather homogeneous conditions. A zone that stands out in the main dam is the high resistivity region in the left part of the dam. These high resistivities might be caused by internal structures such as concrete objects. The absolute values of resistivity within the dyke itself are in the same range as it is for the main dam. Below the bedrock level the resistivities are naturally increasing, however a very distinct low resistivity zone is located below bedrock level with its centre around at section 450 metres. This is interpreted as a variation in rock type or rock quality of the underlying rock.

On the main dam the variation is rather low apart from the leftmost region where a larger variation is evident. One explanation for this variation may be a larger temperature variation in and around the concrete structure at the end of the embankment dam. On the dyke the different electrode arrays mostly present rather small variation, with the most prominent exception around 430 metres along the dam where a deep zone of larger variation is clearly indicated. Some shallow zones of higher variation are also visible in the leftmost part of the L_1-norm results.

13.3 Analysis of errors in resistivity data

Spacing errors should normally be a minor problem in resistivity monitoring using permanently installed electrodes, provided the installation of electrodes has been carried out with suitable quality assurance, but may become a significant if this is not the case. With permanently installed electrodes the spacing errors will be constant in time. However, if monitoring is carried out with electrodes that are put back in place at each time of measurement, the influence of spacing errors can become a very important source of noise.

The observed potential errors will in dam applications largely be a function of the electrode contact resistances, since high contact resistances does not allow the transmission of sufficient current with associated low signal levels and possible coupling problems. High contact resistances are generally most problematic in the winter when freezing of the dam crest is prevalent, resulting in orders of magnitude higher resistivities in near surface part of the dam.

Using real data sets, it was shown that the smoothness-constrained least squares inversion is much more sensitive to the potential errors, whereas the robust inversion is quite insensitive to the outliers of data, as expected. The two inversion schemes produce very similar models with a high data quality, except more ‘blocky’ and slightly better data misfit with the robust inversion. It can be recommended to try using both approaches in real situations, and the difference between the results be used as an indicator on the data quality.

13.4 Comparison between arrays

Numerical modelling work shows that pole-dipole, dipole-dipole, gradient and Schlumberger electrode configurations are most suitable for 2D resistivity imaging survey. These arrays are relatively robust in terms of imaging quality with the data densities of a multi-electrode layout investigated here.

It can be pointed out that a relatively high anomaly effect, high signal-ratio and low noise contamination does not always produce a good resolution image. This is demonstrated by the limited resolution capabilities of the pole-pole, Wenner, Wenner-β and gamma arrays.

For dam applications dipole-dipole is probably least suitable of the four arrays mentioned above due to the low signal-to-noise ratio, and poor vertical resolution. A further limitation of the dipole-dipole array is that is appears to be more sensitive to 3D effects. Pole-dipole might be unpractical for dam monitoring installations due to difficulties in secure installation of a suitable remote electrode, if it can be arranged the array appears very suitable. Both gradient and Schlumberger arrays are suitable for dam monitoring, but the gradient array holds a clear advantage in the better sensitivity near the ends of the electrode layout, which is often crucial in dam applications.

13.5 2.5D modelling of embankment dams

The 3D effect caused by the dam geometry is a general problem when using standard two-dimensional resistivity measurements. These effects may be very much enhanced by a design with high-resistive rockfill, which is the case in both Hällby and Sädva. The long-term solution is a 3D inversion code that takes care of geometrical factors, but that is not yet practically feasible. It should be mentioned that in the case of studying processes over time (monitoring) the 3D effects is of less importance.

Reservoir level fluctuations were not a problem when evaluating data from Hällby as they are very small and may be neglected. In Sädva however, large fluctuations occur and the resistivity change caused by the variations is significant. Results from this modelling study will be considered in the data evaluation process.

Modelling of different placement of layouts has been helpful for interpretation of data from Hällby where layouts are not only placed along the crest but also on the upstream and the downstream side. Assuming damages with changes limited to the dam core, detection is not possible by the downstream or upstream layouts.

13.6 Self potential

At Hällby no significant seasonal variation in the strength and location of the streaming potential sources is expected, as the changes in reservoir water levels are minor. Consequently the seasonal variation found in the land-based profiles must have another origin. This variation also shows very high repeatability, except for part of the upstream side on the left dam where a clear increase in variation is detected for the last years. The

magnitude of this seasonal variation is generally comparable to the magnitude of the SP-anomalies. Even though the polarisation effects appear stable and repeatable, they are so large that it becomes necessary to try to remove them before attempting to interpret the SP-anomalies in terms of streaming potentials. One would expect the SP to increase from the upstream area to the downstream area, as influx areas generally acquire a negative charge, and outflux areas a positive. This assumption is not really borne out by the comparison of all the profiles. The reason is probably that polarisation effects offset the mean SP levels differently for each profile, and is a further indication of the importance of minimising these effects. One known problematic area on the left dam appears to be detectable in the offshore SP-data.

The observation period at Sädva is short but some general observation can still be made. The time variation of SP appears to correlate with the resistivity variation. There is also a correlation with the reservoir level, but this is very weak probably due to the use of an electrode on the dam as reference (see below).

In order to maximize the signal-to-noise ratio in the SP observations it is important to locate the electrodes where there is significant variation of SP. As an example consider a hypothetic dam that is perfectly symmetric and has upstream and downstream SP sources of equal strength and geometry. The centre line of such a dam would be a zero potential line, and consequently a poor place to put the electrodes. Considering realistic dam and seepage geometries such a model is much too simple, and a suitable location should ideally be found through modelling of the SP response for the particular dam.

A second important electrode placement consideration is the location of the reference electrode. As discussed in section 12.2.3, the use of an electrode on the dam as reference will mask the time variation of SP as the potential of the reference electrode will follow that of the observation electrodes. For this reason it is advisable to use reference electrodes placed at such a distance from the dam that changes in SP sources in the dam has little influence on the reference.

14 CONCLUSIONS AND FUTURE WORK

The long-term measurements show that seasonal variation of both resistivity and SP is significant both at Hällby and Sädva dams. The seasonal resistivity variation in the dam can be explained by freezing, moisture variation and seasonal change of water temperature and conductivity, where the latter depends on the seepage flow rate. The monitoring data can thus be used for seepage detection, which should be the next step in this research.

The data recorded at Hällby is affected by strong noise whereas the Sädva data is much cleaner, the latter thanks to the good electrode contact achieved by installing the electrodes inside the upper part of the dam core. However, data-filtering routines that we have developed remove the noise while maintaining the seasonal variation in the data, so that the Hällby data can be successfully interpreted.

For future installations, large efforts should be made to obtain a good installation as was done at Sädva. Although noisy data (as at Hällby) can be significantly improved by advance data-filtering routines, data quality improvement will never compensate an insufficient installation.

The seasonal variation of SP at Hällby cannot be explained by reservoir water level variations since the water level variation is less than 0.8 m. The seasonal variation is larger than the spatial variation of SP and can be seen for all years. With reservation for the polarization problems with the electrodes this large variation indicates that a single SP survey may not be enough to determine the seepage flow in the dam.

The seasonal SP variation is probably mostly caused by resistivity variations. This implies that:

- One-time resistivity and SP measurements may be affected by seasonal variation that is larger than the spatial variation, i.e. interpretation from one survey may be misleading, and;
- SP measurements should be performed in combination with resistivity unless it can be shown that the resistivity variation can be neglected.

The two-dimensional assumption used for the resistivity model inversion will not give true values neither of the resistivity nor the depth location. The errors strongly depend on the design of the dam. Measured absolute resistivities along dam crests may be several times higher than the resistivity of the core material, for dams with high contrast between a low resistive core and a high resistive rockfill. However, the current channelling of the conductive material of the core serves to focus the sensitivity of the investigation, which should improve the detection capabilities of the monitoring. Furthermore, inverted data can be used for relative comparisons, as the distortion from the inversion is essentially constant over time with low water level fluctuations. In addition, this distortion mainly affects the absolute resistivity values, which are of low importance in long-term monitoring. To some extent the resolution in depth location is

probably also distorted whereas the resolution in lateral location should remain unaffected.
An increase of seasonal variation in resistivity as well as an increasing trend, which might be caused by internal erosion or deteriorating of the old grouting, has been found in a specific region at Hällby left dam. This might be the cause of the increased seasonal variation in SP in a zone on the upstream slope of the left dam, recorded through the offshore electrodes. However, this change cannot yet be fully explained due to lack of knowledge about material properties and behaviour at internal erosion. Near future monitoring results from this region will be followed with high interest, and increasing water pressure in the dam foundation recorded on the downstream side of the dam core suggests that something is going on. The laboratory tests that are to be performed at UBC will hopefully lead to a better way of understanding such situations.

At Sädva a zone of increased resistivity variation in the foundation below the dyke may be indicative of a zone of anomalous leakage.

15 REFERENCES

Bergström, J. (1998). *Geophysical Methods for Investigating and Monitoring the Integrity of Sealing Layers on Mining Waste Deposits*, Licentiate thesis, Luleå University of Technology, ISSN 1402–1757, ISBN LTU-LIC--98/24—SE, 77p.

Claerbout, J.F. and Muir, F., 1973, Robust modeling with erratic data: Geophysics, 38, 826-844.

Dahlin, T and Zhou, B. (in press) A Numerical Comparison of 2D Resistivity Imaging with Ten Electrode Arrays, *Geophysical Prospecting*.

Dahlin, T. and Zhou, B. (2002) Gradient and mid-point-referred measurements for multi-channel 2D resistivity imaging, Procs. 8th Meeting Environmental and Engineering Geophysics, Aveiro, Portugal, 8-12 September 2002, 157-160.

Dahlin, T. and Zhou, B. (2001) A numerical comparison of 2D resistivity imaging with eight electrode arrays, Procs. 7th Meeting Environmental And Engineering Geophysics, Birmingham, England, 2-6 September 2001, ELEM01, 2p.

Dahlin, T. and Loke, M.H. (1997). Quasi-3D resistivity imaging: mapping of 3D structures using two dimensional DC resistivity techniques, *Procs. 3rd Meeting Environmental and Engineering Geophysics*, Aarhus, Denmark, 8-11 September 1997, pp. 143-146.

Dahlin, T. (1996). 2D resistivity surveying for environmental and engineering applications, *First Break*, 14(7), pp. 275-283.

Dahlin, T. (1993). *On the Automation of 2D Resistivity Surveying for Engineering and Environmental Applications*, Ph.D.Thesis, ISRN LUTVDG/TVDG--1007--SE, ISBN 91-628-1032-4, Lund University, 187p.

deGroot-Hedlin, C. and Constable, S., 1990, Occam's inversion to generate smooth, two-dimensional models from magnetotelluric data: Geophysics, 55, 1613-1624.

Ellis, R.G. and Oldenburg, D.W., 1994, Applied geophysical inversion: Geophysical Journal International, 116, 5-11.

Farquharson, C.G. and Oldenburg, D.W., 1998, Non-linear inversion using general measured of data misfit and model structure. Geophysical Journal International, 134, 213-227.

Johansson, S., Dahlin, T. and Friborg, J. (2000). *Seepage Monitoring by Resistivity and Streaming Potential Measurements at Hällby Embankment Dam 1996-1999*, Elforsk Rapport 00:15.

Johansson, S. and Dahlin, T. (1996) Seepage monitoring in an earth embankment dam by repeated resistivity measurements, European Journal of Engineering and Environmental Geophysics, 1(3), 229-247.

Loke, M.H. (1999) Time-lapse resistivity imaging inversion, *Procs. 5th Meeting of the European Association for Environmental and Engineering Geophysics*, 5-9 September 1999, Budapest, Em1, 2p.

Loke, M.H. (2001) Constrained time-lapse resistivity imaging inversion. *Procs. SAGEEP 2001 (Symposium on the Application of Geophysics to Engineering and Environmental Problems)*, Denver, Colorado, March 4-7 2001.

Loke, M.H., Acworth, I and Dahlin, T. (2001) A comparison of smooth and blocky inversion methods in 2-D electrical imaging surveys, *Procs. ASEG 15th Geophysical Conference and Exhibition, August 2001, Brisbane.*

Loke, M.H. (2003) Rapid 2-D Resistivity & IP inversion using the least square method, *Manual to RES2DINV ver. 3.52, Geoelectrical Imaging 2-D & 3D GEOTOMO SOFTWARE, 125p*

Militer, H., Rosler, R. and Losch, W. (1979) Theoretical and experimental investigations for cavity research with geoelectrical resistivity methods. *Geophysical Prospecting*, 27: 640-652.

Oldenburg, D.W and Ellis, R.G. (1993) Efficient inversion of magnetotelluric data in two dimensions, *Phys, Earth Planet. Inter., 81*, 177-200.

Ward, S.H. (1990) Resistivity and Induced Polarization Methods, in *Investigations in Geophysics no. 5: Geotechnical and Environmental Geophysics, vol I*, ed. S. Ward, Society of Exploration Geophysicists, Tulsa, p 147-189.

Wolke, R. and Schwetlick, H., 1988, Iteratively reweighted least squares algorithms, convergence analysis, and numerical comparisons: SIAM Journal of Scientific and Statistical Computations, 9, 907-921.

Zhou, B. and Dahlin, T (2003) Properties and Effects of Measurement Errors on 2D Resistivity Imaging Surveying, *Near Surface Geophysics*, 1(3), 105-117.

Zhou, B. and Greenhalgh, S.A. (2000) Crosshole resistivity tomography using different electrode configurations. *Geophysical prospecting*, 48, 887-912.

Zhou B, 1998, Chapter 3, Crosshole resistivity and acoustic velocity imaging: 2.5-D Helmholtz equation modeling and inversion (PhD thesis), The University of Adelaide

APPENDICES

A SÄDVA ACQUISITION SYSTEM DETAILS

A.1 Sädva data acquisition computer configuration

Table A-1: Serial port configuration of data acquisition computer at Sädva.

Port	Address	IRQ
COM1	3F8	4
COM2	2F8	3
COM3	3E8	4
COM4	2E8	5

Table A-2: Set-up of AUTOEXEC.BAT. The comments in italics are not included in the file

```
C:\DOS\SMARTDRV.EXE /X
@ECHO OFF
PROMPT $p$g
PATH C:\DOS;c:\util;c:\res;c:\aw      include needed directories in path
SET TEMP=C:\DOS
MODE CON CODEPAGE PREPARE=((850) C:\DOS\EGA.CPI)
MODE CON CODEPAGE SELECT=850
KEYB SV,,C:\DOS\KEYBOARD.SYS
mouse.exe

aw /o:h /m:a                          put pcAnywhere in background

cd resdata                            move to data directory
make_bat.exe saedva.scr saedva.bat    create batch file of the day
wait_min 5                            wait 5 minutes before starting
call saedva.bat                       start data acquisition

nc                                    call Norton Commander
```

Table A-3: System configuration in CONFIG.SYS:

```
DOS=SINGLE
DOS=HIGH,UMB
Device=C:\WINDOWS\Himem.Sys
rem device=c:\util\interlnk.exe /drives:6
```

A.2 Relay Switch Connections at Sädva

Table A-4: Electrode cable and reservoir probe connection to RSW16 combined relay switch and lightning protection.

Input	Function	Addresses
1-A	Dyke electrodes 1-32	1-32
1-B	Main dam Pb/PbCl electrodes	1-32
1-C1	Reservoir resistivity/temperature probe at mini powerplant	1-6
1-C2	Reservoir resistivity/temperature probe at old spillway t	9-14
1-A	Dyke electrodes 33-64	33-64
1-B	Main dam steel electrodes	33-64

A.3 Reservoir water probe configuration at Sädva

Table A-5: Reservoir water resistivity and temperature probe connection.

Function	Cable colour	Connector pin	Address #1	Address #2
A (C1)	white	1 (A)	1	9
B (C2)	brown	2 (B)	2	10
M (P1)	red	3 (C)	3	11
N (P2)	blue	4 (D)	4	12
Temp signal +	green	5 (E)	5	13
Temp signal –	grey	6 (F)	6	14
Temp 12 VDC	yellow	7 (G)	-	-
Temp 0 VDC	pink	8 (H)	-	-

B CALIBRATION OF TEMPERATURE SENSORS AT SÄDVA

B.1 Probe 1 – In mini power plant

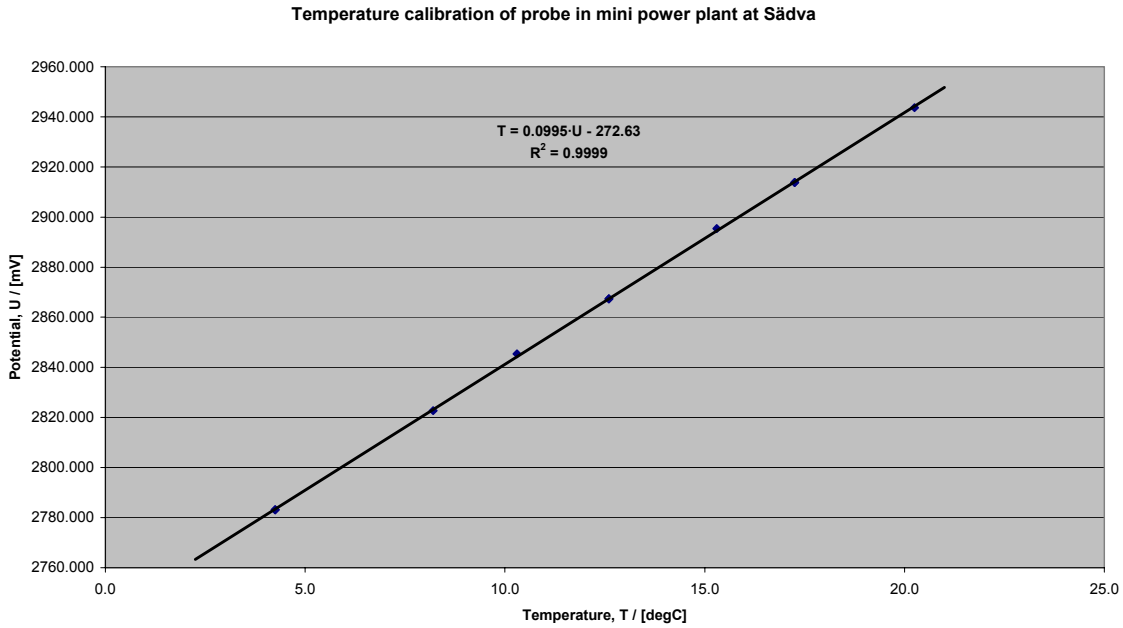

Figure B-1: Calibration of temperature sensor in probe 1.

B.2 Probe 2 – In upstream reservoir

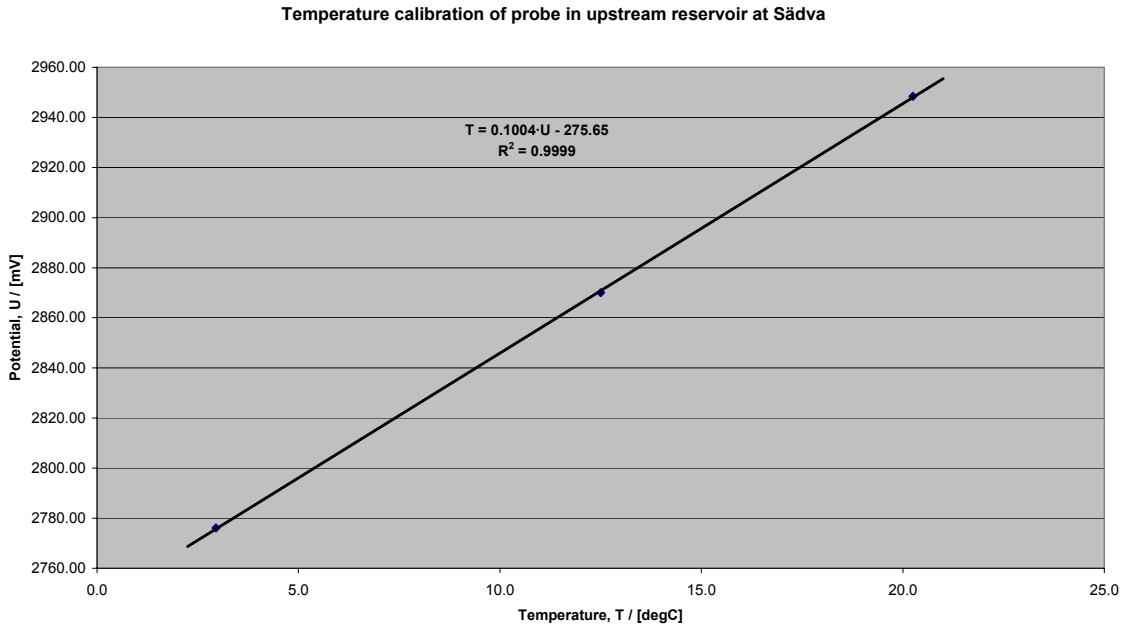

Figure B-2: Calibration of temperature sensor in probe 2.

C POSITIONING OF UPSTREAM ELECTRODES AT HÄLLBY

C.1 Original data

Table C-1: Original data from positioning of upstream electrodes at Hällby.

#	Longitude (WGS-84)	Latitude (WGS-84)	Y (RT 90)	X (RT 90)	Z (m.b.w.s)	Zadj (m.a.s.l)
1	17.197304	63.884251	1568407.023	7087067.845	9.4	282.2
2	17.197126	63.884287	1568398.191	7087071.667	9.1	282.5
3	17.197052	63.884340	1568394.427	7087077.495	8.6	283.0
4	17.196961	63.884383	1568389.853	7087082.190	8.0	283.6
5	17.196819	63.884428	1568382.767	7087087.053	7.5	284.1
6	17.196693	63.884464	1568376.490	7087090.931	6.6	285.0
7	17.196505	63.884460	1568367.264	7087090.284	8.1	283.5
8	17.196372	63.884431	1568360.801	7087086.909	7.9	283.7
9	17.196291	63.884412	1568356.868	7087084.705	8.2	283.4
10	17.196233	63.884387	1568354.080	7087081.856	7.6	284.0
11	17.196165	63.884374	1568350.771	7087080.335	7.7	283.9
12	17.195977	63.884353	1568341.586	7087077.793	8.1	283.5
13	17.195767	63.884334	1568331.316	7087075.451	7.5	284.1
14	17.195640	63.884310	1568325.130	7087072.665	8.0	283.6
15	17.194810	63.885778	1568280.800	7087235.370	12.9	278.7
16	17.194662	63.885837	1568273.387	7087241.787	13.0	278.6
17	17.194501	63.885982	1568265.126	7087257.776	12.4	279.2
18	17.194550	63.885927	1568267.667	7087251.699	13.0	278.6
19	17.194414	63.886028	1568260.741	7087262.810	12.8	278.8
20	17.194288	63.886078	1568254.431	7087268.248	12.4	279.2
21	17.194058	63.886170	1568242.909	7087278.257	13.5	278.1
22	17.194163	63.886122	1568248.184	7087273.019	13.0	278.6
23	17.193968	63.886232	1568238.338	7087285.071	13.0	278.6
24	17.193906	63.886253	1568235.242	7087287.345	11.9	279.7
25	17.193753	63.886304	1568227.602	7087292.866	12.5	279.1
26	17.193620	63.886343	1568220.975	7087297.071	13.4	278.2
27	17.193532	63.886405	1568216.502	7087303.887	14.0	277.7
28	17.193493	63.886459	1568214.455	7087309.864	12.9	278.7
29	17.193502	63.886502	1568214.793	7087314.666	13.4	278.2
30	17.193531	63.886529	1568216.152	7087317.706	11.7	279.9
31	17.193564	63.886545	1568217.734	7087319.525	11.4	280.2
32	17.193519	63.886586	1568215.424	7087324.047	11.3	280.3
33	17.193543	63.886530	1568216.739	7087317.831	12.5	279.1

- WGS-84 represent raw field data
- Approx. +/- 1 meter accuracy in WGS-84 coordinates
- Approx. +/- 1 meter total accuracy in the transformation from WGS-84 to RT90 (no or small relative transformation errors between individual electrodes)
- Z (meter below water surface) represents raw field data
- Zadj (meter below sea level) is calculated from Zadj=291.60-Z.

D LISTS OF MONITORING PROTOCOLS AT HÄLLBY AND SÄDVA

D.1 Monitoring protocols at Hällby

Table D-1: Complete list of monitoring protocols at Hällby 1996-10-12 – 2003-03-30.

CODE	ARRAY	LINE	NAME PROTOCOL FILE	NUMBER OF POINTS	START	FINISH
W1	Wenner	Left Crest	HWENNER1	35	961012	990224
W2	Wenner	Right Crest	HWENNER2	108	961012	990224
W3	Wenner	-	-	-	-	-
W4	Wenner	Right Downstream	HWENNER4	51	961012	990224
W5	Wenner	Left Upstream	HWENNER5	26	961012	990224
W6	Wenner	Right upstream	HWENNER6	84	961012	990224
R1	Reciprocal Wenner	Left Crest	HWENREC1	35	961012	990224
R2	Reciprocal Wenner	Right Crest	HWENREC2	108	961012	990224
R3	Reciprocal Wenner	-	-	-	-	-
R4	Reciprocal Wenner	Right Downstream	HWENREC4	51	961012	990224
R5	Reciprocal Wenner	Left Upstream	HWENREC5	26	961012	990224
R6	Reciprocal Wenner	Right Upstream	HWENREC6	84	961012	990224
SP	Old SP	-	H_SP1, H_SP2, H_SP3, H_SP4, H_SP5, H_SP6	16 , 27 , 2 , 19 , 14 , 24	961012	970306
C1	Pole-Dipole 1	Left Crest	PoleDIP1	112	961023	990224
C2	Pole-Dipole 1	Right Crest	PoleDIP2	338	961023	990224
C3	Pole-Dipole 1	-	-	-	-	-
C4	Pole-Dipole 1	Right Downstream	PoleDIP4	162	961023	990224
C5	Pole-Dipole 1	Left Upstream	PoleDIP5	84	961023	990224
C6	Pole-Dipole 1	Right Upstream	PoleDIP6	264	961023	990224
C1	Pole-Dipole 2	Left Crest	H-PD1XL	228	990226	IN PROGRESS
C2	Pole-Dipole 2	Right Crest	H-PD2XL	734	990226	IN PROGRESS
C3	Pole-Dipole 2	-	-	-	-	-
C4	Pole-Dipole 2	Right Downstream	H-PD4XL	336	990226	IN PROGRESS
C5	Pole-Dipole 2	Left Upstream	H-PD5XL	168	990226	IN PROGRESS
C6	Pole-Dipole 2	Right Upstream	H-PD6XL	564	990226	IN PROGRESS
TE	Water Temperature	-	TEMPERAT	1-5	970210	IN PROGRESS
VA	Water Resistivity	-	VATTEN	2-5	970210	IN PROGRESS
S1	SP	Left Crest	H_SP1	16	970310	IN PROGRESS
S2	SP	Right Crest	H_SP2	27	970310	IN PROGRESS
S3	SP	-	H_SP3	2	970310	IN PROGRESS
S4	SP	Right Downstream	H_SP4	19	970310	IN PROGRESS
S5	SP	Left Upstream	H_SP5	14	970310	IN PROGRESS
S6	SP	Right Upstream	H_SP6	23.-24	970310	IN PROGRESS
X1	Wenner-Schlumberger	Left Crest	HWENSCH1	48	970924	IN PROGRESS
X2	Wenner-Schlumberger	Right Crest	HWENSCH2	201	970924	IN PROGRESS
X3	Wenner-Schlumberger	-	-		-	-
X4	Wenner-Schlumberger	Right Downstream	HWENSCH4	78	970924	IN PROGRESS
X5	Wenner-Schlumberger	Left Upstream	HWENSCH5	33	970924	IN PROGRESS
X6	Wenner-Schlumberger	Right Upstream	HWENSCH6	147	970924	IN PROGRESS
Q1	Reciprocal PoleDipole	Left Crest	RPoleDIP1	112	981019	990324

D.2 Monitoring protocols at Sädva

Table D-2: Complete list of monitoring protocols at Sädva 2001-05-11 – 2003-03-30.

CODE	ARRAY	LINE	NAME PROTOCOL FILE	NUMBER OF POINTS	START	FINISH
MD	Dipole-Dipole	Main Dam	Main_Dip	126	010511	IN PROGRESS
MP	Pole-Dipole	Main Dam	Main1PDP, Main2PDP	406+406	010511	IN PROGRESS
MW	Wenner	Main Dam	Main_Wen	126	010511	IN PROGRESS
MG	Gradient	Main Dam	Main_Grd	560	020825	IN PROGRESS
DD	Dipole-Dipole	Dyke	Dyke_Dip	651	010511	IN PROGRESS
DW	Wenner	Dyke	Dyke_Wen	651	010511	IN PROGRESS
DG	Gradient	Dyke	DYKE1GRD, DYKE2GRD	600+436	011006	IN PROGRESS
DQ	Reciprocal Dipole-Dipole	Dyke	RDYK_DIP	651	020824	IN PROGRESS
DR	Reciprocal Wenner	Dyke	RDYK_WEN	651	020824	IN PROGRESS
RD	Reciprocal Dipole-Dipole	Main Dam	rMai_Dip	117	010511	010512
RP	Reciprocal Pole-Dipole	Main Dam	rMAI_PDP	392	010511	010514
RW	Reciprocal Wenner	Main Dam	rMai_Wen	126	010511	010514
QD	Reciprocal Dipole-Dipole	Dyke	rDyk_Dip	606	010511	010512
QP	Forward and reverse Pole-Dipole	Dyke	rDy1FPDP, rDy2FPDP, rDy1RPDP, rDy1RPDP	465+465+465+465	010512	010512
QW	Reciprocal Wenner	Dyke	rDyk_Wen	651	010511	010512
S1	SP	Dyke	Dyke_SP	64	010512	IN PROGRESS
S2	SP	Main Dam	Main_SP1	32	010512	IN PROGRESS
S3	SP	Main Dam	Main_SP2	29	010512	IN PROGRESS
T1	Water Temperature	Mini power plant	Temp1	8	011120	IN PROGRESS
T2	Water Temperature	Old outlet	Temp2	8	010809	IN PROGRESS
V1	Water Resistivity	Mini power plant	Vatten1	8	011120	IN PROGRESS
V2	Water Resistivity	Old outlet	Vatten2	8	010809	IN PROGRESS
Z1	Check instrument	-	ZERO1	16	020824	IN PROGRESS
Z2	Check instrument	-	ZERO2	16	020824	IN PROGRESS

ELFORSK

SVENSKA ELFÖRETAGENS FORSKNINGS- OCH UTVECKLINGS – ELFORSK – AB
Elforsk AB, 101 53 Stockholm. Besöksadress: Olof Palmes Gata 31
Telefon: 08-677 2530. Telefax 08-677 2535
www.elforsk.se